**T.C.**

**AKSARAY UNIVERSITY**

**GRADUATE SCHOOL OF NATURAL AND APPLIED SCIENCE**

**DEPARTMENT OF ELECTRICAL-ELECTRONIC AND COMPUTER ENGINEERING**

# INTELLIGENT INDOOR NITROGEN DIOXIDE SENSORS NETWORK BASED FSO COMMUNICATION

**DOCTORAL THESIS**

**Mohammed Hussein ALI**

**SUPERVISOR**

**Assist. Prof. Yusuf Erkan YENICE**

**AKSARAY, 2021**

Aksaray University, Graduate School of Natural and Applied Sciences Approval, Mohammed Hussein Ali, Doctor of Philosophy with thesis, student No. 172353803, successfully presented the Doctor of Philosophy Thesis titled "**INTELLIGENT INDOOR NITROGEN DIOXIDE SENSORS NETWORK BASED FSO COMMUNICATION**", prepared after satisfying all the requirements identified in the concerned bylaws, before the jury whose signatures are affixed below.

**Thesis Advisor: Assist. Prof. Dr. Yusuf Erkan YENICE**
Aksaray University
I approve that this thesis is a Doctor of Philosophy in scope and quality ……

**Member: Prof. Dr. Mehmet Reşit TOLUN**
Konya Food and Agriculture University
I approve that this thesis is a Doctor of Philosophy in scope and quality ……

**Member: Assoc. Prof. Dr. Yunus UZUN**
Aksaray University
I approve that this thesis is a Doctor of Philosophy in scope and quality ……

**Member: Assoc. Prof. Dr. İsmail BAYRAKLI**
Aksaray University
I approve that this thesis is a Doctor of Philosophy in scope and quality ……

**Member: Assoc. Prof. Dr. Özkan Ufuk NALBANTOĞLU**
Erciyes University
I approve that this thesis is a Doctor of Philosophy in scope and quality ……

Date of Defense: 25 / 1 / 2021

I agree that this thesis which is accepted by the jury, has fulfilled the requirements for being a Doctor of Philosophy Thesis.

……

Assoc. Prof. Dr. Mehmet Ali HINIS

Director of Natural and Applied Science

## DECLARATION

The idea for this Ph.D. thesis was taken from the literature regarding the topics. It was announced here that the whole work presented in this project has been composed and originated by myself unless otherwise specified. The study was conducted completely under the supervision of Asst. Prof. Dr.Yusuf Erkan YENICE.

**Mohammed Hussein Ali**

## ACKNOWLEDGEMENT

Firstly, I would like to express my sincere gratitude to my advisor Assist. Prof. Dr. Yusuf Erkan YENICE for the continuous support of my Ph.D. study and related research, for his patience, motivation, and immense knowledge. His guidance helped me in all the time of research and writing of this thesis. I could not have imagined having a better advisor and mentor for my Ph.D. study.

Besides my advisor, I would like to thank the rest of my thesis committee: Prof. Dr. Mehmet Resit TOLUN, and Assoc. Prof. Dr. Yunus UZUN, for their insightful comments and encouragement, but also for the hard question which incented me to widen my research from various perspectives.

My sincere thanks also to my family Father, Mother, and all of my colleagues for all support and encourages given through this journey.

Mohammed Hussein Ali
AKSARAY, 2021

**TABLE OF CONTENTS**

**DOKTORA TEZİ**

# AKILLI BİNA İÇİ NITROJEN DIOKSIT SENSORLERI AĞINA DAYALI SERBEST UZAY OPTİK İLETİŞİMİ

**MOHAMMED HUSSEIN ALI**

**Aksaray Üniversitesi**
**Fen Bilimleri Enstitüsü**
**Elektrik Elektronik ve Bilgisayar Mühendisliği Bölümü**

**Danışman: Öğr. Üyesi Dr. Yusuf Erkan YENICE**

## ÖZET

Akıllı Kablosuz Sensor Ağı (AKSA) günümüzde yaygın olarak kullanılan uygulamalardan biri olup, şu alanlarda kullanılmaktadır: 1) Dünyamızda meydana gelen doğal olgu ya da çevresel koşulların algılanmasında; 2) sensorlarından gelen verilerin işlenmesinde; 3) girilen verilere dayanarak uygun bir kararın sunulmasında. Bu çalışmada karbonmonoksit gaz algılama uygulamalarında kullanılabilecek bir Akıllı Kablosuz Sensor Ağı tasarlanıp uygulanmıştır. Bu sistem ana parçadan oluşmaktadır: akıllı sistem, sensor arayüz birimi ve kablosuz iletişim sistemi. Önerilen akıllı sistem karbonmonoksit sensorlardan gelen verileri işlemek ve ardından bu verilerin bir ortalama değerini sunmak için kullanılmıştır. Sensor arayüz birimi de nitrojendioksit sensorlarından gelen analog sinyalleri akıllı sisteme aktarılması gereken ve bunlarının sonuncusunun Alanda Programlanabilir Kapı Dizisi'nde(APKD) saklanması gerektiği ikili verilere dönüştürmekte kullanılmıştır. Kablosuz iletişim sistemi uzak mesafelerde sensor düğümü ile akıllı sistem arasında dijital verilerin aktarılması amacıyla uygulanmıştır. Bu çalışma için akıllı sistem olarak bir Geri Yayılımlı sinir ağı kullanılmış ve bu ağda 'girdi', 'tekli gizli' ve 'çıktı' katmanları şeklinde üç tabaka tasarlanmıştır. Bu ağ çeşitli eğitim işlevleri tarafından eğitilmiş olup, gizli katman için SATLINS işlevi ve çıktı katmanı için SATLIN işlevi olmak üzere iki doğrusal aktivasyon işlevi kullanmıştır. TRAINPSO (Parçacık Sürü Optimizasyonu) eğitim işlevi kullanılarak optimal bir sonuç da sunulmuş, ancak sıfır Ortalama Hata Karesi'ne yalnızca gizli katmandaki üç nöron kullanılarak 46 tekrarlamada ulaşılmıştır. Bu çalışmada, önerilen sistem için kablosuz iletişim birimi olarak bir lazerli Serbest Uzay İletişim(SUI) Sistemi tasarlanmış ve uygulanmıştır, çünkü bu teknik aynı iletim aralığına yönelik diğer tekniklerden daha düşük enerji tüketimine ve daha yüksek bant genişliğine, yönelme yeteneğine ve bağışıklığa sahiptir. Bu teknikte sensor birimlerinin dijital verilerinin bir kızılötesi lazer ışık taşıyıcısıyla modüle edilmesi için, güçlü ve lazer iletişim sistemlerinde yaygın olarak kullanılan bir teknik olan AÇIK/KAPALI anahtarlama modülasyonu kullanılmıştır.

**Anahtar Kelimeler:** AKSA (Akıllı Kablosuz Sensor Ağı), APKD (Alanda Programlanabilir Kapı Dizisi'nde), TRAINPSO (Parçacık Sürü Optimizasyonu), SUI (Serbest Uzay İletişim).

**Ocak, 2021; 120 sayfa**

**Ph.D. THESIS**

# INTELLIGENT INDOOR NITROGEN DIOXIDE SENSORS NETWORK BASED FSO COMMUNICATION

**MOHAMMED HUSSEIN ALI**

**Aksaray University**
**Graduate School of Natural and Applied Sciences**
**Department of Electrical Electronic and Computer Engineering**

**Supervisor: Assist. Prof. Yusuf Erkan YENICE**

## ABSTRACT

The Intelligent Wireless Sensor Network (IWSN) is one of the widely used applications in present time, whereas it is utilized for: 1) sensing of the natural phenomenon or environmental conditions that occur in our world, 2) processing the incoming data from their sensors, 3) presenting a appropriate decision according to the entered data. In this work, an Intelligent Wireless Sensor Network has been designed and implemented, which can be used for applications of carbon monoxide gas sensing, it involves three main parts, the intelligent system, the sensor interface unit, and the wireless communication system. The proposed intelligent system has been utilized to processing the incoming data from carbon monoxide sensors, then presenting the average value of these data. The sensor interface unit has been used for converting the incoming analog signals from the nitrogen dioxide sensors to binary data that should be driven to the intelligent system, where the last one should be saved in FPGA (Field Programmable Gate Array). The wireless communication system has been implemented for transferring the digital data between the sensor node and the intelligent system for remote distances. A Back-Propagation neural network has been utilized as an intelligent system for this work, three layers had been designed in this network, input, single hidden, and output layers. This network has been trained by several training functions, and has used two linear activation functions, the SATLINS function for the hidden layer, and the SATLIN for the output layer. Using TRAINPSO (Particle Swarm Optimization) training function, an optimal result has been also presented, but with reaching the MSE to zero value in 46 iteration using of only three neurons in the hidden layer. A laser FSO(Free-Space-Optical) system has been designed and implemented as a wireless communication unit for the proposed system, cause this technique possesses low power consumption and high bandwidth, directivity, immunity than other techniques for same range of transmission. The ON/OFF keying modulation has been used in this technique for modulating the digital data of the sensor units with an infra-red laser light carrier, which is a powerful widely used modulation technique in the laser communication systems.

**Keywords:** IWSN (Intelligent Wireless Sensor Network), FPGA (Field Programmable Gate Array), TRAINPSO (Particle Swarm Optimization), FSO (Free-Space-Optical)

**January, 2021; 120 Pages**

**LIST OF FIGURES**

## LIST OF TABLES

## LIST OF ABBREVIATIONS

| | |
|---|---|
| $\mathbf{A_o}$ | Strength of turbulence at ground level. |
| **A[k]** | Normalized number. |
| $\mathbf{A_v}$ | Voltage gain. |
| **A** | Learning rate. |
| $\mathbf{a_t}$ | Present learning rate. |
| $\mathbf{a_{t+1}}$ | Next learning rate. |
| **BER** | Bit-Error-Rate. |
| **B.W** | Bandwidth. |
| **C** | Capacitance. |
| $\mathbf{C_n^2}$ | Refractive index structure parameter. |
| $\mathbf{c_1}$ | Local weight. |
| $\mathbf{c_2}$ | Global weight. |
| **D** | Distance length between the transmitter and receiver |
| **D** | Desired output vector. |
| $\mathbf{d_1}$ | Transmitter aperture diameter. |
| $\mathbf{d_2}$ | Receiver aperture diameter. |
| **E** | A vector of network error. |
| **F** | Frequency. |
| **GL** | Geometric Losses. |
| **G** | Gradient of MSE with respect to weight. |
| $\mathbf{g_o}$ | Primary gradient. |
| **Gt** | Gradient of next vector. |
| **g(t)** | Best known position vector found by any particle in the swarm. |
| **H** | Planck's constant = $6.626\times10^{-34}$. |
| **H** | Height. |
| **I** | Identity matrix. |
| $\mathbf{I_{LD}}$ | Laser diode operating current. |
| **I** | Distribution of size scattered particles. |
| **J** | Jacobian Matrix. |
| **K** | A measurement constant. |
| **K** | Wave number. |
| **L** | Link range in km unit. |
| **L** | Link range in m unit. |
| **MSE** | Mean-Square-Error |
| **N** | A constant has a values range(0.3-0.8) |
| $\mathbf{N_M}$ | Volumetric density of air particles. |
| **N** | No. output neurons. |
| **P** | Average amplitude of the intensity x(t). |
| $\mathbf{P_{out}}$ | Output power. |

| | |
|---|---|
| $\mathbf{P_r}$ | Received power. |
| $\mathbf{P_t}$ | Transmitted signal power. |
| $\mathbf{p_o}$ | Primary search direction. |
| **Q** | Quality factor. |
| **R** | Resistance. |
| **R** | Aerosol particle size included in atmosphere. |
| $\mathbf{r_1}$ | Random variable number at range (0-1). |
| $\mathbf{r_2}$ | Random variable number at range (0-1). |
| **S** | Spot Size. |
| **SNR** | Signal-to-Noise ratio. |
| **T** | Transpose. |
| **Tp** | Tuning parameter. |
| $\mathbf{t_p}$ | Pulse duration. |
| **U** | Viewed object distance from the lens. |
| **V** | Visibility. |
| $\mathbf{V_{LD}}$ | Laser diode operating voltage. |
| $\mathbf{V_{th}}$ | Threshold voltage. |
| **V** | Wind velocity. |
| **v(t)** | Current velocity vector. |
| **v(t+1)** | New velocity vector. |
| $\mathbf{W_g}$ | Energy gap. |
| $\mathbf{w_c}$ | Cut off frequency in radian unit. |
| $\mathbf{w_t}$ | Present weight vector. |
| **wt+1** | Next weight vector. |
| **wt-1** | Previous weight vector. |
| $\mathbf{x_o}$ | Characteristic size constant. |
| **x(t)** | Current position vector. |
| **x(t+1)** | New location vector. |
| **Y** | Actual output vector. |
| **Z** | Image distance from the lens. |
| **A** | Attenuation of Atmosphere. |
| $\boldsymbol{\alpha_M}$ | Mie scattering cross-section. |
| **B** | Total attenuation coefficient. |
| $\mathbf{B_{abs}}$ | Absorption coefficient. |
| $\boldsymbol{\beta_M}$ | Mie scattering coefficient. |
| $\boldsymbol{\beta_R}$ | Rayleigh scattering coefficient. |
| $\mathbf{B_{scat}}$ | Scattering coefficient. |
| $\boldsymbol{\beta_t}$ | Fixed value varies with the different types of conjugate gradient methods. |
| **Θ** | Divergence angle. |
| **Δt** | Individual update value. |
| **H** | Sensitivity of the received power. |

# 1. INTRODUCTION

In modern times, the use of technology applications in health care is an important area of research. As previous research has highlighted the dangers of nitrogen dioxide gas and its relationship with asthma, lung disease, and death in some cases [1], it has become necessary to find solutions to keep the people exposed to this gas safe. Chronic exposure to $NO_2$ can damage the respiratory system, including airway inflammation in healthy people and increased respiratory symptoms in people with asthma. $NO_2$ creates ozone which causes eye irritation and exacerbates respiratory conditions, leading to increased hospital admission and visits to the emergency room for respiratory issues, especially asthma [2]. Furthermore, exposure to $NO_2$ in some cases can lead to death. In this work, an Intelligent Wireless Sensor Network has been designed and implemented, which can be used for nitrogen dioxide gas detection applications. It involves three main parts: the intelligent system, the sensor interface unit, and the wireless communication system. The proposed intelligent system can be utilized to process incoming data from nitrogen dioxide sensors and present the average value of these data. The sensor interface unit is used to convert the incoming analog signals from the nitrogen dioxide sensors to binary data that is then driven to the intelligent system, with the last one being saved in FPGA (Field Programmable Gate Array). The wireless communication system has been implemented for transferring the digital data between the sensor node and the intelligent system for remote distances.

## 1.1 Problem Background

Gaseous $NO_2$ is classified as one of the most dangerous and most toxic gases. Indoors, the prominent sources of $NO_2$ include: exposure to cigarette smoke [3], butane, kerosene heaters and stoves [4]. Because workers in industries where $NO_2$ is used are also exposed and are at risk for occupational lung diseases, NIOSH has set exposure limits and safety standards [5]. Astronauts in the Apollo–Soyuz Test Project were almost killed when $NO_2$ was accidentally vented into the cabin [6]. Agricultural workers can be exposed to $NO_2$ arising from grain decomposing in silos; chronic exposure can lead to lung damage in a condition called “Silo-filler's disease”

[7][8]. Historically, nitrogen dioxide was also produced by atmospheric nuclear tests, and was responsible for the reddish color of mushroom clouds [9].

Nitrogen dioxide has the following effects on humans:

1. Inhalation can lead to significant damage to the lungs and the occurrence of suffocation and inability to breathe, with major impact to the mucous membranes in the nose and eyes [10].
2. Episodes of allergies and poisoning are also common, especially if particles of the gas are concentrated in the air, that may lead to death [11].

It also causes significant health damage to animals and plants.

Outdoors, $NO_2$ arises from internal combustion engines burning fuel and as a result of traffic from motor vehicles. Its harmful effects include:

1. It causes a hole in the ozone layer, which allows harmful sunlight to reach the earth in larger quantities. It is worth mentioning that nitrogen oxides from human activities are the most harmful to the environment [12].
2. The occurrence of acid rain phenomenon that causes significant negative effects on the environment is a result of increased nitrogen dioxide levels [12].

Toxicity:

The Acute harm due to $NO_2$ exposure is only likely to arise in occupational settings. Direct exposure to the skin can cause irritations and burns. Only very high concentrations of the gaseous form cause immediate distress: 10–20 ppm can cause mild irritation of the nose and throat, 25–50 ppm can cause edema leading to bronchitis or pneumonia, and levels above 100 ppm can cause death due to asphyxiation from fluid in the lungs. There are often no symptoms at the time of exposure other than transient cough, fatigue or nausea, but over an hour's inflammation in the lung’s causes edema [13].

### 1.2 Motivation

The effects of toxicity on health have been examined using questionnaires and in person interviews in an effort to understand the relationship between $NO_2$ and asthma. It was discovered that most people who were exposed to the nitrogen dioxide gas, whether industrial workers or children in their homes, suffer from asthma and

mild irritation of the nose and throat. Therefore, $NO_2$ is classified as an extremely hazardous substance in the United States as defined in Section 302 of the US. Emergency Planning and Community Right-to-Know Act (42 U.S.C. 11002) [14]

### 1.3 Problem Statement

The influence of indoor air pollutants on health is important, because the majority of people in the world spend more than 80 percent of their time indoors. Therefore, considering that nitrogen dioxide is considered one of the most dangerous air pollutants, the question can be worded as: "How can we keep indoor areas where nitrogen dioxide could be produced, such as homes and factories, safe for people and workers, based on the known dangers of this gas?"

For this purpose:

- It becomes necessary to keep indoor areas safe from the dangers of the $NO_2$ gas by using an automated system to detect the level of gas in a limited area and to make a proper decision according to the level of $NO_2$ in that area.
- Because the sensor uses analog reading, it is required to develop a new technique to convert the data from analog to digital.
- FSO (Free Space Communication) is necessary to implement a system with low power consumption and to increase the bandwidth channel.
- The system must be intelligent to give accurate results and reduce MSE (Mean Square Error).

### 1.4 Challenges

The main challenges that facing this work are:

1. Difficulties of line of sight (LoS).
2. The light sources operate by the main AC 220 Volt.
3. The power consumption.

### 1.5 Scope of Project

Indoors, there is a wide range of applications for this project due to the multiplicity of sources of this type of gas from homes that are almost devoid of nitrogen dioxide

sources, such as gas stoves, cigarette smoke, and heaters that use butane and kerosene. Unlike the home, factories use $NO_2$ as an intermediate in the manufacturing of Nitric Acid, as well as oil refineries and power plants. Many workers in these industries are also exposed to $NO_2$ gas despite the use of this gas being banned to reduce the chances of occupational lung disease and meet the safety standards set by the National Institute of Occupational Safety and Health.

### 1.6 Aim of The Project

The aim of this work is to design and implement an automated system that uses an intelligent wireless sensor network to sense and present the average level of nitrogen dioxide ($NO_2$) gas over a limited area, determine its level based on given parameters (Normal, Critical or Fatal), and then make the appropriate decision to avoid $NO_2$ gas toxicity, such as "ventilation." This project should be achieved with the following considerations:

1. The proposed system should be performed with two nitrogen dioxide gas sensors as a prototype model.
2. The Back-propagation neural network should be designed and simulated as an intelligent system for the proposed system using MATLAB v 2014b software package.
3. The Particle Swarm Optimization (PSO) technique should be used as a training function for the proposed Back-propagation neural network.
4. The FPGA Xilinx Spartan-6 SP-605 evaluation kit should be used to save the proposed Back-propagation neural network.
5. An infra-red IR laser communication system should be realized as a wireless communication system for the proposed system.
6. The IR laser communication system should be performed by Free-Space-Optical (FSO) technology.
7. The link range for the proposed laser communication system should be equal to 50 meters, because of the proposed system used for indoor application.

## 1.7 Main Contributions of This Work

The proposed intelligent wireless sensor network has been realized with the following main contributions:

1. Using the Trainpso (Particle Swarm Optimization) function as a training function for the proposed Back-propagation neural network, with four neurons in the input layer, three neurons in the hidden layer, and four neurons in the output layer. An optimal result has been obtained when the mean square error reaches zero value. Another important result has been obtained by this training: the size of the proposed neural network has been reduced.
2. A new proposed technique of Analog-to-digital A/D conversion circuit has been utilized in this work, which has been used for converting the analog output signal of the $NO_2$ gas sensor to binary data that is driven to the input of the proposed neural network. The concept of this proposed A/D converter circuit is the conversion of the analog output signal of the $NO_2$ gas sensor to a single pulse with a specific duration, then converting this generated pulse to a binary data by a pulse period decoding unit. This new proposed A/D converter circuit has been named pulse period coding A/D converter circuit. The main feature of this A/D converter circuit is the low conversion time.
3. The information of the output of the $NO_2$ gas sensor has been represented by a single pulse (single bit), which is sent by the laser transmitter as a single laser pulse to the receiver circuit of the laser communication system. The duration value of this pulse (bit) depends on the represented signal level of the sensor, whereas each signal level of the sensor is represented by a single pulse (bit) with a specific duration. The main feature of this proposed technique is the probability of error that occurs in a single representing pulse (bit) of this system is much lower than that of the related systems which represent the analog signal of the sensor by multiple bits (mostly they represent the analog level by 8-bit binary data).

## 1.8 The Proposed System

Within the proposed system, one of the two nodes is considered an indoor wireless sensor network responsible for nitrogen dioxide ($NO_2$) gas sensing, processed by an

intelligent system saved in an FPGA (Field programmable Gate Array). The proposed system consists of two nodes of $NO_2$ gas sensor systems, each of these systems involves two main parts: hardware and software. The hardware component is composed of the sensor interface unit and the FSO (Free-Space-Optical) laser communication system, which is composed of four main units: the data transmitter, data receiver, ON/OFF switching key transmitter, and ON/OFF switching key receiver. The software is considered a simulation of a Back-propagation neural network used for processing the incoming data from the two sensors and producing the average output of these two pieces of data. Figure 1.1 below shows the basic block diagram for one sensor unit of the proposed system.

The role of the data transmitter unit is to read the sensor output level and then translate this level to a pulse with a specific width. After, this pulse is transmitted by the FSO laser communication system as a laser pulse to the data receiver unit. Then, the last one decodes this laser pulse to a binary data driven to the input of FPGA.

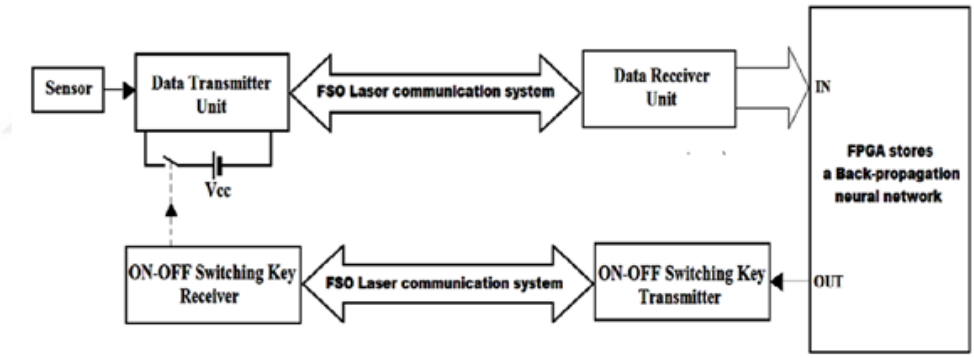


**Figure 1.1.** The basic block diagram of one sensor unit of the proposed system.

The duty of the ON/OFF switching key transmitter is to receive the key signal from the FPGA and then produce a suitable switching key pulse that is transmitted by the other FSO laser communication system to the ON/OFF switching key receiver unit. Then the last one decodes this laser pulse to binary data that is used for switching ON the power supply terminal to the supply feeding terminal of the data transmitting unit. Finally, the laser pulse of the ON/OFF switching key transmitter is used as a key signal for activating the data transmitter unit.

The output signal of each sensor is divided into three levels: the NORMAL level represented by the binary data (01), CRITICAL level represented by the binary data (10), and FATAL level represented by the binary data (11). As such, one can observe that the output signal of each sensor is represented by two bit data. Therefore, the simulation of the intelligent system should have four input lines, with each two lines specialized for a single sensor.

Four output lines are proposed for the simulation system output the proposed system: (x, y, z, and f). The x output line is activated by NORMAL level result, the y output line is activated by CRITICAL level result, and the z output line is activated by the FATAL level result.

For the FSO laser communication system, the NORMAL level has been represented by a pulse with a duration of 1 msec, the CRITICAL level has been represented by a pulse with duration 2 msec, and the FATAL level has been represented by a pulse with duration 3 msec. Thus, one can see for these levels, only a single pulse should be transmitted in each situation. For this reason, the probability of error of the proposed system has been minimized as much as possible with respect to the traditional wireless sensor networks.

The software of the proposed system is a Back-propagation neural network, which is trained by Trainpso training functions. Only by using this training function, the proposed intelligent system has produced optimal results, where the mean square error has reached to zero.

## 1.9 System Components

The proposed system has been designed with two main components, the hardware and software component requirements.

### 1.9.1 Hardware requirements

The hardware part is composed of: the sensor interface unit, FSO (Free-Space-Optical) laser communication system, and FPGA board.

- The Sensors Interface Unit composed of:

1. Two $NO_2$ sensors.
2. Power supply.

❖ The FSO (Free Space Optical) component:

**1.** Data Transmitter Unit which is composed of:

a. Analog-to-Digital converter which done using:

- Four comparators
- Timer
- AND gate and OR gate
- Mono-stable-multi vibrator

b. Pulse period coder which is composed of:

- One-shot-to circuit
- Binary counter
- Latch
- Timer

c. Laser transmitter part

**2.** Data Receiver Unit:

a. Laser pulse Receiver which is composed of:

- Laser pulse detector
- Low noise amplifier
- Notch filter
- Low pass filter
- Voltage comparator

b. Pulse period decoder

❖ The FPGA Xilinx Spartan-6 SP-605 evaluation kit should be used to Save the proposed Back-propagation neural network.

**Software requirement:**

❖ Computer system with minimum requirements:

a. Hard disk with 2.00 GB available storage

b. 3GB of RAM

c. CPU with 2.2 GHz

d. Windows7 Operating System

❖ The Back-propagation neural network has been designed and simulated as an intelligent system for the proposed system using MATLAB v 2014b software package.

### 1.10 Expected Result

At the end of this project, we expect to get an optimal result using the Trainpso (Particle Swarm Optimization) function as a training function for the proposed Back-propagation neural network and faster training method. As a result, one can conclude that the training by the particle swarm optimization is the fast training method compared to other training functions used in previous work, while the MSE (Mean Square Error) reached zero and the size of simulation software got reduced. Likewise, using the proposed method of Analog to digital conversion will produce a faster system because of the minimum required time to convert the data from analog to digital. Furthermore, we expect that the system bandwidth will be big enough to carry data using a laser pulse in data transmission.

# 2. LITERATURE REVIEW

## 2.1 Literature Survey

In this section, the findings of several previous research have been presented, which relate to the proposed system work. These studies have utilized several intelligent systems, such as Back-propagation Neural Network (BPNN), Particle Swarm Optimization (PSO), or other types for the specific functions of their wireless sensor networks. The research has been divided into three groups related to the utilized intelligent system. All of them have presented acceptable results.

## 2.2 BPNN Studies

The following research utilized the Back-Propagation Neural Network as an intelligent system for the wireless sensor network. Each study uses the BPNN for a specific function, such as clustering, localization, data recognizing, etc. They had utilized several training functions, such as Trainlm and Traindgx, for their proposed neural network.

In 2012, [15] used a trainable Back-Propagation Neural Network for basic gates and image compression for the wireless sensor network. This work used linear activation functions for the hidden and output layers of their proposed neural network and used gradient descent training function for their work. They have implemented this work on FPGA.

In 2012, [16] described the implementation of the Back-propagation algorithm for use in Wireless Sensor Network (WSN) applications. This application had been performed over an FPGA (Field Programmable Gate Array) and the MATLAB software package. This paper studies the architecture of a neural wireless sensor network designed to identify technical conditions (temperature, humidity, light, etc.) of the base station of wireless sensor networks. This work used A/D converter ICs and microcontrollers for the sensor units and used linear activation functions for the hidden and output layers of their proposed work.

In 2013, [17] proposed a design and implementation of a Back-Propagation Neural Network for node localization to a wireless sensor network, where the node positions in the overall wireless sensor network can be recognized by these nodes themselves.

The Back-Propagation Neural network used in the study was based on a Multilayer Perceptron Neural Network. The study used a non-linear activation function for the hidden layer and linear activation function for the output layer. She used the Levenberg-Marquardt training function for their proposed work. This work is not implemented on FPGA.

In 2014, [18] presented a design and implementation of wireless sensor network nodes using a Back-Propagation Neural network based on a Multilayer Perceptron Neural Network. The research used a non-linear activation function for the hidden layer and linear activation function for the output layer. The Levenberg-Marquardt training function was used for their proposed work. This work is not implemented on FPGA.

In 2014, [19] presented a design and implementation of wireless sensor network nodes based on Back-propagation Neural Network. The proposed Back-propagation neural network was trained by the parameters of Routing protocol for wireless mobile sensor networks, which can be active or passive depending on the proposed design. This work is not implemented in an FPGA because it uses a non-linear activation function for the proposed neural network

### 2.3 Other ANNs Studies

The following research used other Artificial Neural Networks (ANNs) to perform several functions in wireless sensor network applications.

In 2013, [20] developed a basic gas recognition system to distinguish between the industrial gas brands. This system involves an array of eight micro-hotplate-based $SnO_2$ thin film gas sensors with various selectivity patterns. A signal conditioning and analyzing system was used for processing the output signals of the proposed system. This gas recognition was performed by a Multi-Layer Perceptron (MLP) Neural Network, which was implemented on appropriate FPGA using the VHDL code program.

In 2015, [21] presented a design and implementation of an algorithm of embedded and distributed target location method using the Received Signal Strength Indicator (RSSI). The estimation of target location in a distributed fashion against anchor

failure was performed using an Embedded Feed-Forward Artificial Neural Network (EFFANN). This artificial intelligence system was implemented on an FPGA.

In 2015, [22] presented a design and implementation of an algorithm for an embedded and distributed target location method using the Received Signal Strength Indicator (RSSI). The estimation of the target location in a distributed fashion against anchor failure was performed using an Embedded Feed-Forward Artificial Neural Network (EFFANN). This artificial intelligence system was implemented on an FPGA.

### 2.4 Using WSNs In Gas Detection

The following research used wireless sensor networks in hazard gas detection implemented in the use of microcontrollers.

In 2012, [23] developed a wireless sensor network to detect methane gas. The study used a WSN to focus on the power consumption of the sensor node. The sensor node was designed based on the planar catalytic sensor with improved power consumption characteristics. This work was done using a microcontroller without the use of a neural network.

In 2017, [24] designed and implemented a wireless sensor network to detect $CO_2$ gas. The work was carried out using a microcontroller and back propagation network, the network used two linear activation functions: the SATLINS function for the hidden layer and the SATLIN for the output layer. Using the TRAINGDA (Gradient Descent with Adaptive Learning Rate) training function, an optimal result has been presented by reaching the zero value of the MSE (Mean-Square-Error) in 87 iterations using ten neurons in the hidden layer.

# 3. THEORETICAL BACKGROUND

The wireless sensor network (WSN) has been described in detail in this chapter. A WSN is defined as many sensor nodes connected to a control station (HUB) via a wireless communication system. Each sensor node includes one or more sensors and a serial transmitting unit. The control station consists of a central processing unit with a serial receiving unit [25].

A Free-Space-Optical (FSO) communication system can be utilized in the wireless sensor networks. This is because FSO communication systems consume less power than other communication systems, like RF and microwave communication systems, with the same range of communication [26].

The Back-Propagation (BP) Neural Network has been described in detail within this chapter, along with utilizing its essential training functions. This type of neural network is considered as a powerful artificial intelligent system that has an optimal algorithm for updating the weights and biases of its overall system connections.

The Particle Swarm Optimization (PSO) technique has been also described in this chapter, which is considered an optimal method for obtaining a best solution for specific problems.

## 3.1 Wireless Sensor Networks (WSNs)

The star topology is mostly used in wireless sensor networks. In this topology, each sensor node should communicate with the control station via a specific channel and each sensor node has its own energy source. The HUB receives data from the sensors via the sensor nodes and the communication channels, then these data should be collected and processed by the HUB for producing a specific decision. A model of star topology wireless sensor network is shown in Figure 3.1. The following wireless communication systems can be utilized to communicate the sensor nodes with the HUB [27].

1. RF communication system

2. Optical communication system

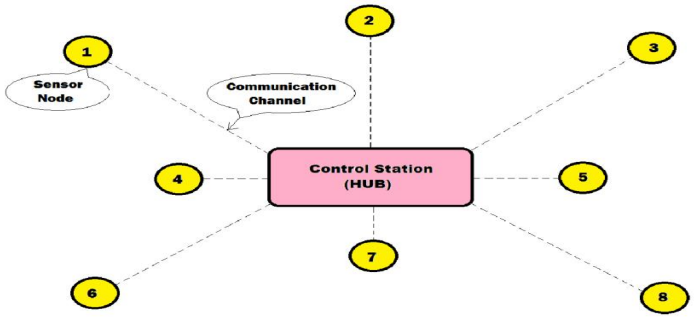


**Figure 3.1.** A model of star topology wireless sensor network [28].

The sensor nodes (sensor units) are mini-power, low cast, small, and distributed devices that have wireless communication and local processing abilities. Limited quantity processing can be performed by a single sensor node. The detailed measuring of a specific physical environment can be performed by collecting data from these sensor nodes. Therefore, the sensor network can be defined as a network of many sensor nodes, collected for producing a specific function [29].

Antique sensor networks involve few sensor nodes that connect to a control station (or central processing station) via wires. However, at the present time, there is great focus on distributing these sensor nodes in a wireless fashion, such as in wireless sensor networks. In modern wireless sensor networks, if the location of sensing a specific physical or chemical phenomenon is harsh or rough in relation to a single sensor node, we can substitute this sensor node by dense distributed sensor nodes around or close to this harsh location. To surmount environmental deterrents, like line of sight limitations and obstructions, a dense distribution of sensor nodes are also required in a specific location [30]. In many situations, the monitored environment does not have a strong foundation for the energy or communication, so the designers must consider the requirements to conserve the sensor nodes with little and limited sources of energy to communicate through a wireless communication channel [31]. The sensor networks have another requirement for their distributed processing ability, where the communication function is the most energy consumer. Sometimes the centralized system is the solution, such as in long distances where communication is needed for some sensor nodes, i.e. more energy is consumed [32].

Another requirement for the sensor network is the local processing of sensor nodes, which is the best concept to process a huge quantity of information locally at the sensor node for the minimization of total bits of the transmitted signal [33].

There are many advantages of the wireless sensor networks over the old technology of sensing due to their deployed nature and embedded construction. The most noticeable one is their cost, as the sensor nodes use inexpensive, low-power transceivers and microcontrollers. Furthermore, the cost of sensor nodes used in wireless sensor networks are always less than one hundred dollars. This feature allows the easy application of wireless sensor networks in many military or commercial applications [34].

The low cost of the sensors allows for the use of many sensors in the sensor nodes or in the overall wireless sensor network for maximum coverage of the sensing area. For such networks, if a few of sensors fall or drop, their effect will be ignored and they will not affect the overall wireless sensor network, unlike the old sensor systems [35].

### 3.2 The Communication Link Between Sensor Node And HUB

The communication link has two channels. The first one is used for transferring the ON/OFF key signal from the HUB to the sensor node, where this signal is used to switch ON the power supply terminals to the overall circuit of the sensor node. The second one is used for transferring the data signal from the sensor node to the HUB [36]. The first role of control station (HUB) in the wireless sensor network is to process the incoming data from the sensor nodes and present specific decisions, while the second role is to provide the ON/OFF key signal to the sensor nodes [37][38].

There are three types of communication links used in wireless sensor networks: RF, Microwave, and optical communication links. The last one is divided into two kinds: Free-Space-Optical (FSO) system and fiber-optic communication links [39].

The RF communication link uses an electromagnetic carrier wave with a frequency range of several hundred kilohertz to several hundred megahertz. Generally this type

of link uses a receiver and transmitter antennas for transmitting and receiving the propagated wave. These are considered non-directed links.

The microwave communication link uses an electromagnetic carrier wave in the frequency range of several gigahertz and always uses horn or dish antennas at the transmitter and receiver ends. This type of link is considered directed links [40].

The optical communication link uses light as a carrier wave and a light transmitter and detector at the transmitter and receiver ends. This type of communication link usually utilizes the infra-red light band for communication because this band is not visible and offers negligible attenuation [41].

Free-Space-Optical (FSO) communication links have been utilized as the wireless communication system for the proposed system because these links consume less power than other link types with the same range of communication [42].

### 3.3 Advantages of FSO Communication

FSO communication systems are powerful communication systems at present day which have the following advantages [42]:

1. They have a long range respective to communication: they can be applied up to 11 km.
2. The used bit rates are quite high: the FSO has a high bandwidth capability in the range (2.5-10) Gbps.
3. They possess high immunity, are secure, and have ultra-narrow and very directional beams: this system is not affected by electromagnetism.
4. Interference: they are not detected by RF instruments like the RF meter and the spectrum analyzer.
5. They usually use infra-red light, which is not visible and does not harm the eye. Therefore, there are no health hazards.
6. The Bit Error Rates (BER) are quite low in this system.
7. There are no side lobes in the light beam.

8. FSO systems are quick and easy to apply.
9. They are quite practical systems as they can be applied with little maintenance.
10. There are lower costs compared to fiber-optic networks: FSO costs about 1/5 of fiber-optic network costs.
11. They can operate without a license for operation in long distances (when we compare it with RF communication).

### 3.4 FSO Disadvantages

In ground FSO applications, there are several basic limiting factors can be presented, they are [42]:

a. There is variable signal attenuation due to scattering and absorption of the atmosphere conditions.
b. There is interference between the transmitted light beam with the background light or radiation from the sun.

### 3.5 Basic Optical Communication Link Between Sensor Node And HUB

The optical communication link is widely used in the present time because it consumes lower power than the other types of communication links for a given distance length. FSO depends on the line-of-site between the light source (light transmitter) and the light detector. Figure 3.2 shows the basic FSO link between the sensor node and the control station for a specific wireless sensor network.

For short distance optical communication links, the LED (Light Emitting Diode) can be used as a light transmitter, which operates at about 2.2 Volt, while the laser diode can be used for long distance optical communication links, usually operated at 3 Volt. The light beam of the laser diode is so narrow and can provide more power than the LED. Usually, the LED is used for short distance fiber-optic communication links, while the Laser Diode is used for both FSO communication links and long distance fiber-optic links. The fiber-optic communication system has higher immunity and lower loss of the transmitted power than the FSO communication

system, but it has a higher cost. For this reason, fiber-optic is used for limited distances [43]. The FSO communication system utilizes the atmosphere for propagating the light.

As shown in Figure 3.2, the optical communication link consists of three main parts: the sensor node, the control station (HUB), and the communication channel. Included in the sensor node are the sensor, the analog-to-digital A/D converter, the microcontroller (1), external memory, and the laser transmitter unit.

The sensor is a device that converts the chemical or physical event to an electrical signal. Many types of sensors exist, each depending on the effecting element and the type of conversion. Examples of these types include sound, thermal, pressure, light, and gas sensors. Of these, one type is the MOS (Metal Oxide Semiconductor) gas sensor. This sensor type has been utilized in this work. The output signal produced from these types of sensors is in an analog form. They must always be supplied by a DC or AC voltage source, with 5 Volt being most common [44].

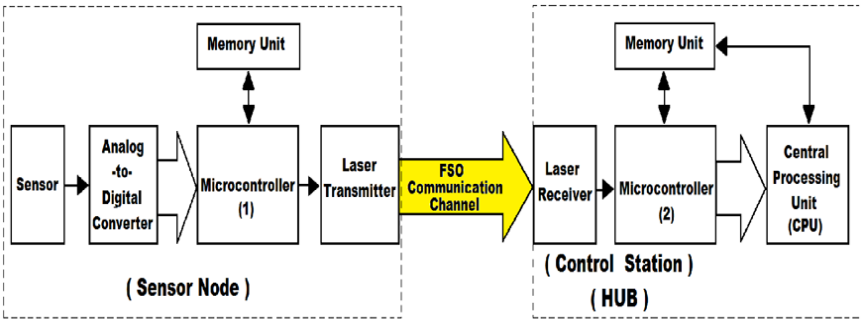


**Figure 3.2.** FSO link of the sensor node and the control station (HUB) [32].

The Analog-to-Digital (A/D) converter is an integrated circuit chip used for converting the analog output signal of the sensor to digital or binary parallel data. The control station does not understand the output analog signal of the sensors unless it is translated to binary data. The resolution of the A/D converter depends on its output bits; the more output bits mean increasing the accuracy of the A/D converter. Usually, most A/D converters include an analog comparator and logic circuit, with the analog comparator always being used to compare the input analog signal with a reference analog signal. Several examples of A/D converters are: counter ramp, tracking counter ramp, successive approximation, single slope integrating, dual slope

integrating, multi-slope integrating, flash, and VCO. The flash A/D converter is the fastest type, but it is the most complex and costly [45]. An 8-bit A/D converter is commonly used in wireless sensor networks because it has good resolution and accuracy. The IC AD 574 successive approximation A/D converter is a good example of this.

The microcontroller (1) is a microprocessor-based integrated circuit chip, shown in Figure 3.3 below. The microcontroller IC (integrated circuit) consists of: a microprocessor, RAM (Random Access Memory), ROM (Read Only Memory), two timers, control registers, I/O (input/output) ports, and general purpose registers. Its frequency depends on the internal oscillator and the crystal frequency [46]. The microcontroller consumes very low power when compared to the microprocessor of the microcomputers, but it operates at a lower frequency and has lower cost when compared with microcomputers. Very low power consumption is the main feature of the microcontroller [46].

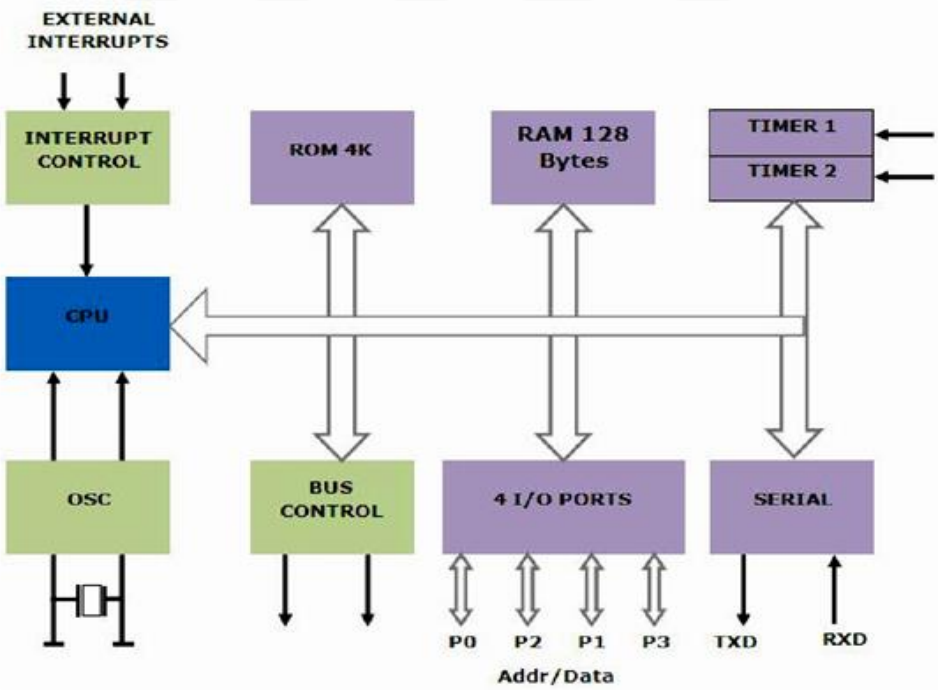


**Figure 3.3.** Internal block diagram of the microcontroller [46].

The role of the microcontroller in the sensor node unit is to convert the parallel output data of the A/D converter to serial data which is easy for transmission through a single channel. In the sensor node, the microcontroller converts the 8-bit parallel

data of the A/D converter to 8-bit serial data, through the addition of a start bit at the beginning of the 8-bit and an end bit at the end of the 8-bit serial data (i.e the total bits number of the serial data is equal to 10-bit). This addition of start and end bits is used to synchronize the serial communication [47].

As shown in Figure 3.3, the Timers (1) and (2) are responsible for the serial communication. The output serial data is produced from the TXD pin of the microcontroller (1), while the parallel output data of the A/D converter is entered from the input ports of the same microcontroller. Some microcontrollers add a parity bit at the end of the serial data for data error detection.

The laser transmitter unit consists of a modulator and a laser source. Wireless sensor networks most often use the laser diode because it consumes very low power and draws few currents in milli-amperes.

The modulator circuit modulates the carrier laser light by the output serial binary data of the microcontroller (1) through one of the following modulation techniques: pulse-position, direct intensity (ON/OFF keying), ASK, FSK, and QSK. Generally, with low bit rate transmission, the ON/OFF keying modulation is used in wireless sensor network application because it is a powerful method of modulation for such transmission [48].

The laser diode (LD) is used to generate the modulated laser light that propagates through the atmosphere or the optical fiber. The laser receiver unit usually consists of a laser detector circuit, DC eliminator, low noise amplifier, 50Hz Notch (Band Reject) Filter, and low pass filter. The laser receiver unit converts the received laser light to electrical serial binary data. The laser detector circuit consists of a photodiode like a PIN or an Avalanche Photodiode [49] and a series resistor connected to the Vcc for generating an output electrical signal to the input of the low noise amplifier [50]. The DC eliminator is used to cancel the effect of the sunlight or the light supplied by the DC power supply then amplify it to an acceptable level because this amplifier has an ultra-low noise for amplifying. The 50 Hz notch filter is used for canceling the effects of light supplied by the 50 Hz Main Power Supply. The low pass filter is used to cancel the undesired high frequency noise from the system.

The laser transmitter with the atmosphere channel and the laser receiver compose the Free-Space-Optical (FSO) communication link, which is discussed in detail later in this chapter.

The microcontroller (2) converts the incoming 10-bit serial data from the output of the laser receiver to 8-bit parallel data that enters to the input of the control station. The last one always involves a central processing unit (CPU) that receives the 8-bit parallel data from the microcontroller (2) and then processes them to present specific decisions.

The memory units in the sensor node and the control station are used for temporary storing of the incoming data. They are Random Access Memory (RAM) types.

## 3.6 Nitrogen Dioxide MOS Sensors

MOS means Metal Oxide Semiconductor. The tin oxides are mainly used by the MOS sensors, which are utilized as a sensing thick film, they are based and deposited on two variant substrates. The first are applied in thick film sensors, which are called Alumina Substrates, and the second are applied in micro sensors, which are called silicon Micro Machined Substrates. Electrodes are produced with these substrates to enable the measuring of the sensing layer resistance. Tungsten heaters are used in these sensors, they are supplied by AC or DC power supply. The variation of the sensing layer resistance leads to changing of the sensor response [51].

### 3.6.1 Operation concept of MOS sensors

The sensing layer of the Metal Oxide Semiconductor (MOS) sensor is considered a percolating thick film of polycrystalline ($SnO_2$). At the surface of the $SnO_2$, the oxygen atoms and the water vapor molecules are absorbed at normal environment conditions. The reaction occurs with oxygen atoms and the water vapor molecules to minimize the carbon monoxide (CO) or hydrogen ($H_2$) gases. The sensor resistance reduces from this absorption, as the sensor resistance increases because of oxidation of the gases such as ozone ($O_3$) or nitrogen dioxide ($NO_2$). The material base doping or the composition, the microstructure of the sensor, the morphology and geometrical characteristics of the sensing layer, and the temperature at the sensor layer are

required for the resistance changing magnitude [52]. The chemical reaction at the sensing layer of the MOS sensor has been demonstrated in Figure 3.4. The change of sensing layer resistance is caused by a chemical reaction at the sensing surface.

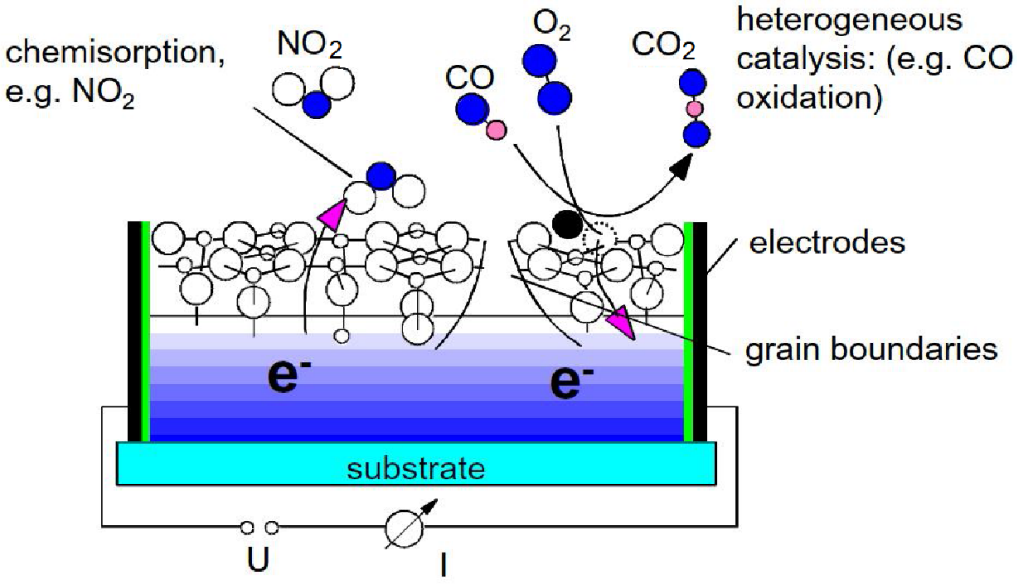


**Figure 3.4.** The chemical reaction at the sensing layer of the MOS sensor [52].

The $NO_2$ gas concentration can be determined by this analog signal output. The analog signal output will increase when the sensing layer resistance decreases. In this work, the $NO_2$-SS (Appendix A) Nitrogen Dioxide gas sensor has been used. Increasing the output voltage of the $NO_2$-SS is in the range (0.22-4.2) Volt.

Changing the sensing layer resistance of the MOS sensors depends on the composition changes in the environment. This has been determined by the following expression of the relationship between the resistance and the concentration of the sensed Nitrogen Dioxide $NO_2$ gas, which is called the power law [53]:

$$R = K.N\mp^{n} \tag{3.1}$$

where,

*R*: Resistance of the sensor.

*N*: Concentration of sensed NO gas.

*K*: A measurement constant.

*n*: a constant has a values range (0.3-0.8), where the (+) sign is used for oxidized gases, while the (-) sign is for reduced.

### 3.7 Nitrogen Dioxide ($NO_2$) Affecting Levels

The effects of $NO_2$ depend on its concentration in the environment, the exposure duration, and the health state and activity level of the person. Direct exposure to the skin can cause irritations and burns. Only very high concentrations of the gaseous form cause immediate distress: 10–20 ppm can cause mild irritation of the nose and throat, 25–50 ppm can cause edema leading to bronchitis or pneumonia, and levels above 50 ppm can cause death due to asphyxiation from fluid in the lungs. There are often no symptoms at the time of exposure other than transient cough, fatigue or nausea, but inflammation in the lungs for over an hour causes edema [54].

There are several National Standards for the effects of $NO_2$ concentration levels exposure. They are described as follows:

- It is classified as an extremely hazardous substance in the United States as defined in Section 302 of the U.S. Emergency Planning and Community Right-to-Know Act (42 U.S.C. 11002) [55].

- Both the ACGIH and NIOSH have recommended maximum limits for nitrogen dioxide. The current ACGIH recommendation is for a 3 ppm and a 5 ppm. The NIOSH REL is 1 ppm as a 15-minute short-term limit. OSHA's former PEL was 5 ppm as a ceiling value. The Agency proposed, and the final rule establishes, a permissible exposure limit for nitrogen dioxide of 1 ppm as a 15-minute STEL. NIOSH agreed with the selection of this PEL. Nitrogen dioxide is a reddish-brown gas.

- EPA: Environmental Protection Agency, this National Standard says that a human must not breathe 10 PPM or more of concentrated $NO_2$ over the span of 15 hours.

### 3.8 FSO IR Communication Link

The Infra-Red (IR) Free-Space-Optical (FSO) communication link is an optical communication system with free space or atmosphere channel. It consists of three

main units: the transmitter, FSO communication channel, and receiver. Figure 3.5 illustrates the block diagram of the FSO communication system which was used in this work. The FSO communication system can be used in terrestrial applications with a link range up to 11km. This distance is sufficient for using the wireless sensor network. In spatial applications, the FSO can be used up to a hundred-millions kilometers [56]. The infra-red (IR) light band has been used in the proposed communication system because the total losses can be minimized as much as possible when it is used in the FSO communication channel.

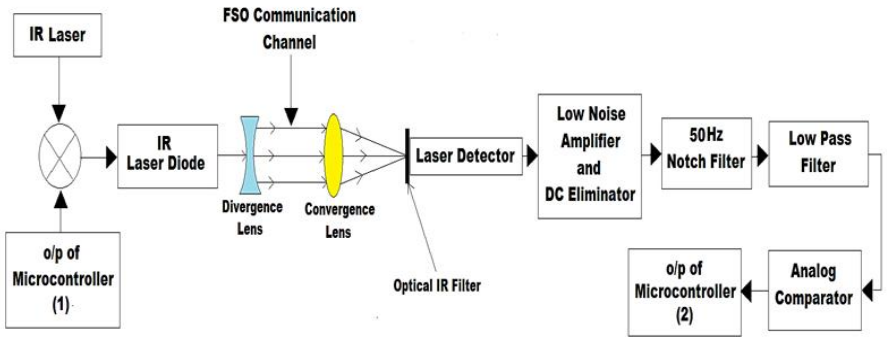


**Figure 3.5.** The Block diagram of the FSO communication link [57].

To reduce the difficulties related to the Line-of-Site (LOS) and increase the received light power, two lenses are used [57]:

a) A divergence lens is used at the transmitter side to direct the beam and to spread the light signal into a wide area at the receiver side.

b) At the receiver side, a convergence lens is used to increase the intensity of light (which means increasing the signal power). The optical detector is located at the focal point of this lens.

### 3.9 IR Laser Transmitter Unit

The role of this unit is to modulate the IR laser light by the digital signal incoming from the sensor and then propagate the modulated IR laser light through the atmosphere. The circuit diagram of the IR laser transmitter unit has been illustrated in Figure 3.6, which consists of buffer (IC1) and IR laser diode [58].

As shown in this figure, the Buffer (IC1) is a logic buffer integrated circuit which is used as a modulator circuit that modulates the incoming digital data from the output of the microcontroller (1). The type of the digital modulation used in this unit is the ON/OFF keying or direct intensity modulation [59]. Using this unit, the ones (1s) output bits of the microcontroller (1) with a specific durations are translated to constant levels of emitted laser light with the same durations, while the zeros (0s) output bits of the microcontroller (1) that have specific durations are translated to no emitted laser light with the same durations. Generally, the IC 7407 is used as a Buffer IC1, where this IC is an open-collector buffer IC and supplied by 5 Volt power supply. The resistor *R* in Figure 3.6 can be calculated as follows:

$$R = \frac{5 - V_{ld}}{I_{ld}} \tag{3.2}$$

where,

$V_{LD}$ : Laser diode operating voltage (in Volt).

$I_{LD}$ : Laser diode operating current (in Amp.).

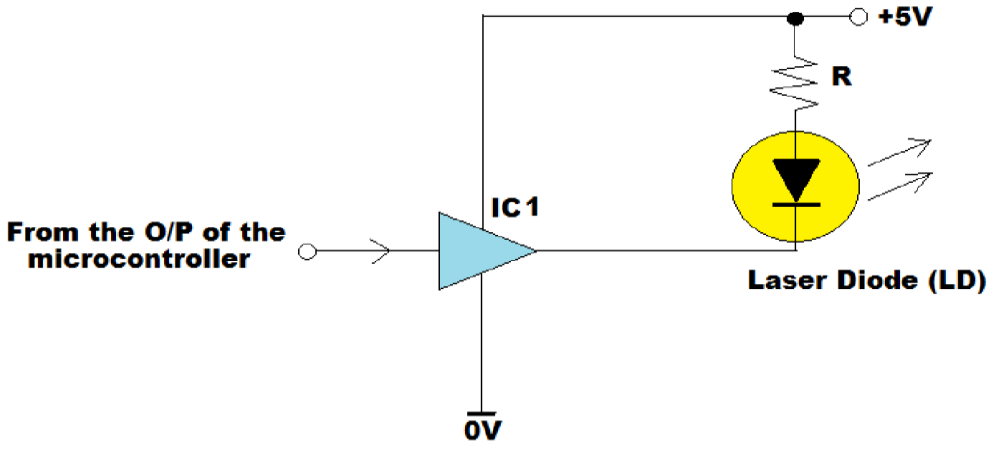


**Figure 3.6.** The laser transmitter unit [59].

### 3.10 FSO communication channel

FSO communication system uses the air or atmosphere as an optical communication channel, which suffers from several turbulences suchlike, atmospheric absorption and scattering attenuations, scintillation…, etc. The transmitter unit propagates the binary data into the FSO communication channel as light ray pulses, where the zeros

(0s) with specific durations are represented by no transmitting light ray with the same time durations, while the ones (1s) with specific time durations are represented by transmitting a constant level of light ray with the same time durations. Usually, IR light bands are used in FSO communication systems. FSO communication systems can utilize two types of free space channels: the terrestrial, and the spatial communication channels [60].

The Data Rate (in Bits/sec) of the transmitted signal through the FSO communication channel can be calculated by the following expression [50][55]:

$$DataRate = \frac{1}{n} p_r \tag{3.3}$$

where,

$P_r$: Received power (in photons/sec).

$\eta$: The sensitivity of received power (in photons/bit).

The small-divergence angle $\theta$ between the transmitter and the receiver can be measured in *mrad* unit, which it can be converted to degree unit by the following expression [50][45]:

$$1° \approx 17 m\text{rad} \rightarrow 1\text{mrad} \approx 0.0573° \tag{3.4}$$

The relation between the small-divergence angle and the spot size can be shown in Figure 3.7, it can be expressed by the following expression [50][56]:

$$\theta = D \,.\, S \tag{3.5}$$

where,

$\theta$: The divergence angle (in *mrad*).

*D*: The distance length between the transmitter and receiver (in *km*).

*S*: The spot size (in *meter*).

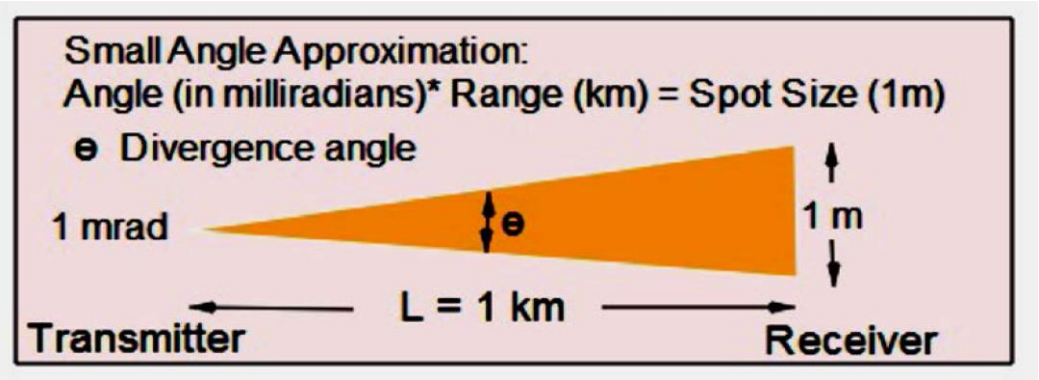


**Figure 3.7.** The relation between small divergence angle and spot [61].

### 3.11 FSO Atmospheric Attenuation

The loss of energy that results from a transmitting light beam transferring through the atmosphere is named atmospheric attenuation. In fact, the signal attenuation caused by atmosphere effects in the FSO communication system is divided into two types: absorption and scattering. All of these phenomena are dependent on environmental and weather factors and they vary with the time. Generally, atmospheric attenuation can be expressed by the following equation from Beer's Law :

$$a = exp\,[\beta L] \tag{3.6}$$

where,

$\alpha$: Attenuation of the atmosphere.

$\beta$: Total attenuation coefficient that be calculated as follows ( in $km^{-1}$) [62]:

$$\beta = \beta_{abs} + \beta_{scat} \tag{3.7}$$

where,

$L$: Transmitter distance from the receiver (in km);

$\beta_{abs}$: Absorption coefficient ( in $km^{-1}$).

$\beta_{scat}$: Scattering coefficient ( in $km^{-1}$).

When photons from the light rays collide with microscopic particles of liquids, water vapor, fog, dust, and more, absorption and scattering attenuation can result. The

major gases that affect atmospheric absorption at infra-red light bands are $O_2$, $O_3$, and $CO_2$. However, the effect of these gases can be reduced to acceptable or negligible values for ranges necessary for limited communication.

Gases that are found in the air, as well as their concentrations, affect the absorption coefficient $\beta_{abs}$. In the spectral transmitting of the atmosphere, the Molecular absorption phenomenon occurs and produces transparent zones, named the atmospheric transmission window. This window has been demonstrated in Figure 3.8. As illustrated in the figure, only some light ray spectrums can enter the atmosphere with negligible losses of energy . As shown in Figure 3.8, at infrared wavelengths near the wavelength 850 nm, the transmission has an opened window and the atmospheric absorption coefficient $\beta_{abs}$ can be neglected in the attenuation calculation due to its negligible value. Therefore, it is possible to consider $\beta_{abs}$=0 [63].

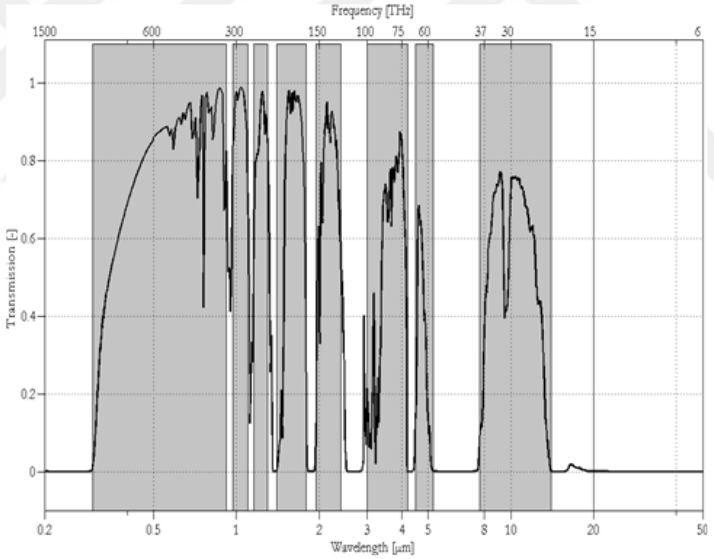


**Figure 3.8.** The models of Rayleigh, Mie, and Non-selective scattering [63].

### 3.11.1 FSO atmospheric scattering

Whenever the light ray intercepted by a particle exists in the atmosphere, some light rays are removed, then re-emitted in a specific solid angle at the particle center. A scattering that stores the wavelength occurs at the scattered light. The three common

types of scattering are: Rayleigh scattering, Mie scattering, and non-selective. The three scattering types have been demonstrated in Figure 3.9.

The characteristic size constant $x_o$ is dependent on the scattering effect, as [64]:

$$x_0 = \frac{2\pi r}{\lambda} \tag{3.8}$$

where,

$r$: aerosol particle size included in atmosphere (in meter) .

$\lambda$: the wavelength of the light spectrum (in meter).

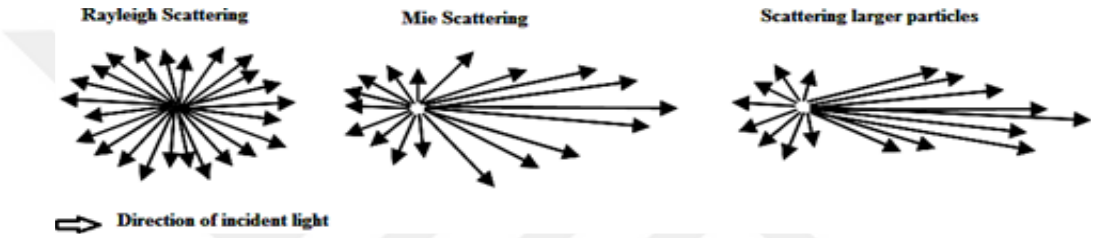


**Figure 3.9.** The models of Rayleigh, Mie, and Non-selective scattering [64].

If $x_o$ is much smaller than one (1), the side lobes will be hidden, and the main back-lobe will be much larger. This is named Rayleigh scattering and is illustrated in Figure 3.9. If $x_o$ is nearly equal to one (1), the back-lobe and the forward-lobe will be symmetrical, which is named Mie scattering. Finally, if $x_o$ is much greater than one (1), a big forward-lobe and very small side-lobes will appear at the particle, which is named non- selective scattering. The total scattering coefficient is given by [66]:

$$\beta scat = \beta_R + \beta_M \tag{3.9}$$

where,

$\beta_M$: Mie scattering coefficient.

$\beta_R$: Rayleigh scattering coefficient.

For infra-red laser FSO applications (such as in this work), Rayleigh scattering can be neglected because it is most prevalent in the ultraviolet to visible wave range [65]. Non-selective scattering, such as the effect of rainfall and some atmospheric turbulence, are not calculated because it randomly occurs at variable concentrations

during the year. The solution to this problem is to increase the output power of the laser diode nearly ten times (at the times when they occur) to substitute the loss of transmitted light energy caused by turbulence [50].

In this work, only Mie scattering has been considered. This is because it has an important effect on the FSO communication system. Therefore, for the mentioned reasons, the total scattering coefficient can be written as follows [66]:

$$\beta_{scat} = \beta_M \tag{3.10}$$

### 3.11.2 Effects of Mie scattering

When the particle diameter is equal or larger than one-tenth of the incoming light beam wavelength, the effect of Mie scattering should be generated. Generally, droplets of fog and haze mostly attenuate the transmitted light ray from Mie scattering effects at the interested wavelengths range (0.35-0.9) μm. The Mie scattering coefficient can be calculated as follows [66]:

$$\beta_M = a_m \, . \, N_m \tag{3.11}$$

where:

$\alpha_M$: the Mie scattering cross-section [$km^2$].

$N_M$: the volumetric density of air particles [$km^{-3}$].

The Mie scattering coefficient also can be calculated using the visibility parameter, this parameter can be easily given by the airport or whether information. Using the visibility parameter, the Mie scattering coefficient can be given as follows [66]:

$$\beta_M = \left(\frac{3.91}{V}\right) . \left(\frac{0.55m}{\lambda}\right) i \tag{3.12}$$

where:

$V$: Visibility (in km).

$\lambda$: Incoming laser wavelength( in μm).

$i$: Distribution of size scattered particles, its value in the range (0.7- 1.6) depending on the visibility conditions as follows [67]:

$$i = 1.6 for V > 50km \tag{3.13}$$

$$i = 1.3 for 6km \leq v \leq 50km \tag{3.14}$$

$$i = 0.585 V^{\frac{1}{3}} for V < 6km \tag{3.15}$$

and the total atmospheric attenuation $\alpha$ can be represented by the following expression [67]:

$$a = exp\ (\beta_m L) \tag{3.16}$$

The total atmospheric attenuation also can be given in (dB), as shown in the following expression:

$$a = 4.3429 \beta_m L \tag{3.17}$$

The ratio of the received signal power to the transmitted signal power is represented by the total attenuation of the link, which can be calculated by the following expression [67]:

$$P_r = P_t \tag{3.18}$$

where,

$P_t$: Transmitted signal power (in dB).

$P_r$: Received signal power (in dB).

$\alpha$: Total attenuation coefficient (in dB).

### 3.12 The Receiver Unit

The role of the receiver unit is to detect the transmitted laser light beam and to translate it to an electrical signal, and then amplify this electrical signal to a suitable level which can be compatible with the input of the microcontroller (2). The receiver unit involves the following parts: the PIN photodiode, Low Noise Amplifier with DC

elimination, Notch Filter, Low Pass Filter, and the Voltage Comparator [43]. Each of these components have been discussed in detail below:

### 3.12.1 Low noise amplifier (LNA)

The duty of this amplifier for our research is to amplify the incoming signal from the PIN photo-detector and minimize the noise as much as possible. The low noise amplifier is an amplifier with very low noise, 0.7 nV/√Hz or lower. A model of low noise amplifier has been illustrated in Figure 3.10. As shown in this figure, the amplifier consists of a Darlington amplifier with two complementary transistors. The two transistors have been connected in common-emitter amplifier mode. The maximum obtained gain from this amplifier is 200. The first transistor is an NPN BC 337, derived by the second PNP transistor BC 559. This amplifier requires supply current of 3 mA, with a supply voltage of 5 Volt. The ratio of R5 to R6 determines the gain of this amplifier. The bandwidth of this amplifier is respectively high, exceeding 1 MHz. There are two main feedbacks in this amplifier. The first feedback is achieved by the resistor R4, while the second is achieved by the resistor R5. The capacitors C1 and C3 are used for DC voltage elimination. The noise of resistor R6 is added to the input noise. The resistors R3 and R6 are also feedback resistors are used to increase the stability of the two transistors [68].

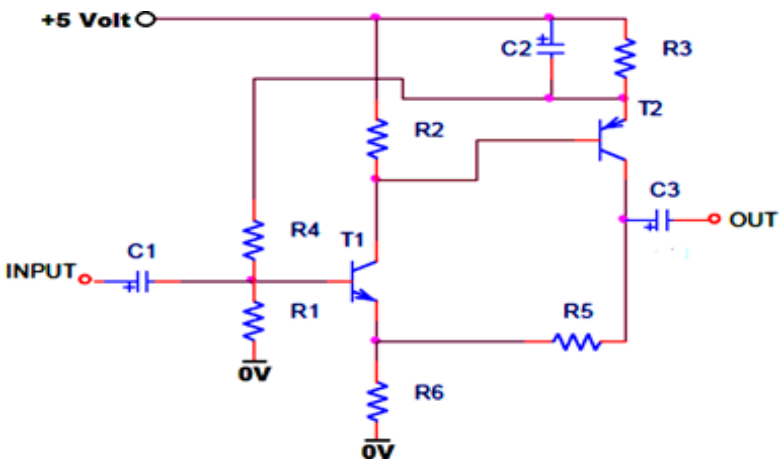


**Figure 3.10.** Circuit diagram of the low noise amplifier [68].

### 3.12.2 The notch filter

The notch filter is used in this work to reject the center frequency (50 Hz) with its narrow bandwidth (59-52 Hz) that is generated by the light sources operating along the main AC 220 Volt. The notch filter passes all frequencies except for a band of frequencies that are called the rejected band. This filter has been shown below.

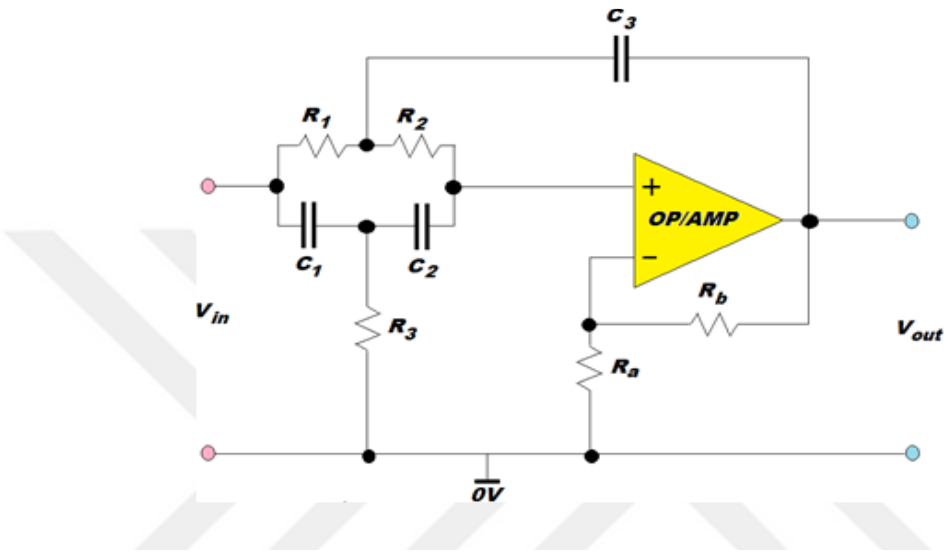


**Figure 3.11.** The notch filter circuit diagram [69].

For $R_1 = R_2 = R$, $C_1 = C_2 = C$, *and* $R_3 = R/2$, $C_3 = 2C$, one can calculate the center cut-off frequency by the following expression [53]:

$$w_c = \frac{1}{R.c} \tag{3.19}$$

and the gain of the operational amplifier can be calculated by [69]:

$$A_v = 1 + \frac{R_b}{R_a} \tag{3.20}$$

Note, that stability requires $A_v < 2$, and the quality factor can be expressed by [69]:

$$Q = \frac{1}{2 - A_v} \tag{3.21}$$

the bandwidth of this notch filter is calculated as follows [69]:

$$B.W = \frac{W_0}{Q} \tag{3.22}$$

### 3.12.3 Low pass filter

The role of this filter is to reject the frequency spectrum that exceeds the maximum used frequency of the proposed optical communication system. This filter passes only the frequency band range (0-$w_c$), where the frequency $w_c$ is the cut-off frequency. The low pass filter has been shown in Figure 3.12 and is called Sallen and Key circuit. This is a second order low pass filter, which consists of a non-inverting operational amplifier (Op-Amp) to provide a positive feedback.

For $R_1 = R_2 = R$, $C_1 = C_2 = C$, the cut-off frequency is expressed as follows [69]:

$$W_0 = \frac{1}{R.c} \tag{3.23}$$

and the gain of the operational amplifier is given as follows [69]:

$$Av = 1 + \frac{R_b}{R_a} \tag{3.24}$$

For good stability, the gain of the operational amplifier $A_v$ must be less than

The Quality factor $Q$ is expressed as follows [69]:

$$Q = \frac{1}{3 - A_v} \tag{3.25}$$

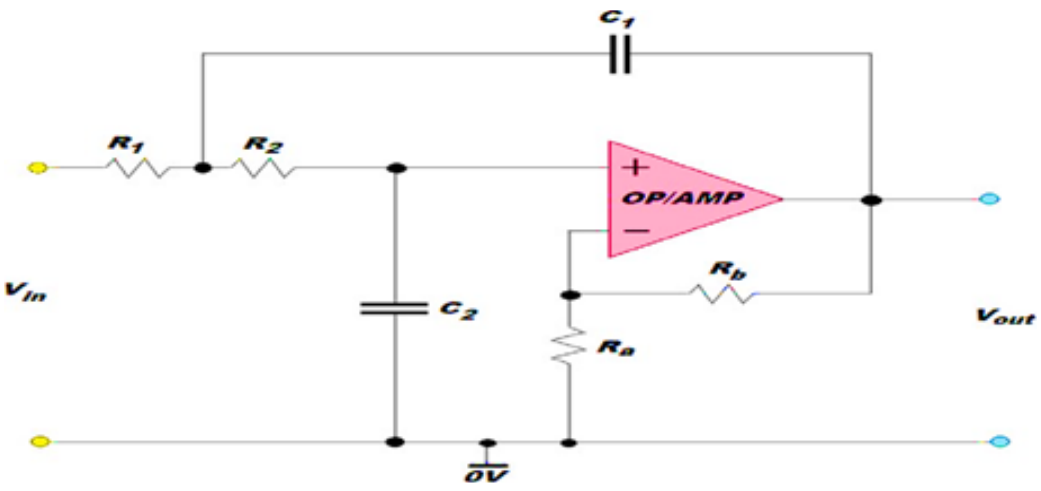


**Figure 3.12.** The low pass filter circuit diagram [69].

### 3.12.4 Voltage comparator

In this work, the main role of this circuit is to reshape the incoming pulses from the low pass filter. This circuit is used for converting the incoming distorted pulses from the output of the low pass filter to pure digital pulses, before directing them to the input of the microcontroller (2). The voltage comparator circuit has been demonstrated in Figure 3.13. The threshold voltage of this comparator is calculated as follows [70]:

$$R_{th} = \frac{R2}{R1+R2}.V_{cc} \tag{3.26}$$

The output signal level depends on the threshold voltage $V_{th}$. When the input voltage value falls below the threshold voltage, the output voltage becomes zero value (LOW level). When the input voltage exceeds the threshold voltage, the output voltage becomes (5) Volts (HIGH level). The main property of the voltage comparator is its high slew rate. The voltage comparator is considered as a high speed operational amplifier circuit with open loop feedback.

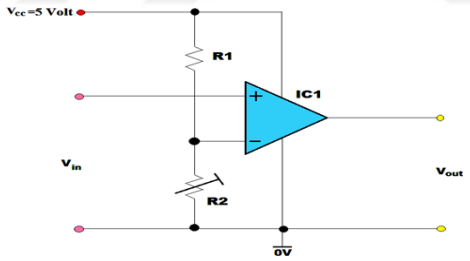


**Figure 3.13.** The voltage comparator circuit using Op-Amp [70].

## 3.13 Back-Propagation Neural Network

Back-Propagation Neural Networks are the most used Multi- Layer Artificial Neural Network (MLANN). They are considered training modules with rules and an optimization method for updating their weights and biases. Figure 3.14 illustrates the configuration of the BP neural network. Generally, BP neural networks consist of three layers: the input layer, hidden layer, and output layer. It is considered a supervised ANN, which means that a target output value should be needed to present the error signal. By succession of the training process, this error signal should be

minimized as much as possible to reach the best result (minimizing the Mean-Square-Error MSE). During this process, an updating should take place on the weights and biases of the input connection of the hidden and output layers. Whenever this error signal (MSE) reaches the minimum value, the training process will stop, and the best output will be presented.

As shown in Figure 3.14, the hidden and output layers are sequentially represented by layers *j* and *k*. The learning rate is represented by the $\eta$ symbol, while *O* represents the output of the network and $V_z$ and $W_y$ represent the weights of input connections of the hidden and output layers. As demonstrated in the same figure, the updating of input connection weights of the hidden layer depends upon 1) the activation function differentiation of the output and hidden layers, 2) the difference between target and actual outputs, and 3) the learning rate. The updating of input connection weighs of the output layer depends upon 1) the activation function differentiation of the output layer, 2) the activation function differentiation of just the related neuron of the hidden layer, 3) the difference between target and actual outputs, and 4) the learning rate [70].

The BP neural network can be trained by several training functions, each having its own characteristics, such as: speed of learning, accuracy, number of training iterations to reach the best result, updating of the learning rate, etc.

The following expression represents the Mean-Square Error of the BP [71]:

$$\text{MSE}=\frac{1}{2}\Sigma n(d-y)^2 \tag{3.27}$$

While the gradient of the MSE can be calculated as follows [71]:

$$g=\frac{\partial(MSE)}{\partial w} \tag{3.28}$$

where:

*MSE*: The Mean Square Error

*n*: The no. of output neuron.

*d*: The desired output vector.

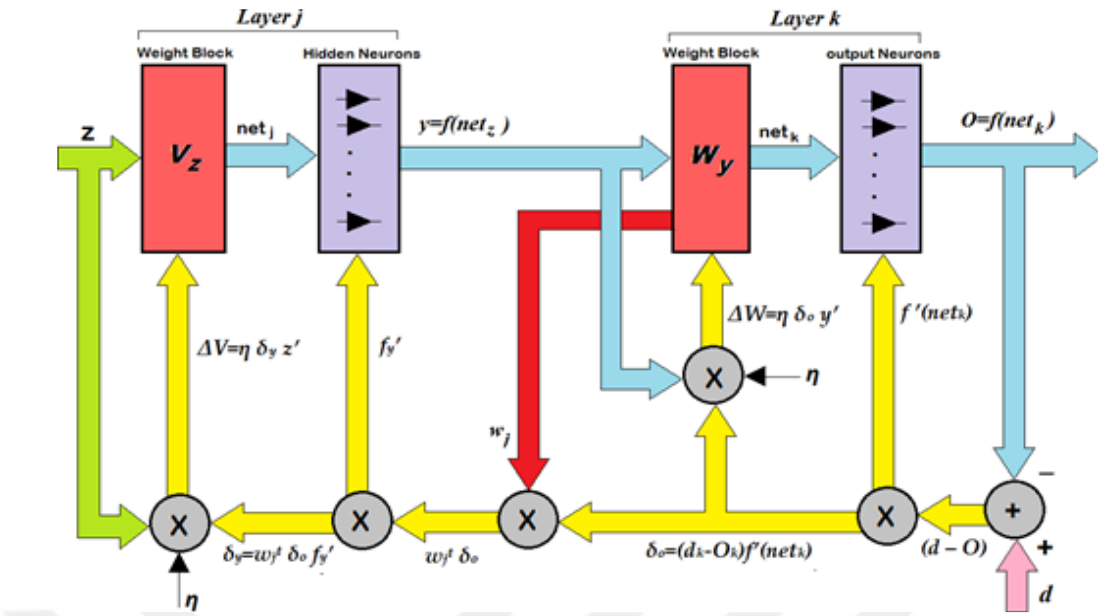


**Figure 3.14.** The block diagram with the details of a typical BP neural[71].

The linear activation function can be used in practical applications because they can be converted to the VHDL code program, which can be saved in FPGA. Several essential activation functions have been shown in Figure 3.15 [72].

| Activation function | Equation | Example | 1D Graph |
|---|---|---|---|
| Unit step (Heaviside) | $\phi(z) = \begin{cases} 0, & z < 0, \\ 0.5, & z = 0, \\ 1, & z > 0, \end{cases}$ | Perceptron variant | |
| Sign (Signum) | $\phi(z) = \begin{cases} -1, & z < 0, \\ 0, & z = 0, \\ 1, & z > 0, \end{cases}$ | Perceptron variant | |
| Purelin | $\phi(z) = z$ | Adaline, linear regression | |
| Satlin | $\phi(z) = \begin{cases} 1, & z \geq \frac{1}{2}, \\ z + \frac{1}{2}, & -\frac{1}{2} < z < \frac{1}{2}, \\ 0, & z \leq -\frac{1}{2}, \end{cases}$ | Support vector machine | |
| Logistic (sigmoid) | $\phi(z) = \frac{1}{1 + e^{-z}}$ | Logistic regression, Multi-layer NN | |
| Hyperbolic tangent | $\phi(z) = \frac{e^{z} - e^{-z}}{e^{z} + e^{-z}}$ | Multi-layer NN | |

**Figure 3.15.** Some non-linear and linear activation functions [72].

### 3.14 Training by Particle Swarm Optimization (PSO)

The PSO technique is an optimization method for finding the best solution for a given problem. As such, one can use PSO to train the back-propagation neural network for updating the weights and biases of the network. In the MATLAB software package, the PSO training process can be executed by using the "trainpso" function. The "groups coordinated behavior" can loosely represent the PSO technique, such as schools of fish or flocks of birds. A given solution for some minimization of a specific problem can be represented by each particle of the PSO model having a virtual position. The position of particles in the PSO model can represent the network's weights and biases values in the neural network situations. The aim of these neural network cases is determining the weights (positions) of the overall network that makes the desired output approaches (or fits) to the actual outputs of the network[73].

An iteration process and a group of particles should be used in PSO. In every iteration, each particle can travel to a new position that resembles a better solution for a given problem. The base of the particle's movement depends on three items: 1) the particle's present velocity and direction, 2) the best location detected at any time by the particle, and 3) the best position detected in the swarm by other particles. Figure 3.17 shows the process of the PSO technique at iteration (0) when the particles are distributed randomly far from the best solution (labeled by a star), and at iteration (N) when the particles are collected around the best solution (labeled by a star).

The updating of the new velocity and location in the PSO technique can be expressed mathematically as follows [74]:

$$v(t+1) = w.v + C_1.R_1\big(p(t) - x(t)\big) + C_2.R_2.\big(g(t) - x(t)\big) \quad (3.29)$$

$$x(t+1) = x(t) + v(t+1) \quad (3.30)$$

where,

$v(t+1)$: The new velocity vector. $x(t+1)$ : The new location vector. $w$ : The inertia weight value.

$c_1$: The local weight.

$c_2$: the global weight.

*x(t)*: The current position vector.

*v(t)*: The current velocity vector.

$r_1$ and $r_2$: The random variable numbers at range (0-1).

*p(t)*: The particle's best position vector.

In fact, the suggested Equations (3.29) and (3.30) are more complex than the update processing. Equation (3.29) represents the updating of the velocity of particles, while Equation (3.30) represents the updating of the particle location. Once the new velocity *v(t+1)* vector has been calculated, it can be utilized for calculating the new particle position vector *x(t+1)*.

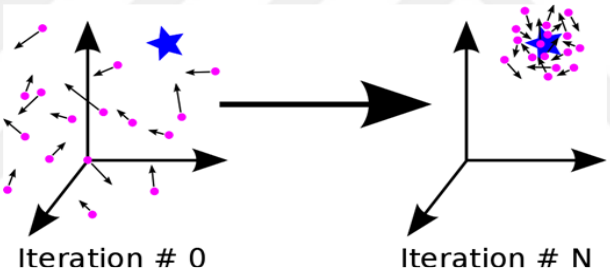


**Figure 3.16.** the PSO process at iteration (0), and iteration (N) [69].

# 4. RESEARCH METHODOLOGY

The purpose of this chapter is to explain in detail the research methods and the methodology implemented for this study. The chapter will first explain all of the choices regarding the research approach, before moving on to the research design and discussing the advantages and disadvantages of the chosen research tools. This will be followed by a discussion on their ability to produce valid results in order to meet the aims and objectives set by this thesis. The chapter then goes on to the data analysis methods which have been used. It concludes with a brief discussion on the ethical considerations and limitations posed by the research methodology, as well as problems encountered during the research.

## 4.1 Research Approach

This dissertation makes use of qualitative research strategy, while implementing the research approach of interpretivism. Willis (2007) defines interpretivism as “an approach which is implemented by the researcher in order to synthesize facts which are derived mainly from secondary sources, and which are qualitative in nature.”

## 4.2 Process of Research Methodology

In this section, we introduce a methodology that has been modeled as a process characterized in steps illustrated in Figure 4.1. The process is characterized by six sequential phases: *identify the problem, Informal Domain Description, Design, Static Verification, Deployment and Runtime Verification; the entire process consists of 12 tasks.*

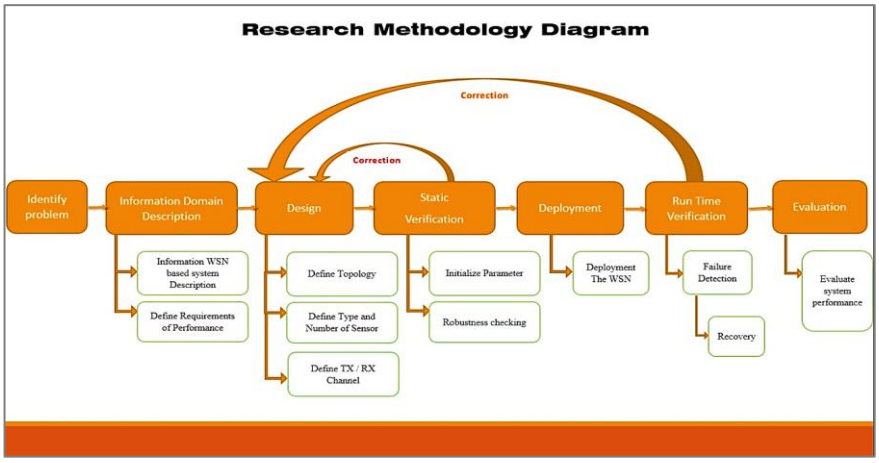


**Figure 4.1.** Research Methodology Diagram.

### 4.2.1 Identify the problem

This section will present the main problem and motivation of this research: air pollution is one of the most harmful agents to the health of people, so pollutant detection and monitoring in an environment has become very necessary. The proposed system has been designed and implemented as an automating intelligent system that detects and monitors $NO_2$ gas, which is considered one of the most dangerous and toxic gases.

Nitrogen dioxide has the following harmful effects on humans:

1. Inhalation of trace amounts can lead to significant damage to the lungs and the occurrence of suffocation and inability to breathe, as well as harm the mucous membranes in the nose and on the eyes [10].

2. When concentrated in the air, it can cause episodes of allergies and poisoning, and eventual death [11].

### 4.2.2 Information Domain Description

#### 4.2.2.1 Informal WSN-based system description

This section will present a description of the proposed system. The practical circuit of the proposed system has been utilized for detecting the output analog signal of the nitrogen dioxide sensor, then converting this analog signal to digital form before transmitting the resulting digital signal to the intelligent system stored in the FPGA.

The reason for converting the analog signal to digital form is that the FPGA only deals with digital signals.

The practical circuit of the proposed system consists of two main parts: the sensor interface unit and the FSO laser communication system. The latter is composed from four main units: the data transmitter, the data receiver, the ON/OFF switching key transmitter, and the ON/OFF switching key receiver.

#### 4.2.2.2 Define the performance requirements

After having defined the application domain, in this task, the performance and dependability characteristics are described. In this system: “We want to guarantee at least 65% of coverage for an area against occurred failure events” and “We want the number of failure events active at the same time to be no higher than half of the total number of sensors.”

The dependability metrics considered in this paper, are:

- *Connection resiliency* represents the number of node failures and disconnection events that can be sustained while preserving a given number of nodes connected to the sink.
- *Coverage* is the time interval in which the WSN can operate, while preserving a given number of nodes connected to the sink.

The computation of these metrics is threshold-based. The threshold expresses the fraction of failed and isolated nodes that the user can tolerate, given its design constraints. For instance, a WSN of 20 nodes and a threshold set to 50% means that, at most, 10 isolated nodes can be tolerated.

### 4.2.3 System Design

This phase includes the design of a WSN defining the topology represented by means of a star topology with the hub node as the center. Since several WSNs are composed of sensors that are in a fixed place (for example in monitoring structural integrity, hospitals, fires, and homes), we focus on static routing topologies that can be

represented by a star topology. Dependability metrics are formalized and number and type of sensors are defined.

#### 4.2.3.1 Define topology

The star topology is considered in design of the wireless sensor network for the proposed system, whereas, in this topology, each sensor node should communicate with the control station via a specific channel and each sensor node has its own energy source. The FPGA receives data from the sensors via the sensor nodes and the communication channels, then these data should be collected and processed by the FPGA to produce a specific decision. A model of star topology wireless sensor network is shown in Figure 4.2. The following wireless communication systems can be utilized to communicate the sensor nodes with the FPGA.

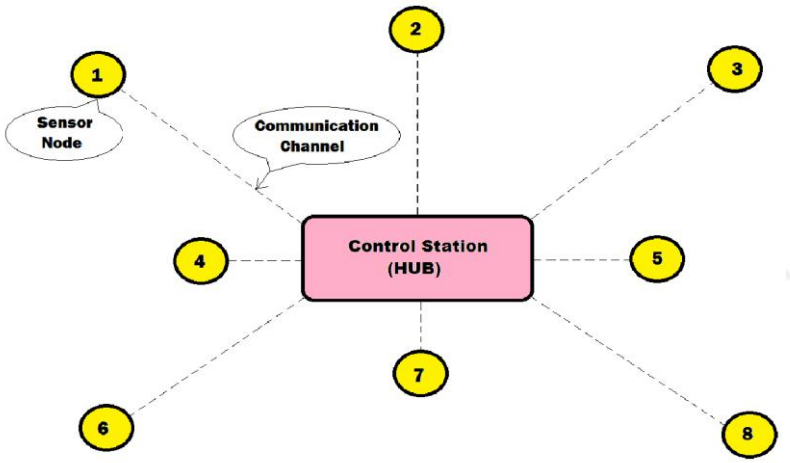


**Figure 4.2.** A model of star topology wireless sensor network [30].

#### 4.2.3.2 Define the type and number of sensor

In this work, we are going to use two Nitrogen dioxide sensors of the MOS (Metal Oxide Semiconductor) type. The tin oxides are mainly used by the MOS sensors, which are utilized as a sensing thick film, they are based and deposited on two variant substrates.

#### 4.2.3.3 Define the communication link

The Infra-Red (IR) Free-Space-Optical (FSO) communication link is considered in this system because it is an optical communication system with free space or atmosphere channel. It consists of three main units: the transmitter, the FSO communication channel, and the receiver. The FSO communication system can be used in terrestrial applications with a link range up to 11km. This distance is sufficient for use in the wireless sensor network. In spatial applications the FSO can be used up to hundreds millions kilometers [60].

### 4.2.4 Static verification

The designed WSN is verified in terms of the defined dependability properties. The verification is static in the sense that the network is not still operating.

The effects of the reasoning, performed on the basis of the defined specifications (general and structural), impact the designed WSN. For instance, if the results of the static verification do not meet the dependability requirements, it could be necessary to modify the topology of the WSN or relax the requirements.

#### 4.2.4.1 Initialize parameters

This task focuses on the choice and initialization of the parameters needed to perform static verification. After the designed topology is loaded, users can set several parameters, such as number of time points, sensors and tolerated failures. Moreover, dependability thresholds are set.

#### 4.2.4.2 Robustness checking

In this task, the WSN design is verified by means of an event-based formal approach. Dependability is evaluated against random sequences of undesired events, useful to identify corner cases and dependability bottlenecks.

### 4.2.5 Deployment

In this phase, the WSN, verified at design time, is actually deployed distributing wireless sensors in one or more environments.

#### 4.2.5.1 Deployment WSN

The aim of this task is to physically deploy the WSN in one or more environments.

#### 4.2.5.2 Runtime verification

Runtime verification is performed on the final running system. The aim is to formally check the running system (the WSN) against some correctness properties. The detection of the violation of a correctness property may be used either to trigger a recovery procedure for the running system or to handle the incorrect status in a safe way. This feature is very useful as long as (although the correctness of the models of the system is granted by formal static verification activities) the quality of the running system may degrade to an unacceptable level, which can be identified just by runtime verification activities.

### 4.2.6 Failure-Detection

In this task, failure events (node failures, disconnections, etc.) that occur in the wireless sensors are detected during the system running and an event is generated in a particular formalism in order to start the computing of the new dependability degree.

#### 4.2.6.1 Recovery

In this task, if the current value of metrics is lower than the desired threshold, the network characteristics (topology, position of the nodes, power of transmission, etc.) can be modified to let the WSN be able to satisfy the required dependability level.

### 4.2.7 Evaluation

In this stage of system, design will evaluate the result of system and it performance to mate the expected result, The goal can be characterized by one or more of three simple questions:

1. “Which one is better?” The evaluation aims to compare the developed systems, with the available system in performance, quality, accuracy, and cost.

2. “How good is it?” This goal aims at the determination of the degree of desired qualities and performance of a finished system.

3. “Why is it bad?” The evaluation aims to determine the weaknesses of a software such that the result generates suggestions for further development. A typical instance of this procedure is a system developing approach using prototypes or a re-engineering of an existing system.

## 5. DESIGN OF PROPOSED BP NEURAL NETWORK

In this chapter, a back-propagation (BP) neural network has been designed and simulated for the proposed intelligent wireless sensor network. The proposed neural network has been utilized as an intelligent system for the proposed sensor network for processing the incoming binary data from the sensor nodes, and then presenting a specific decision according to the incoming data. The proposed neural network has four input lines and four output lines. Two essential activation functions have been applied in the proposed neural network, satlin and satlins, and one training function has been utilized in the proposed neural network, Trainpso.

In fact, the back-propagation neural network is a training method includes an optimization technique performed for determining the best values of weights and biases that minimizes the error signal as much as possible. The error signal can be defined as the difference between the output signal and the desired (target) signal. In this chapter, a contribution has been achieved by using the Particle Swarm Optimization (PSO) method as a training function for determining the best values of input connection weights and biases for the proposed back-propagation neural network, whereas, an optimal result has been obtained by reaching the mean square error to zero value.

### 5.1 Simulation Design Considerations

There are several considerations for designing the proposed simulation system:

1. The outputs of only two sensor nodes should be driven to the input of the proposed simulation system.
2. Each sensor node has two bits output data lines.
3. For the above two considerations, the proposed simulation system must have four input lines, meaning that four neurons should be required for the input layer of the proposed simulation system.
4. The single hidden layer should be used for the proposed simulation system.

5. Four output lines should be driven from the proposed simulation system, meaning that the proposed simulation system has four neurons in its output layer.

### 5.3 Simulation Design Of A BPNN Using Trainpso Training Function

A Back-Propagation Neural Network BPNN can be designed and simulated for the proposed intelligent wireless sensor network depending on the above considerations.

By using the Particle Swarm Optimization (PSO) technique as a training function for the proposed back-propagation neural network, one can get optimal results by reaching the mean square error to zero value. In this contribution, the size of the proposed simulation is four neurons for the input layer, three neurons for the hidden layer, and three neurons for the output layer.

The flowchart of the proposed simulation system is demonstrated in Figure 5.1. In this flowchart, four neurons for the input layer, three neurons for the hidden layer, and three neurons for the output layer have been chosen for the proposed system. The satlins and satlin functions have been utilized as activation functions for the hidden and output layers of the proposed system.

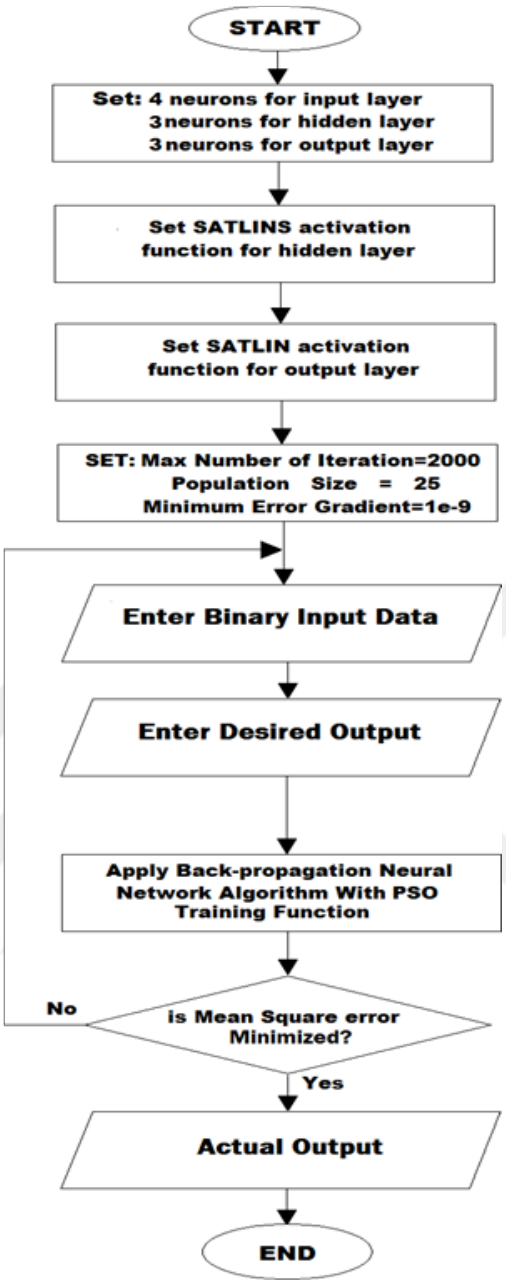


**Figure 5.1.** The flowchart of the proposed simulation system using PSO training function.

Two sensor nodes have been used in the proposed system. The first sensor node has been represented by sensor node (1), and its data should be characterized by (ab). The second sensor node has been represented by sensor node (2), and its data has been characterized by (cd).

In this thesis, the sensor node has been utilized for producing a binary data (represented by two bits) to the proposed simulation system and three output levels have been proposed for the sensor node data as: (01) represented the NORMAL level, (10) represented the CRITICAL level, and finally (11) represented the FATAL level.

When the NORMAL output level of the sensor node was shown, it signified that a low level of the Nitrogen Dioxide gas level (less than 10PPM) had been sensed by the sensor node circuit. When the CRITICAL output level of the sensor node was shown, it signified that a medium level of the Nitrogen Dioxide gas level ((10-50)PPM) had been sensed by the sensor node circuit. Finally, when the FATAL output level of the sensor node was shown, it signified that a high level of the Nitrogen Dioxide gas level (more than 50PPM) had been sensed by the sensor node circuit.

Each sensor node output should be driven to the input of the proposed simulation system. Due to using two sensor nodes in the proposed system, each sensor node must have two bits of output data. Therefore, four input lines should be connected to input of the proposed simulation system. They have been labeled a, b, c, and d

Four output lines (x, y, z, f) have been suggested for the proposed simulation system. The (x, y, z) outputs represented the real output of the proposed simulation system, while the (f) represented the (Fan) output level used for enabling and disabling the (Fan) output signal.

Three output possible levels have been suggested for the proposed simulation system: the output data (1000) represented the NORMAL level, the output data (0101) represented the CRITICAL level, and the output data (0011) represented the FATAL level. Therefore, the overall output of the proposed simulation system has been divided into three levels: NORMAL, CRITICAL, and FATAL.

The non-linear activation function, such as tansig or logsig, cannot be used for the hidden and output layers of the proposed simulation system because the software programs that use such activation functions cannot be translated to VHDL (VHSIC – Very High-Speed Integrated Circuit – Hardware Design Language) code programs,

while the last one can be downloaded into the FPGA (Field Programmable Gate Array).

In this work, the linear activation function satlins and satlin have been sequentially used for the hidden and output layers, where the simulation software that include these activation functions can be downloaded into the FPGA successfully.

The table of the relation between input data patterns and desired output data patterns has been shown in Table (5.1). As shown in this table, the desired output level represents the average of the output levels of the sensor nodes (1) and (2), so when the data of sensor (1) is (ab)=(10) (NORMAL state) and the data of sensor (2) is (cd)=(10) (NORMAL), the desired output is (xyzf)=(1000) (NORMAL state) and the Fan output is in the OFF state; when the data of sensor (1) is (ab)=(11) (FATAL state) and the data of sensor (2) is (cd)=(01) (CRITICAL state), the desired output data is (xyzf)=(0011) (FATAL state) and the Fan output is ON state, and so on.

**Table 5.1.** The relation between the input and desired output data.

| Inputs | | | | Desired Outputs | | | |
|---|---|---|---|---|---|---|---|
| Sensor 1 | | Sensor 2 | | | | | |
| **A** | **b** | **c** | **d** | **x** | **y** | **z** | **f** |
| 1 | 0 | 1 | 0 | 1 | 0 | 0 | 0 |
| 0 | 1 | 1 | 0 | 0 | 1 | 0 | 1 |
| 1 | 1 | 1 | 0 | 0 | 1 | 0 | 1 |
| 1 | 0 | 0 | 1 | 0 | 1 | 0 | 1 |
| 0 | 1 | 0 | 1 | 0 | 1 | 0 | 1 |
| 1 | 1 | 0 | 1 | 0 | 0 | 1 | 1 |
| 1 | 0 | 1 | 1 | 0 | 1 | 0 | 1 |
| 0 | 1 | 1 | 1 | 0 | 0 | 1 | 1 |
| 1 | 1 | 1 | 1 | 0 | 0 | 1 | 1 |

Utilizing the previous mentioned considerations and using the flowchart of the proposed simulation system, one can write a suitable program using the MATLAB software package, finished by the instruction {**gensim(net)**}, which is utilized to generate the proposed system block.

By executing the proposed software program, a system block has been generated. It has four input lines and four output lines. The input lines have been represented by: a, b, c, d, while the output lines have been represented by: x, y, z, f. The input lines a and b represented the output of the sensor node (1), while the input lines c and d represented the output of sensor node (2). The (x) output of the system block represented the (NORMAL) state of Nitrogen Dioxide gas concentration level, while the (y) output of the system block represented the (CRITICAL) state of NO gas concentration level, the (z) output represented the (FATAL) state of NO gas concentration level, and the (f) output signified the (FAN) output state, which is activated when the output level activated is at (y: CRITICAL or z; FATAL). The proposed system has been illustrated in Figure 5.3.

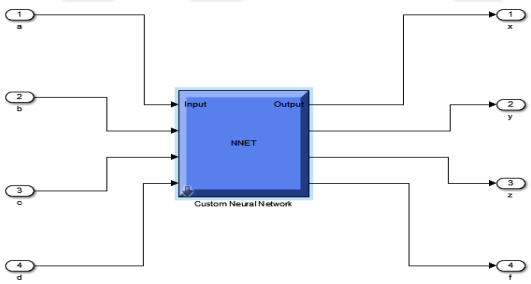


**Figure 5.2.** The proposed simulation system block.

By clicking on the (look under mask) option of the proposed simulation system block, another system block will be presented on the screen of the computer, as demonstrated in Figure 5.4.

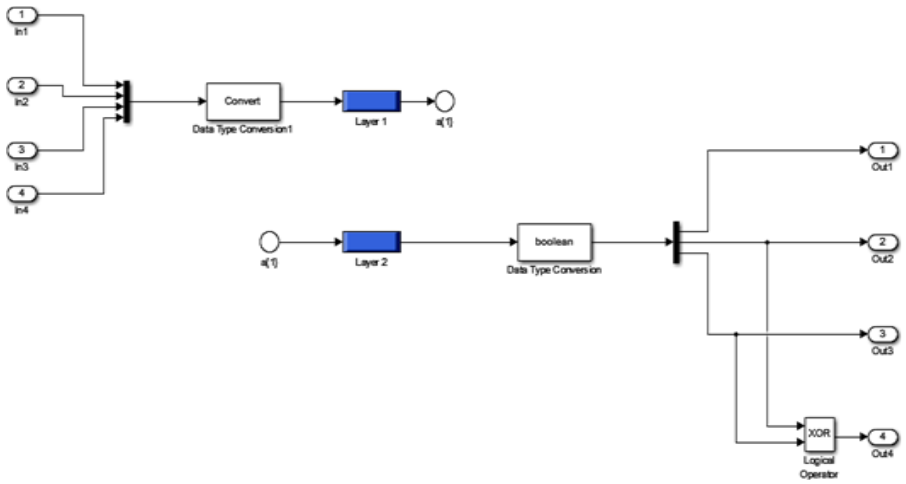


**Figure 5.3.** The detailed system block of the proposed simulation system.

As shown in Figure 5.3, there are two layers in this system block: layer (1) and layer (2). Layer (1) represents the input and hidden layers, while the layer (2) represents the output layer. As shown in this figure, there are four input ports connected at the input of the proposed simulation block, and there are four output ports connected at the output of the same system block. A multiplexer and demultiplexer had been connected in the proposed simulation block. The multiplexer has four inputs and single output, which were connected at the input of the proposed simulation block, while the demultiplexer has single input and four outputs, which were connected at the output of the proposed simulation block. The detailed proposed simulation block system has been illustrated in Figure 5.4.

A four input and single output multiplexer has been connected at the input of this blocks system, while a single input and four output demultiplexer has been connected at the output of the same system. In fact, the proposed design is related with binary type data (Boolean data), while the proposed generated block system is related with Double type data which cannot be converted to Boolean data. Therefore, the second type of data has been converted from Double data to Fixdt data for each element of the proposed system. When using the MATLAB software package, the Fixdt type data can be converted to Boolean data that can be used in the proposed simulation of this work.

Two data type converters had been connected to the proposed blocks system. One was connected between the multiplexer and the input of the proposed blocks system that converts the Boolean data type to Fixdt data type. The other data type converter was connected between the output of the proposed blocks system and the demultiplexer, and it converts the data type from the Fixdt to Boolean data.

By clicking on layer (1), another block system is presented on the screen of the microcomputer, which represents the input and hidden layer. This is shown in Figure 5.5.

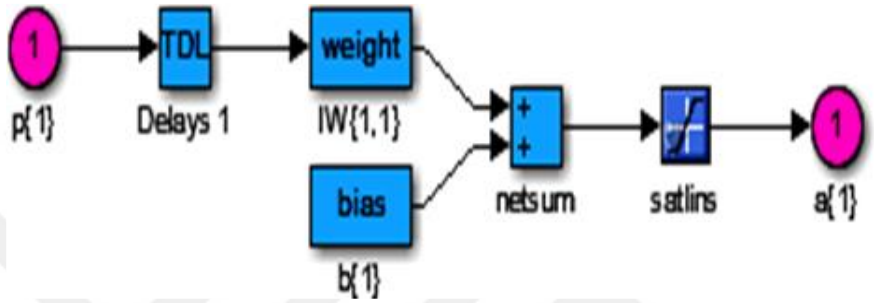


**Figure 5.4.** Internal blocks system of the layer (1) of the proposed.

The block of p{1} has been used to represent the input layer of layer (1), while b{1} block has been used to represent the input biases of the hidden layer of layer (1) and the block of IW{1,1} has been used to represent the input connection weights of the hidden layer of layer (1). The netsum block was used to represent the summation of multiplication of the weights and biases with the input data of the hidden layer of the layer (1). As shown in Figure 5.5, the satlins function has been used in this layer (1).

By clicking on the weight block of layer (1), another block system is presented on the screen of the microcomputer shown in Figure 5.6. As shown in this figure, there are three neurons in this layer (hidden layer) of the proposed simulation system.

By clicking on layer (2) of the blocks system of Figure 5.5, another blocks system is produced on the screen of the microcomputer, as shown in Figure 5.7. Layer (2) has been used to represent the output layer of the proposed simulation system. As shown in Figure 5.7, the LW{2,1} has been used to represent the input connections weights of the output layer of the proposed system, while the b{2} block has been used to represent the input connections biases of the same layer. The netsum block has been used to represent the result of multiplying the weights and biases with the output data

of the layer (1) (hidden layer) of the proposed system. From the Figure 5.7 one can see the satlin function has been used in this layer as an activation function for the same layer (output layer), whereas the configuration of the satlin function has been illustrated in the same figure.


**Figure 5.5.** The internal blocks system of the weight block of the layer (1).

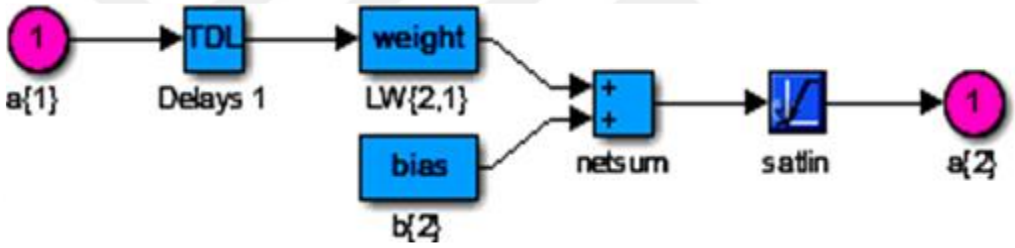


**Figure 5.6.** The internal blocks system of the layer (2) of the proposed simulation system using PSO training function.

By clicking on the weight block of Figure 5.7, another block system is produced on the screen of the microcomputer, as shown in Figure 5.8. As seen from this figure, this layer (output layer) consists of three neurons.

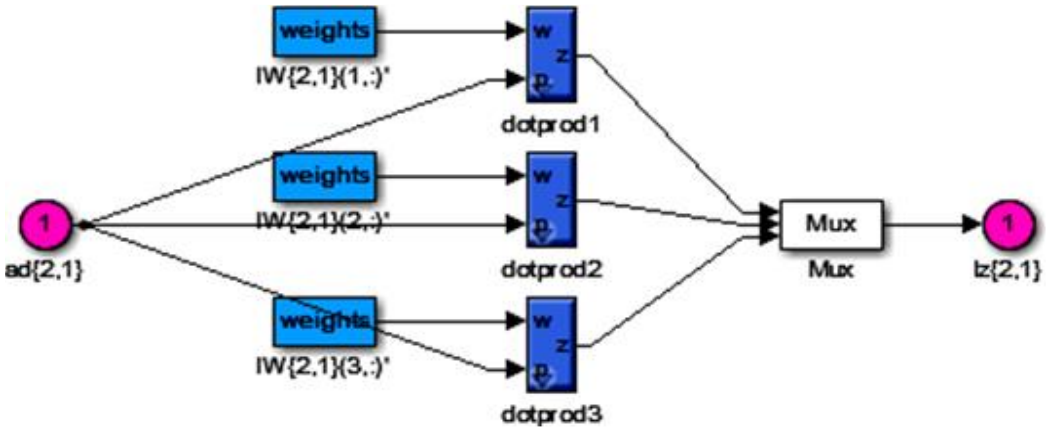


**Figure 5.7.** The internal blocks system of the weight block of layer (2) using PSO training function.

The results of executing these proposed simulation systems have been discussed in detail in the next section.

### 5.4 Output Results Using Trainpso Training Function

After executing the proposed simulation software using the particle swarm optimization training function, a primary result window has been presented on the screen of the computer, as shown in Figure 5.8.

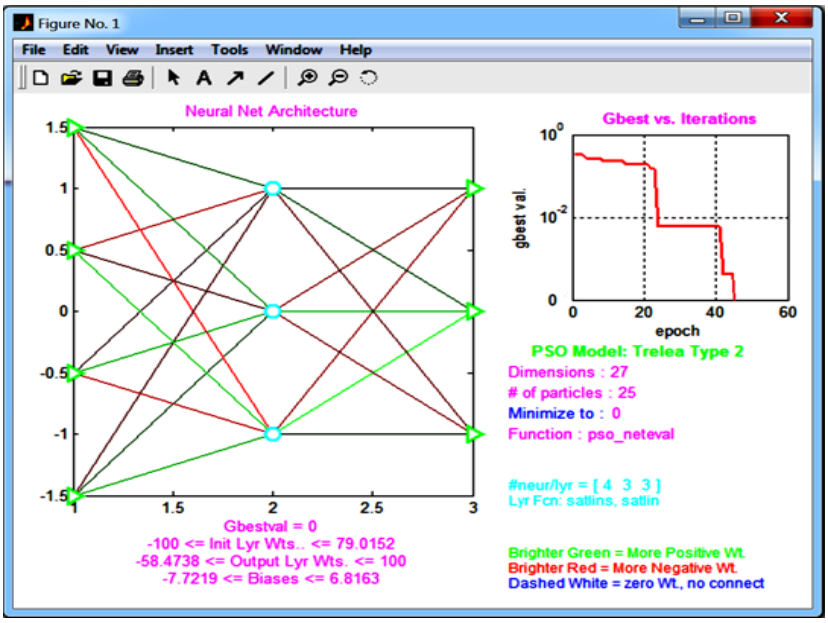


**Figure 5.8.** First output results using trainpso training function.

At the left side of this figure, the network connection has been presented of the proposed simulation system. One can see from the network connection that there are four neurons in the input layer, three neurons in the hidden layer, and three neurons in the output layer. At the right side of the same figure, one can see the relation between the Get best value (Gbest val.) with the number of epochs (iterations). The Gbest value represented the mean square error of the proposed system. As shown in this figure, one can see that the mean square error had reached the zero value at epoch 46, which signified the optimal result with this faster training method. Therefore, one can conclude that the training by the particle swarm optimization is the fast training method with 46 iterations for presenting the optimal result of zero mean square error using three neurons in the hidden layer, which was the least number of neurons used in the hidden layer for the proposed simulation system.

Another result has been presented in the left side of Figure 5.8. The first result is the input connection weights of the hidden layer, where these weights had varied from (-100) to (+79.0152), the input connection weights of the output layer had varied from (-58.4738) to (+100), and the biases had varied from (-7.7219) to (+6.8163).

Another piece of information has been presented in Figure 5.8 is that the first result is the value of the dimensions which was (27), while the number of used particles was (25). Each of these particles had 21 solutions, where each solution represented an individual connection weight of the proposed simulation system.

One can see from the right side of the Figure 5.8 that the Gbest val. (mean square error) had varied non-uniformly and non-linearly with progression of the iterations (epochs) and there is a rapid decrease of the mean square error near epochs 24, 42, and 46, which supports the presented optimal results.

Another result window using the trainpso training function has been presented in this work and is shown in Figure 5.9.

As shown from left this figure, the relation between the Gbest val. (the mean square error) vs. the no. iterations has been presented for another training test, which has been mentioned in Figure 5.9.

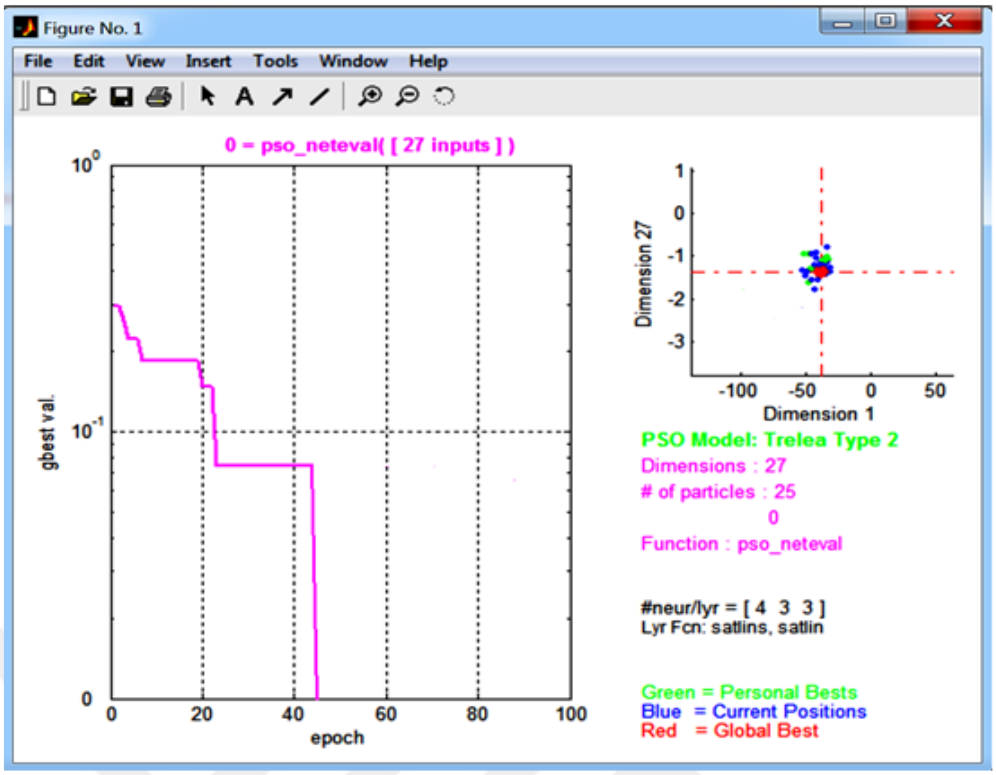


**Figure 5.9.** The second output results using trainpso training function.

At the right side of Figure 5.9, the searching zone (space) has been presented between the dimension 1 (the x- axis) and the 27 dimensions (the y-axis). The intersection point of the red dashed lines has represented the best location of solution (best solution of weights). One can see from this figure that the particles of the proposed system had moved toward the direction of the best solution, which is the intersection of the red dashed lines. As mentioned before, each particle had a single solution for the weights of the proposed simulation system.

## 6. DESIGN OF PROPOSED PRACTICAL CIRCUIT

The practical circuit of the proposed system has been utilized for detecting the output analog signal of the Nitrogen Dioxide sensor, converting this analog signal to digital form, and then transmitting the resulted digital signal to the intelligent system that stored in the FPGA. The reason the analog signal must be converted to digital form is that the FPGA only deals with digital signals.

The practical circuit of the proposed system consists of two main parts: the sensor interface unit and the FSO laser communication system. The latter is composed from four main units: the data transmitter, the data receiver, the ON/OFF switching key transmitter, and the ON/OFF switching key receiver.

The role of the data transmitter unit is transmitting the data of the sensor to the data receiver unit, while the role of the data receiver unit is receiving the data from the data transmitter unit and introduce it to the input of the intelligent system that stored in the FPGA. The role of the ON/OFF switching key transmitter is transmitting the ON/OFF switching key pulse of the intelligent system to the ON/OFF switching key receiver. The role of the ON/OFF switching key receiver is receiving the ON- OFF switching key pulse from the ON/OFF switching key transmitter and then sending it to the relay switching element that used for switching ON and OFF the power supply terminal to the supply the feeding terminal of the data transmitter unit.

### 6.1 Practical Design Requirements

There are several requirements that must be considered when designing the proposed practical circuit:

1- Two Nitrogen Dioxide gas sensors should be used and connected.

2- The analog generated signal of each sensor should be converted to three binary levels. Each binary level is composed of two bits ((ab)and(cd)), where the first is (10), the second is (01), and the third is (11).

3- The binary digit (10) represents the NORMAL level, while the binary digit (01) represents the CRITICAL level and the binary digit (11) represents the FATAL level.

4- Two communication systems must be installed between the two sensors and the FPGA that stores the proposed intelligent system.

5- Each communication system involves two FSO laser communication links.

6- The FPGA has four data input lines (a,b,c,d) and four data output lines (x,y,z,f).

7- The x output represents the NORMAL level, the y output represents the CRITICAL level, the z output represents the FATAL level, and the f output represents the FAN state.

8- TTL (Transistor Transistor Logic) ICs should be used in this design.

### 6.2 Proposing of a novel A/D Converter Circuit

The circuit which is considered is the second contribution for the proposed work, and it is considered a new method of a A/D conversion. This proposed method has been called Pulse-Period Coding A/D conversion. In this conversion method, each analog input sample is translated to only single pulse with a specific width, which makes the conversion faster than other conventional methods.

Simply, the concept of the new proposed A/D converter circuit is the conversion of the analog input signal to a pulse with a specific period related to level of the entered analog input signal. For example, the 1 volt input signal is converted to a pulse with 1 msec, the 2 volt of the input signal is converted to a pulse with 2msec, and so on. Then this pulse converted to binary output data. This process is demonstrated at the block diagram of Figure 6.1.

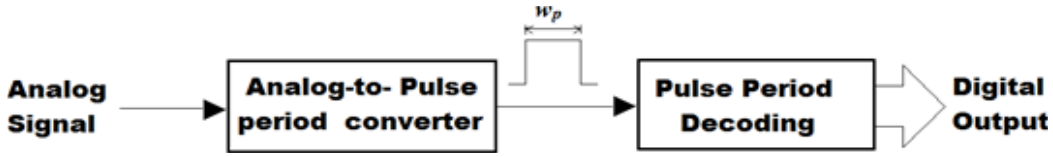


**Figure 6.1.** The block diagram of the new proposed A/D converter circuit.

The analog input voltage is translated to a pulse that has a specific duration using the analog-to-pulse period converter. Then this pulse period is translated to a binary number using the pulse period decoder.

Using the Low Power shotkky technique TTL (Transistor-Transistor-Logic) for the integrated circuits, one can obtain a minimum conversion time of nearly 30 nsec and a maximum conversion time of nearly 2.57 μsec. One can also produce a faster conversion time using faster logic integrated circuits such as Advanced Shotkky TTL ICs [72].

This new proposed A/D converter circuit has been applied in the proposed work. The output analog signal of the sensor has been converted to a laser pulse at the laser transmitter unit. Then this generated pulse has been transmitted to the laser receiver unit. After, this pulse has been translated to a binary number using the pulse period decoder of the laser receiver unit. Finally, this generated binary number has been driven to the input of the FPGA that stores the intelligent system.

Using the proposed A/D converter circuit in the proposed intelligent wireless sensor network, the transmitted signal is considered only a single pulse (single bit) with a specific duration that depends on the value of output voltage of the $NO_2$ gas sensor. Therefore, the probability of error is occurred only on a single bit, whereas the probability of error of the related or traditional wireless sensor networks is performed on multi-bits or pulses (usually 8-bits). It then stands to reason that the probability of error of the proposed transmission technique is much less than traditional WSN systems due to the transmission of only a single bit for representing each character.

In this work, the output signal of the $NO_2$ sensor has been converted to a pulse period using four comparators, a timer, AND and OR gates, and three mono-stable multi-vibrators within the data transmitter unit. The generated pulse period has been converted to a binary number using two one-shot-to circuits, a binary counter, latch,

and timer within the data receiver unit. The overall process of the new proposed A/D converter circuit has been discussed in detail in the next section.

### 6.3 Design of The Proposed Practical Circuit

As shown in Figure 6.2, the proposed practical circuit is composed from two main parts: the sensor interface unit and the FSO laser communication system. The latter of which is composed of four essential units: the data transmitter, data receiver, ON/OFF switching key transmitter, and ON/OFF switching key receiver units.

### 6.4 Design of The Data Transmitter Unit

The data transmitter unit consists of the analog-to-logic level converter, pulse period coder, and laser transmitter parts. The data receiver unit consists of laser receiver and pulse period decoder parts. The ON/OFF switching key transmitter contains of a fixed period pulse generator and the laser transmitter.

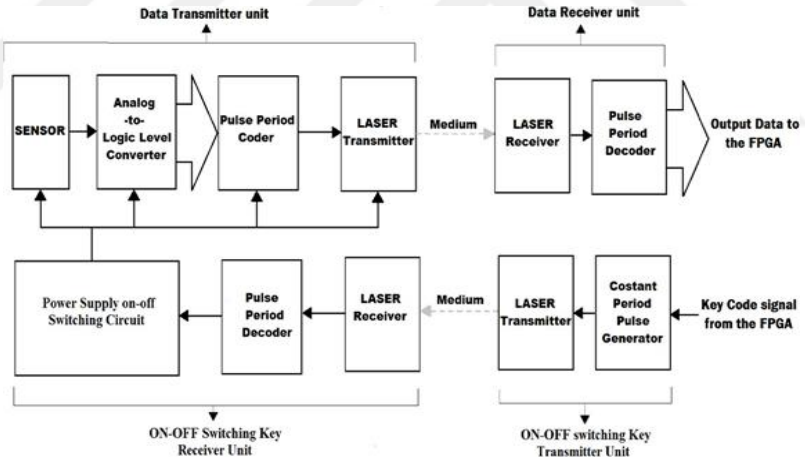


**Figure 6.2.** The block diagram of the proposed practical circuit.

The ON/OFF switching key receiver consists of a laser receiver, pulse period decoder, and the power supply ON/OFF switching circuit parts. The complete circuit diagram of the data transmitter unit has been illustrated in Figure 6.3.

As shown in this figure, the sensor's heater has been supplied with a +5 Volt power supply. The output terminals of the sensor (A, B) have been tied to the input of the analog-to-logic level converter, which is one of the main elements of the new

proposed A/D (analog-to-digital) converter system. The output voltage of the $NO_2$ gas sensor is in the range (0-1) Volt when the concentration of the Nitrogen Dioxide gas is in the range of (0-10) PPM (Parts Per Million), which represents the NORMAL state. The output voltage of the same sensor is in the range of (1-4) Volts when the concentration of the $NO_2$ gas is in the range (10-50) PPM, which represents the CRITICAL state. The output voltage of the sensor is more than 4 Volts when the concentration of the $NO_2$ gas is more than 50 PPM, which represents FATAL state. There are two thresholds voltages that have been supplied at the input of the comparator: $IC_1$, $IC_2$, $IC_3$, and $IC_4$. The first threshold voltage is 1 Volts, the second is 4 Volts.

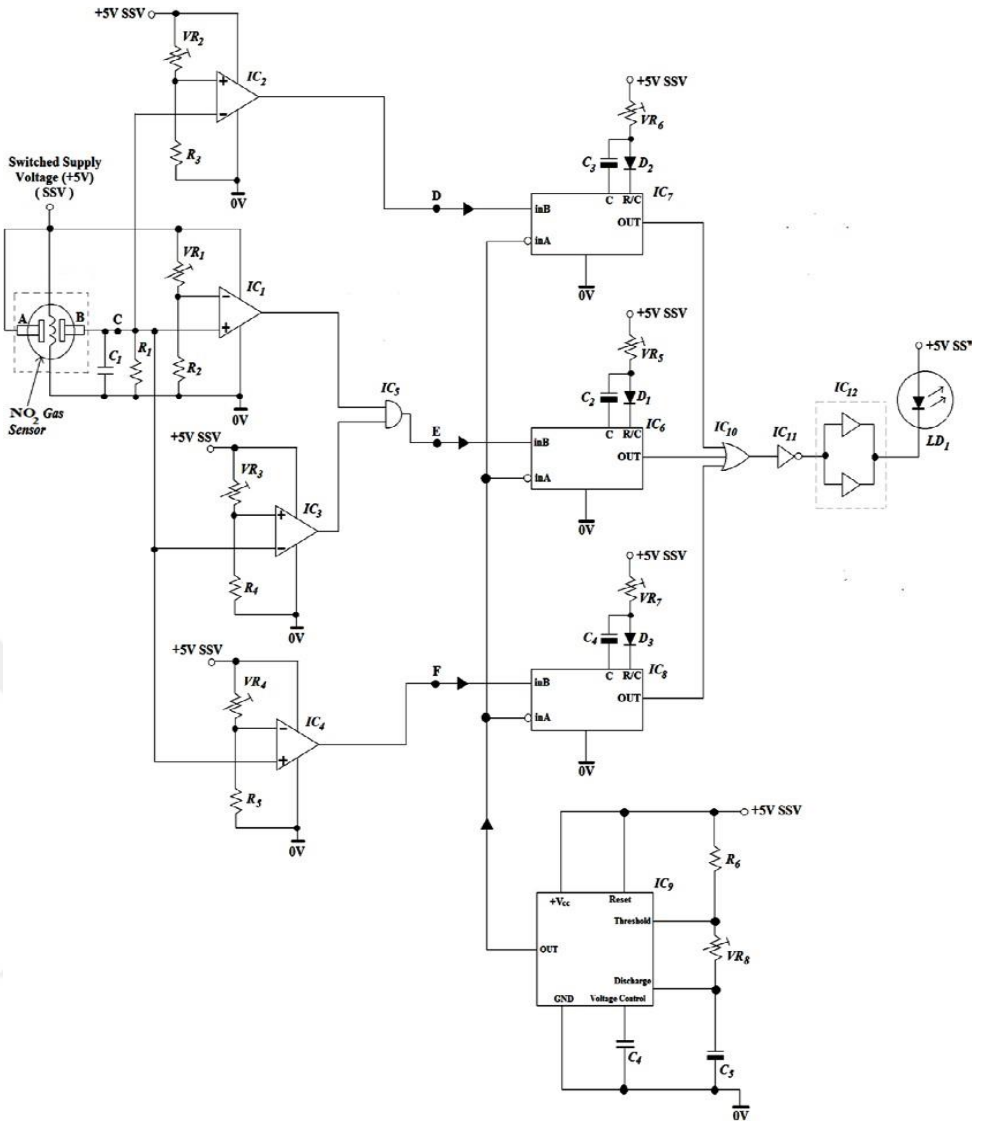


**Figure 6.3.** The complete circuit diagram of the data transmitter unit.

As illustrated in Figure 6.3, $IC_1$, $IC_2$, $IC_3$, and $IC_4$ are type LM 393 analog comparator integrated circuits. $C_1$ is a capacitor used for high frequency noise rejection. The comparator $IC_2$ has a threshold voltage 1 Volt adjusted by the resistor $VR_2$, which is used for producing a HIGH level signal as its output only when the sensor output voltage is in the range of (0-1) Volts, which represents NORMAL level.

The state diagram of the proposed data transmitter unit is shown in Figure 6.4. This figure shows that the synchronization among the main signal started with the output of the $NO_2$ gas sensor for three cases (NORMAL, CRITICAL, and FATAL) and finished with the output of the OR gate $IC_{10}$.

The comparator $IC_4$ has a threshold voltage of 4 Volts adjusted by the resistor $VR_4$, which is used for producing a HIGH level signal as its output only when the sensor output voltage more than 4 Volts for FATAL state. The window comparator is composed of the integrated circuits $IC_1$, $IC_3$, and $IC_5$. They have threshold voltages between 1 and 4 Volts, which is adjusted by the variable resistors $VR_1$, $VR_3$ to produce a HIGH level signal at the output of the AND gate $IC_5$ type SN74LS08 only when the output voltage of the sensor is in the range of (1-4) Volts, which represents the CRITICAL state.

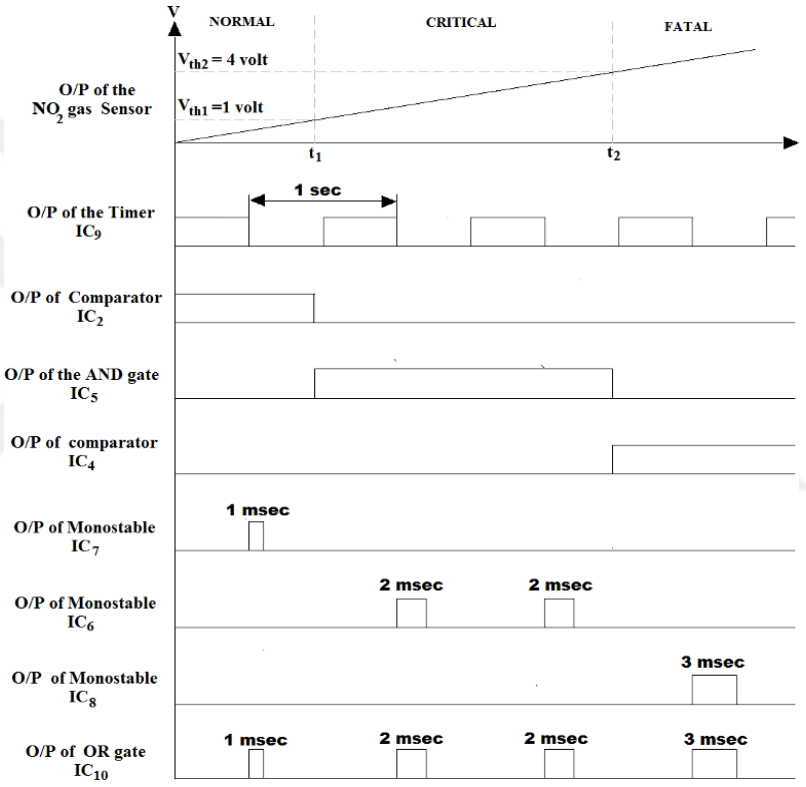


**Figure 6.4.** The state diagram of the data transmitter unit.

$t_{p6} = (0.28) \times 100 \times 10{-}9 \times VR_5 = 2 \times 10{-}3\ sec$

So,

$VR_{5=}\ 71.428\ k\Omega$

and for $IC_7$, the required value for $VR_6$ can be determined as follows:

$t_{p7} = (0.28) \times 100 \times 10{-}9 \times VR_6 = 1 \times 10{-}3\ secF$

So,

$VR_{6=}\ 35.714\ k\Omega$

and for $IC_8$, the required value for $VR_7$ can be determined as follows:

$t_{p8} = (0.28) \times 100 \times 10{-}9 \times VR_7 = 1 \times 10{-}3\ sec$

So,

$VR_{7=}\ 107.143\ k\Omega$

one can select a standard variable resistor 200kΩ for $VR_5$, $VR_6$, $VR_7$.

Note that $IC_6$ is ignited by the output of the window comparator ($IC_1$, $IC_3$, and $IC_5$) at point E, while $IC_7$ is ignited by the output of the comparator $IC_2$ at point D, and $IC_8$ is ignited by the output of the comparator $IC_4$ at point F. The Timer $IC_9$ type NE555 is used to enable the integrated circuits $IC_6$, $IC_7$, and $IC_8$ at the HIGH state of its output frequency. $IC_{10}$ is a 3-input OR gate IC type SN74HC4075 used for summing the outputs of the integrated circuits $IC_6$, $IC_7$, and $IC_8$ that is driven to the input of the Inverter $IC_{11}$ type SN74LS04 to produce the required pulse signal for the Buffer $IC_{12}$ type SN7407, which is used as a modulator and driver for the infra-red laser transmission. There are two Buffer gates, which are $IC_{12}$ type SN7407, that are connected parallel to produce an 80 mA load current to drive the laser diode $LD_1$ type S638505D that has maximum operating current equals to 40 mA. Figure 6.5 shows the practical implementation of the IR laser transmitter circuit.

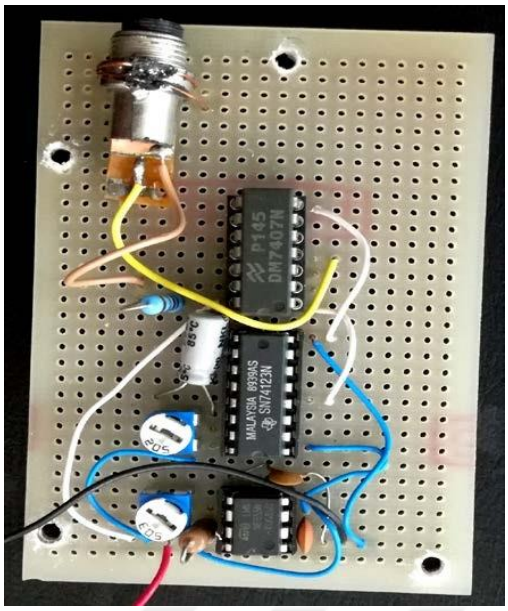

**Figure 6.5.** The practical IR laser transmitter circuit.

$C_5$=100µf, $R_6$=10kΩ, so one can calculate the value of the variable resistor $VR_8$ as follows using the frequency law of the IC NE555:

$$f\frac{1.44}{\big((10*10^3)+2vr8\big)100*10^{-6}}=1Hz$$

So,

$VR_{8=}$ 2.215 $k\Omega$

one can use the standard value of variable resistor 5kΩ for the variable resistor $VR_8$.

The two Buffer gates of $IC_{12}$ are used as parallel connected drivers for the laser diode $LD_1$, which is considered a modulator IC. This modulator IC uses the ON/OFF keying (or Direct intensity) modulation technique to modulate the output pulses of the Inverter $IC_{11}$ with the infra-red laser light generated by the laser diode $LD_1$. The type of laser diode used in this unit is S638505D, which can deliver less than 5mW of infra-red light with wavelength 850nm. Practically, this laser diode can deliver a power of 4.8 mW, as has been measured by the optical power meter device.

### 6.4.1 Calculation of path losses for the laser communication link

The block diagram of the proposed IR laser communication system has been illustrated in Figure 6.6, which consists of three main parts: the IR laser transmitter, The FSO channel, and the IR laser receiver. In this section, the calculation of the path losses and some other parameters has been performed for the proposed laser communication link using some expressions from chapter two to neglect the effects of absorption and Rayleigh scattering attenuation due caused by using the intra-red laser light wavelength with opened window transmission. The scattering losses such as rain, dust, haze, and snow have been neglected due to their random occurrence with variable concentrations during the year. In this design, there are several important assumptions should be considered, such as:

The link range = 50meters.

The laser beam wavelength = 850nm(infra-red band).

The visibility = 10km.

From the Equation (3.15), the exponent variable $i$=(1.3).

One can apply Equation (3.13) to calculate the Mie scattering coefficient $\beta_M$ as follows:

$$\beta_M \left(\frac{3.91}{10}\right)\left(\frac{0.55 * 10^{-6}}{850 * 10^{-9}}\right)1.3$$

$$\beta_M = 0.222\frac{1}{km}$$

So, the total atmospheric attenuation α can be calculated using Equation (3.18) as follows:

$\alpha$ = 4.343 × 0.222 × 0.05

$\alpha$ = 0.0482 $d$B

Using the photodiode type TL 100 PIN with a divergence angle of 1 mrad, the resulted spot size ranged from 50 meter to 5 cm, referring to Equation (3.6). Thus, a

convergence lens with an aperture diameter of 5cm should be used at the receiver side, located at its focal length from the PIN detector face, and an IR filter should be used and located at the receiver side, after the convergence lens but before the laser PIN detector, that passes only the infra-red light beam spectrum to the PIN detector. Now for calculating the geometric loss, assume the following points:

$P_r = -23.188 - 0.0482 = -23.236\ d\mathrm{B}$

And,

$P_r = 4.747 \times 10{-}3\ W\mathrm{aa}t$

Figure 6.7 shows the proto-type of implementation of 50 meter FSO system

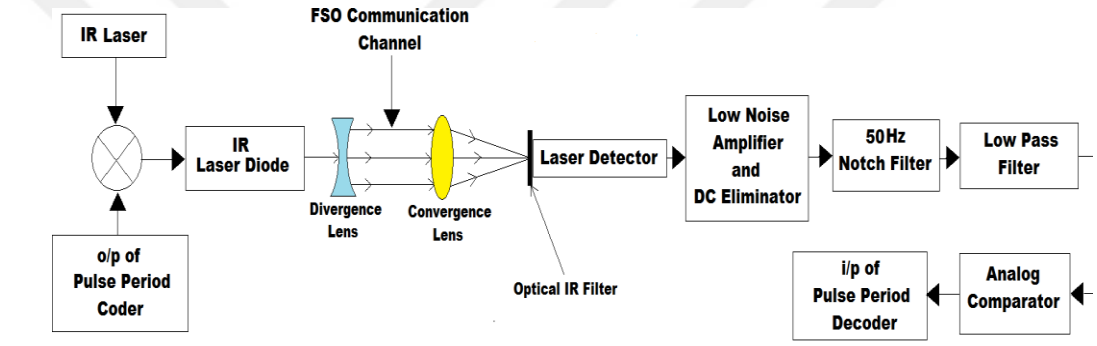


**Figure 6.6.** The block diagram of the proposed IR laser communication system.

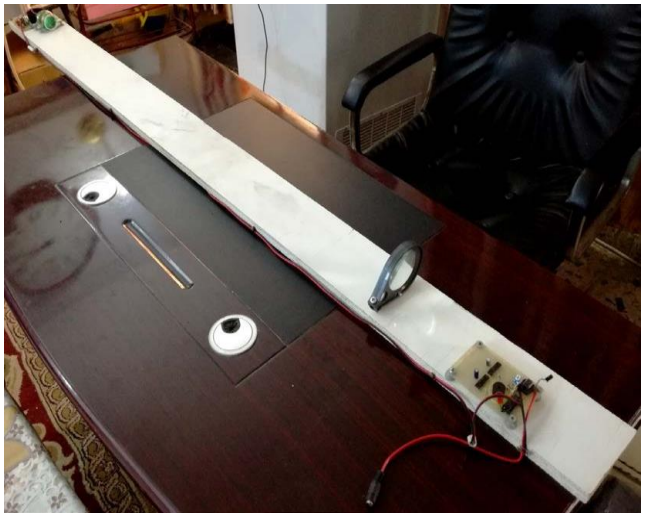

**Figure 6.7.** The practical prototype of the 50 meter laser FSO communication link.

### 6.4.2 Design of the data receiver unit

This unit is responsible for detecting the laser pulses from the data transmitter unit and then decoding them to binary data to be driven to the input of the intelligent system stored in the FPGA.

This unit consists of two main circuits: the laser pulse receiver, and the pulse period decoder. The design of them has been performed as follows:

#### 6.4.2.1 Design of the laser data pulse receiver

This receiver consists of five main parts: the laser pulse detector, low noise amplifier, notch filter, low pass filter, and the voltage comparator.

The laser pulse detector includes photodiode PD1, which was connected in a series with a variable resistor VR9 tied to the +5 Volt power supply. this circuit has been illustrated in Figure 6.8.

If a 100kΩ standard value of variable resistor is used for VR9, then one can calculate the maximum AC peak-to-peak output voltage driven from the VR9 that connected to the input of the low noise amplifier.

The photodiode used in this circuit is type TIL 100, which is a PIN photodiode. Its data sheet has been presented in Appendix A. Using the information of data sheet, the minimum voltage presented across the VR9 can be calculated as follows:

$$V_{out(min)} = \left(I_{ph(min)} * VR_9\right)$$

$$(50 * 10^{-9} * 3860)$$

$$V_{out(min)} = 0.193mV$$

and the maximum output voltage across the VR9 can be calculated as follows:

$$V_{out(max)} = \left(I_{ph(max)} * VR_9\right)$$

$$(10 * 10^{-6} * 3860)$$

$$V_{out(max)} = 38.6 * 10^{-3}Volt$$

so, the maximum peak-to-peak output voltage can be obtained across the VR9 is:

$$V_{out(p.p)max} = 0.0386 - 0.000193$$

$$V_{out(p.p)max} \approx 38.4 \times 10^{-3}$$

which is the practically measured peak-to-peak output voltage across the VR9 when the IR PIN detector is directly located in front of the face of the laser diode that transmits power at 4.8 mW.

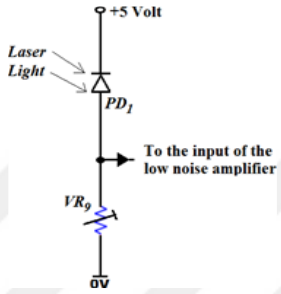


**Figure 6.8.** The laser pulse detector circuit.

### 6.4.2.2 Design of the Low Noise Amplifier

The ready circuit diagram of this amplifier has been demonstrated in Figure 6.9 [52]. This circuit consists of two transistors and several resistors and capacitors. This circuit has a very low noise, equal to 0.7 nV/√Hz (RMS noise) or lower, which is practically measured. The capacitors were used for DC component rejection (the effect of the sunlight rays). The gain of this amplifier is determined by the ratio ($R_{10}$ /$R_9$). As the required gain for this amplifier is 50 or 16.99 dB, one can calculate the value of the resistor $R_{10}$ as follows:

$$Gain = 50 = \frac{R10}{R9} = \frac{R10}{4.7}$$

So,

$$R10 = 235\Omega$$

one can use a 1kΩ variable resistor for $R_{10}$ and set it at the value 235Ω.

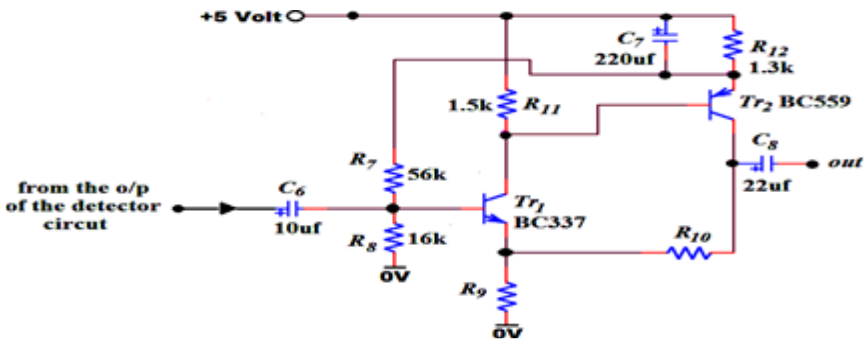


**Figure 6.9.** The complete circuit diagram of the low noise amplifier.

### 6.4.2.3 Design of the notch filter

The role of this filter is rejecting the effect of the 50 Hz light signal dissipated from the AC220Volt light sources. The circuit diagram of this filter has been illustrated in Figure 6.10. The type of the $IC_{13}$ used in this filter is LM124.

The required gain for this filter is 1.9 or 2.7875 dB, which is less than 2, as was considered in chapter two. Using Equation (3.21) and assuming the value of $R_{16}$=1kΩ, then one can calculate the value of $R_{17}$ as follows:

$$Gain_1 = 1.9 = 1 + \frac{R_{17}}{1000}$$

$$R_{17} = 900\Omega$$

So one can use the 1kΩ rheostat for the resistor $R_{17}$.

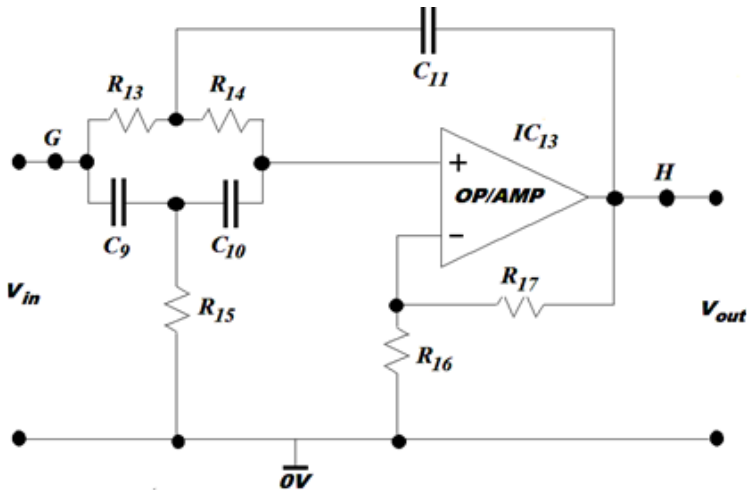


**Figure 6.10.** The complete circuit diagram of the notch filter.

As assumed before at chapter two, $R_{13} = R_{14}$, and $C_9 = C_{10}$,

and

$R_{15} = R_{14}/2$, $C_{11} = 2C_{10}$.

Let $C_{10} = C_9 = 1\mu f$, therefore, $C_{11} = 2\ \mu f$, so one can determine the value of the resistors $R_{13}$, $R_{14}$ and $R_{15}$ using Equation (2.20), where the center frequency of this filter is 50 Hz:

$$f_c = \frac{1}{2\pi R_{13}.C_{10}} = \frac{1}{2\pi R_{13}.(1 * 10^{-6})} = 50HZ$$

So,

$$R_{13} = R_{14} = 159.155K\Omega$$

So,

$$R_{15} = \frac{R_{14}}{2} = 79.5775K\Omega$$

One can use 220kΩ rheostats for the resistors $R_{13}$ and $R_{14}$, and 100kΩ rheostat for the $R_{15}$.

The quality factor can be calculated as follows using Equation (3.22):

$$Q = \frac{1}{2 - Gain_1} = \frac{1}{2 - 1.9} = 10$$

Finally, one can calculate the bandwidth of this filter using Equation (3.23) as follows:

$$B.W = \frac{f_c}{Q} = \frac{50}{10} = 5HZ$$

which is the required bandwidth.

Design of the Low Pass Filter

This filter has been used to reject the frequencies beyond the highest used frequency of the transferred data between the transmitter and the receiver. The type of used integrated circuit $IC_{14}$ is LM124. The circuit diagram of this filter has been demonstrated in Figure 6.11.

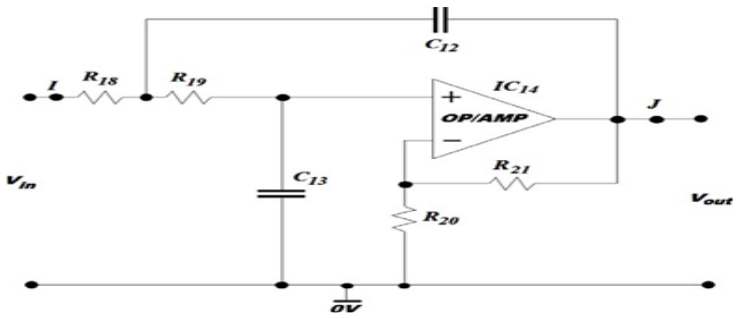


**Figure 6.11.** The circuit diagram of the low pass filter.

The input of this filter is driven from the output of the notch filter, and the output of this filter is connected to the input of the voltage comparator circuit. One can observe that the maximum frequency related to this work is for the NORMAL state pulse to have a duration equal to 1 msec. So the maximum frequency must be equaled to (1/0.001)=1kHz. Therefore, the cutoff frequency of this filter should be equal to 1 kHz. In this design, one can assume a unity gain for this filter, which is less than 3 as was considered in chapter two, so one can calculate the value of the resistor $R_{21}$ using Equation (3.25):

$$Gain2 = 1 = 1 + \frac{R_{21}}{R_{20}}$$

So, $R_{21}$ must be short circuit or $R_{20}$ must be open circuit, i.e. $R_{21} = 0\Omega$ or $R_{20} = \infty\Omega$.

The resistors $R_{18}$ and $R_{19}$ should be equal to each other, and the capacitors $C_{12}$ and $C_{13}$ should also be equaled. One can assume that $C_{12}$ and $C_{13}$ equaled to 0.1μf. So one can calculate the value of the resistors $R_{18}$ and $R_{19}$ using Equation (3.24) as follows:

$$f_c = 1000HZ = \frac{1}{2\pi R_{18}.C_{12}} = \frac{1}{2\pi R_{18}.(0.1 * 10^{-6})}$$

So,

$$R_{18} = R_{19} = 1.591K\Omega$$

one can use the 2.2kΩ rheostats for the resistors $R_{18}$ and $R_{19}$.

Note that the overall gain of the laser pulse receiver circuit should be equal to: $(Gain_1 \times Gain_2)=50\times1.9=95$.

The received peak-to-peak voltage can be calculated using the proportionality law as follows:

$$\frac{P_t}{P_r} = \frac{v_{t(p.p)}^2}{v_{r(p.p)}^2} (5.1)$$

$$V_{r(p.p)} = 38.19 * 10^{-3}$$

Therefore, the peak-to-peak voltage at the output of the low pass filter can be calculated as follows:

$$V_{L.P.F(out)} = V_{r(p.p)} * totalGain$$

$$V_{L.P.F(out)} = 0.03819 * 95 = 3.628volts$$

which is the peak-to-peak output voltage of the low pass filter that produced to the input of the voltage comparator circuit.

### 6.4.2.4 Design of the voltage comparator circuit

This circuit is used to reshape the deformed incoming pulses from the low pass filter and is of the integrated $IC_{15}$ is LM393 type. The circuit diagram of this part of the receiver system is shown in Figure 6.12.

The input of this comparator circuit is driven from the output of the low pass filter, while the output of this circuit is connected to the input of the pulse period decoding circuit. One can assume the threshold voltage for this comparator is equal to 3 Volts and that the value of the resistor $R_{22}$ is 10kΩ. Therefore, using Equation (3.27), one can calculate the value of the variable resistor $VR_{10}$ as follows:

$$V_{th} = 3 = \frac{VR_{10}}{VR_{10} + VR_{22}} = \frac{VR_{10}}{VR_{10} + (10 * 10^3)}$$

$V_{R10} = 15K\Omega$

So, one can use the 22kΩ rheostat for the $VR_{10}$ and set it at the value 15kΩ.

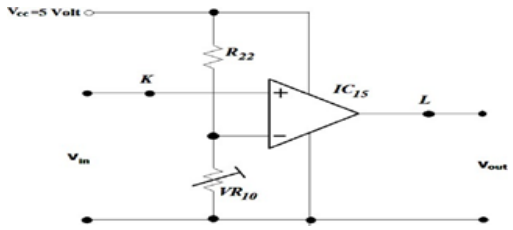


**Figure 6.12.** shows the practical implementation of the laser receiver circuit.

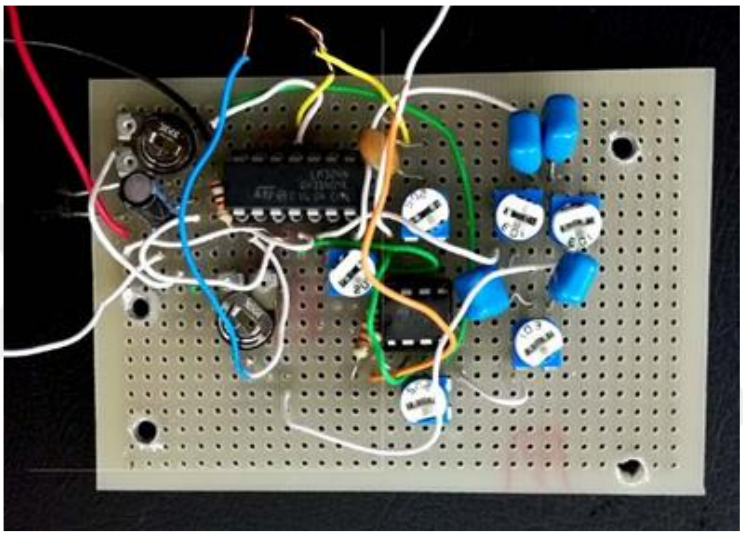

**Figure 6.13.** The practical laser receiver circuit.

### 6.4.2.5 Design of the pulse period decoder

The role of this circuit is converting the periods of the incoming data pulses from the data transmitter unit to binary numbers that are driven to the input jumper J55 of the SPARTAN 6 SP-605 kit FPGA (its data sheet has been shown in Appendix A). The circuit diagram of this decoder circuit is shown in Figure 6.14.

This circuit consists of TTL logic ICs supplied by +5 volt power supply. At the beginning, the incoming pulse enters from the point M, its positive edge trigs the one-shot-to circuit 1 (composed from NOT gate IC type SN74LS04 $IC_{16}$ and the AND gate $IC_{17}$ type SN74LS08) to generate a positive narrow pulse with a duraiton of 10nsec to reset the binary counter $IC_{20}$ type SN74LS93. One can set the capacitor

$C_{14}$ to 10nf to get this pulse period. At the same time, the gated controlled oscillator$_1$ is enabled to generate a clock frequency with 1 kHz, the capacitor $C_{15}$ is set to 0.1µf, and the 2.2kΩ variable resistor is chosen for $VR_{11}$. So one can set the $VR_{11}$ to get this desired frequency. The clock of this gated oscillator feeds the input clock of the binary counter $IC_{20}$, which continuously counts the output pulses of the gated oscillator only if the incoming data pulse from the data transmitter unit at HIGH state.

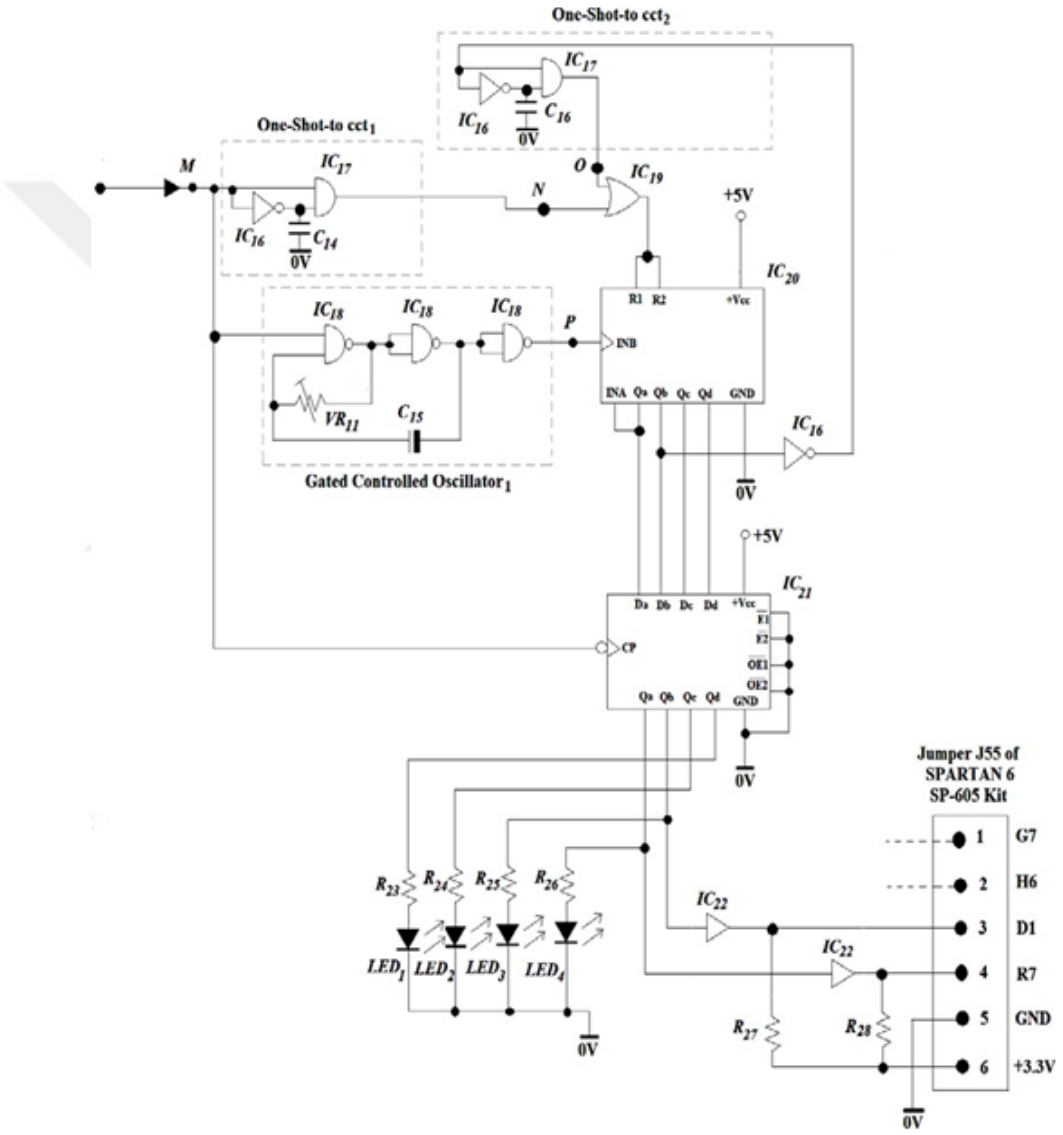


**Figure 6.14.** The circuit diagram of the pulse period decoder.

At the end of incoming pulse of the data transmitter unit, the latch $IC_{21}$ (type SN 74LS175) holds (or latches) the last output count of the binary counter $IC_{20}$, then the output lines ($Q_A$ and $Q_B$) of the latch $IC_{21}$ is buffered and adapted to the input of the SPARTAN-6 SP-605 FPGA kit. The Buffer $IC_{22}$ is used to adapt the output lines of the latch $IC_{21}$, which is supplied by +5 Volts to the input of the FPGA kit that is supplied by +3.3 Volts.

The role of the one-shot-to circuit 2 is to prevent the binary counter to count more than binary number (11), this circuit is trigged from the output line ($Q_B$) of the binary counter $IC_{20}$. The capacitor $C_{16}$ is set to 10nf for getting an output pulse from this circuit with 100nsec period. The binary number (01) (which represents NORMAL state) is presented at the input of the FPGA kit if the incoming pulse from the data transmitter unit has a period of 1 msec. The binary number (10) (which represents CRITICAL state) is presented at the input of the FPGA kit if the incoming pulse from the data transmitter unit has a period of 2 msec. The binary number (11) (which represents FATAL state) is presented at the input of the FPGA kit if the incoming pulse from the data transmitter unit has a period of 3 msec.

The state diagram of the proposed pulse period decoder circuit has been demonstrated in Figure 6.15 for a case of 3 msec period of an incoming pulse from the data transmitter unit, which represents the FATAL state of the $NO_2$ gas level. As shown in this figure, this incoming pulse is converted to a binary number (11), which is presented at the output of the binary counter and the latch ICs.

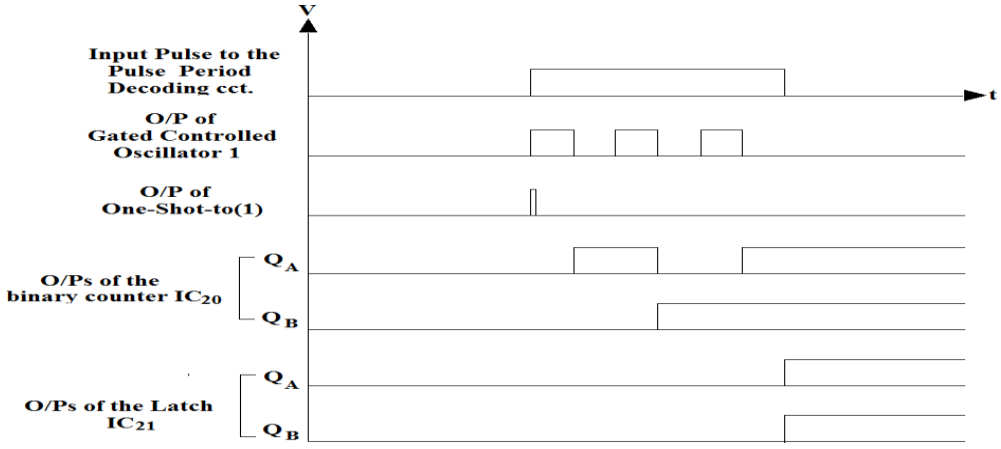


**Figure 6.15.** The state diagram of the main signals of the pulse period decoder.

### 6.4.3 Design of the ON/OFF switching key transmitter unit

The role of this unit is transmitting the ON/OFF switching key pulse with a specific period used for switching ON and OFF the power supply terminal to the supply feeding of the data transmitter unit. The circuit diagram of this circuit has been shown in Figure 6.16. This unit consists of $IC_{23}$, which is a timer type NE555. This timer is used for generating repetitive pulses for igniting the mono-stable multi-vibrator $IC_{24}$ type SN74LS132 to generate the ON/OFF switching key pulses that are modulated with an infra-red laser light by the Buffer $IC_{25}$ type SN74LS07. The required frequency for the timer $IC_{23}$ is 1 Hz. Let the capacitor $C_{18}$ be equal to 100µf and the resistor $R_{29}$ equal 10kΩ, so one can calculate the resistance of the variable resistor $VR_{12}$ using the frequency expression of IC NE555 as follows:

$$f = \frac{1.44}{((10\times10^{3})+2VR_{12})100\times10^{-6}} = 1$$

$$V_{R12} = 2.215K\Omega$$

one can the use the standard value of variable resistor 5kΩ for the variable resistor $VR_{12}$.

The output of the timer $IC_{23}$ is connected to the clock input of the mono-stable $IC_{24}$ type SN74LS123. The $IC_{24}$ is a mono-stable multi-vibrator that is used to generate the ON/OFF switching key pulse with a duration 3 msec. Let the capacitor $C_{19}$ have a value 100n. So one can calculate the value of the variable resistor $VR_{13}$ as follows:

$$t_{p24} = (0.28) * 100 * 10^{-9} * V_{R13} = 3 * 10^{-3}sec$$

$$V_{R13} = 107.143K\Omega$$

one can select a standard variable resistor 200kΩ for $VR_{13}$.

The integrated circuit $IC_{25}$ is a Buffer IC type SN7407 used for modulating the output pulse (ON/OFF switching key pulse) with an infra-red laser light that is generated by the laser diode $LD_2$. There are Two Buffer gates $IC_{25}$ type SN7407 that are connected parallel to produce an 80 mA load current to drive the laser diode $LD_2$ type S368505D that has maximum operating current equals to 40 mA. The laser

diode $LD_2$ is considered a carrier signal generator. The $LD_2$ laser diode used in this on/off switching key transmitter unit is S368505D, which can deliver less than 5mW of infra-red light with wavelength 850nm. Practically, this laser diode can deliver a power equal to 4.8 mW, which has been measured by the optical power meter device. The state diagram of the main signals of this unit has been shown in Figure 6.17. The modulation technique used for this unit design is the ON/OFF keying (or Direct Intensity) modulation.

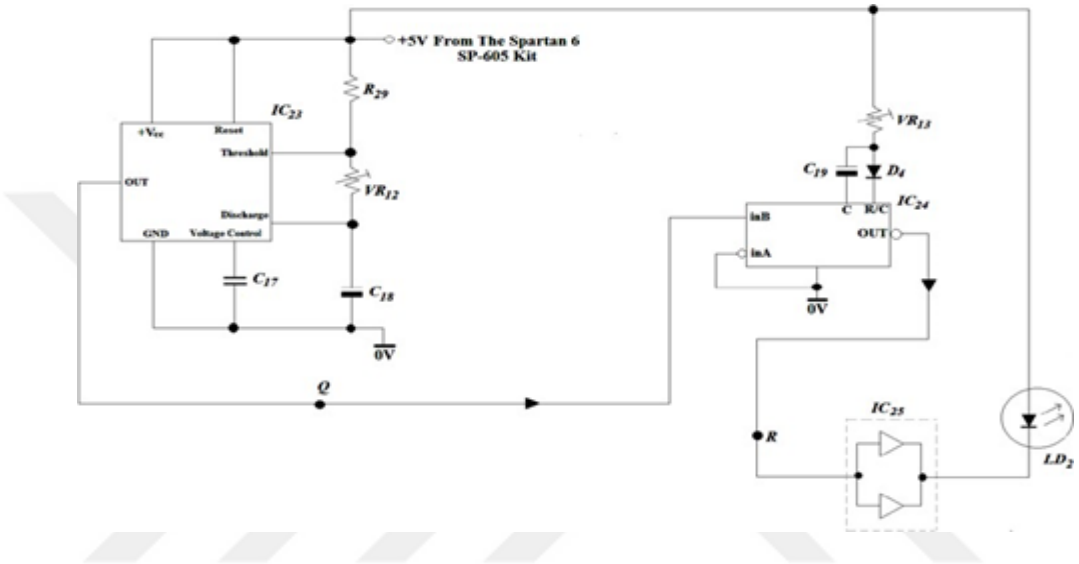


**Figure 6.16.** The circuit diagram of the ON/OFF switching key transmitter.

As shown in this diagram, at only the positive edge of the output pulse of the timer $IC_{23}$, a positive narrow pulse with period 3msec is generated by the mono-stable multi-vibrator $IC_{24}$.


**Figure 6.17.** The state diagram of the main signals.

### 6.4.4 Design of ON/OFF switching key receiver unit

This unit is composed from two circuits: the laser signal receiver and the pulse period decoder. The role of this unit is receiving the laser pulse that transmitted by

the ON/OFF switching key transmitter. Then, this key pulse is converted to a binary number that is driven to the switching element (Relay) used for switching ON and OFF the power supply terminal to the supply feeding of the data transmitter unit.

#### 6.4.4.1 Design of ON/OFF switching key laser pulse receiver circuit

The circuit design of this part of the receiver is exactly the same as the laser data pulse receiver of the data receiver unit, which discussed in details in section 6.4.3.1.

#### 6.4.4.2 Design of the ON/OFF switching key pulse period decoder

The circuit design of this decoder is similar to that of the data pulse decoder that discussed in section 6.4.3.6 with several differences presented at the output of this pulse period decoder. The circuit diagram of this decoder is shown in Figure 6.18.

The first difference is using of a decoder at output of the latch $IC_{31}$ (type SN74LS175). This decoder is composed from the 4-input NAND gate $IC_{32}$ type SN74LS20 and the two inverter gates $IC_{26}$ type SN74LS04. This decoder has an active LOW output, which is used for decoding the output of the latch $IC_{31.}$ This decoder produces an active LOW if the entered binary number is (0011), while the other possible binary numbers produce a non-active HIGH.

The output of the decoder circuit is driven to the one of the two inputs of the OR gate of $IC_{29}$ type SN74LS32, while the other input of this OR gate is driven from the active LOW output of the mono-stable multi- vibrator $IC_{34}$ type SN74LS123. Meanwhile, the $IC_{34}$ is used to produce an active LOW pulse with duration more than of the clock cycle duration of the incoming laser pulses from the ON/OFF switching key transmitter. The role of this active LOW output pulse of the $IC_{29}$ is for continuously switching ON the power supply terminal to the supply feeding of the data transmitter unit whenever the incoming laser pulses from the ON/OFF switching key transmitter is regenerated, i.e. the output of the $IC_{34}$ changes to a non-active HIGH if the laser pulses from the ON/OFF switching key transmitter is stopped. One can assume the output pulse width of this mono-stable multi-vibrator is equal to 2 seconds, which is larger than the duration of repetition of the laser pulses incoming to the input of the on-off switching key receiver that has a duration of 1 second. One

can assume the value of the capacitor equals to 100μf, then the variable resistor $VR_{15}$ can be calculated using the data sheet of the $IC_{34}$ as follows:

$$t_{p34} = 2sec = (0.28) * 100 * 10^{-6} * V_{R15}$$

$$V_{R15} = 71.428K\Omega$$

So, one can use standard 100kΩ variable resistor for $VR_{15}$ and set it at 71.428 kΩ.

Finally, the output of the OR gate $IC_{29}$ is driven to the input of the parallel Buffer gates of $IC_{33}$ type 74LS07 for increasing the load current. The output of this Buffer gate is driven to a switching Relay (1). This Relay is used as a controlled switch to switch ON and OFF the power supply terminal to the supply feeding of the data transmitter unit according to the logic signal produced by the buffer $IC_{33}$.

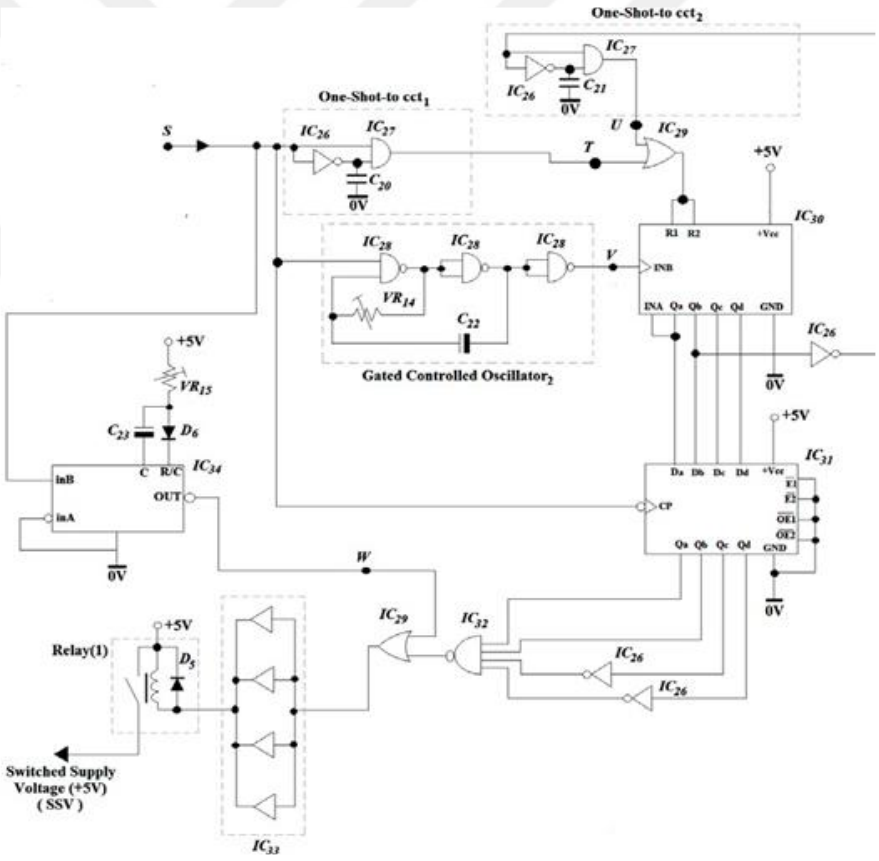


**Figure 6.18.** The circuit diagram of the ON/OFF switching key pulse period decoder.

The state diagram of pulse period decoder of the ON-OFF switching key receiver unit has been shown in Figure 6.19.

The overall implementation of the proposed practical circuit has been shown in Figure 6.20, which shows the connection of the proposed practical circuit to the FPGA kit. Figure 6.21 shows the picture of testing the proposed system using the execution of the proposed simulation software.

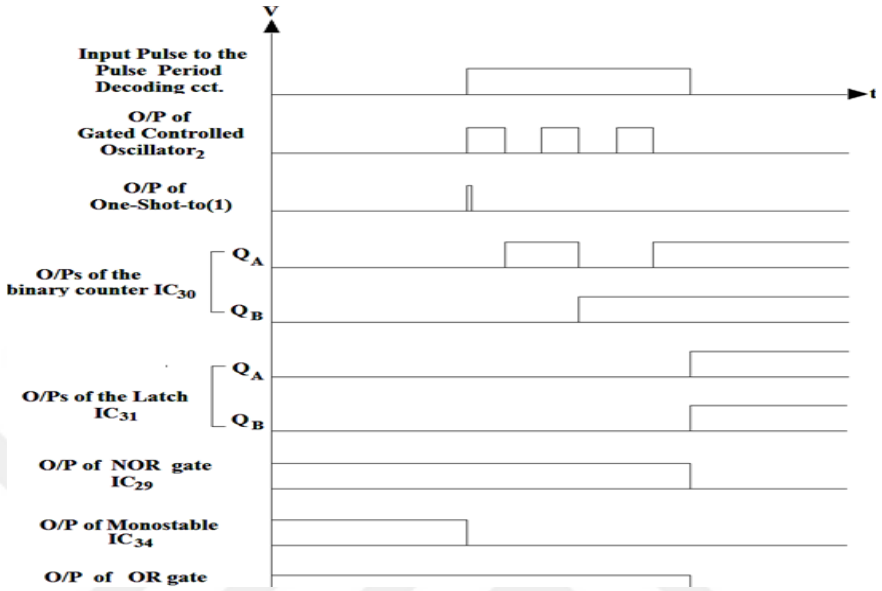


**Figure 6.19.** The state diagram of the pulse period decoder of the ON/OFF switching key receiver.

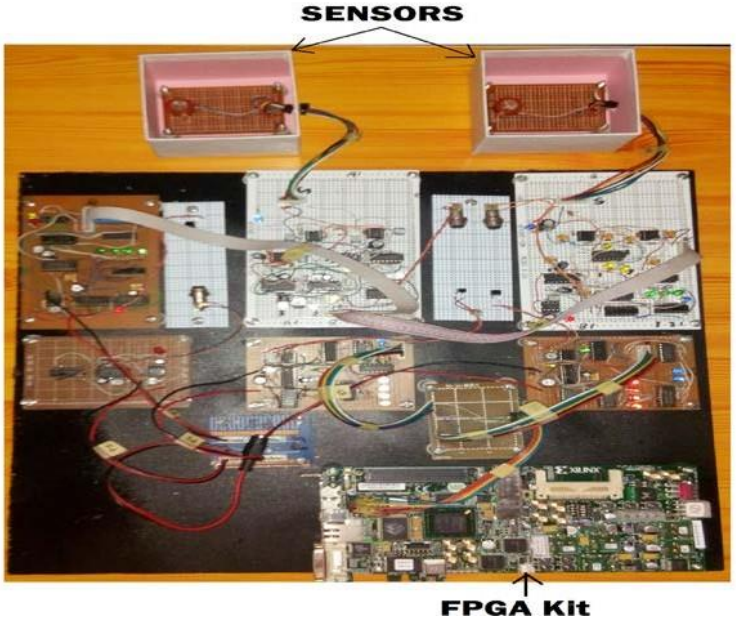


**Figure 6.20.** The implemented proposed intelligent WSN connected to the FPGA.


**Figure 6.21.** SP-605 evaluation kit.

# 7. EXPERIMENT RESULTS

## 7.1 Conclusion And Discussion On Result Of BB System Design Using PSO

The simulation software of the proposed system has been designed, executed, and then tested using the MATLAB and ISE Design Suit software packages. The proposed system software has been ended by the instruction {**gensim(net)**} for generating the system block for the proposed simulation system. Then, using the MATLAB software package, this system block has been translated to the VHDL (VHSIC (Very High-Speed Integrated Circuit) Hardware Design Language) code program. Later, this code program has been tested and downloaded into the FPGA (Field Programmable Gate Array) by the ISE design suit software package.

The proposed simulation system has been trained by Trainpso function. After that, the optimal obtained results have been presented using this training function.

The optimal result has been obtained using the trainpso training function with the setting of three neurons in the hidden layer. Thus, using the Particle Swarm Optimization (PSO) as a training function, one can get the optimal result while reducing the size of the proposed simulation system that leads to a contribution to this work.

## 7.2 Output Results Using Trainpso Training Function

After executing the proposed simulation software using the particle swarm optimization training function, a primary result window has presented on the screen of the computer, as shown in Figure 7.1.

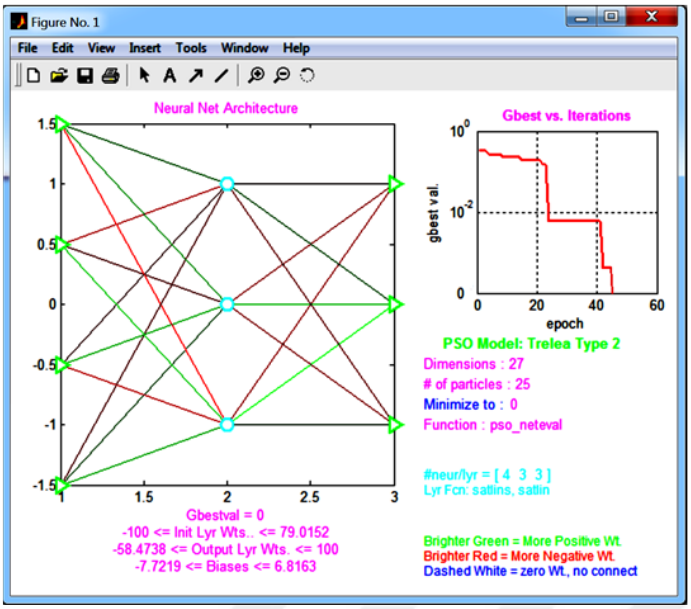


**Figure 7.1.** First output results using trainpso training function**.**

At the left side of this figure, the network connection has been presented of the proposed simulation system, one can see from the network connection that there are four neurons in the input layer, three neurons in the hidden layer, and three neurons in the output layer. At the right side of same figure, one can see the relation between the Get best value (Gbest val.) with the number of epochs (iterations). The Gbest value represented the mean square error of the proposed system. As shown in this figure, one can see that the mean square error had reached to zero value at epoch 46, which signified the second optimal result of this faster training method. Therefore, one can conclude that the training by the particle swarm optimization is the fast training method with 46 iterations for presenting the optimal result of zero mean square error using three neurons in the hidden layer, which was the least number of neurons used in the hidden layer for proposed simulation system. Another result has been presented in the left side of Figure 7.1. The first result is the input connection weights of the hidden layer, whereas these weights had varied from (-100) to (+79.0152), and the input connection weights of the hidden layer varied from (-58.4738) to (+100), with the biases varying from (-7.7219) to (+6.8163).

Another piece information that has been presented in Figure 7.1 is that the value of the dimensions which was (27), while the number of used particles was (25), and

each of these particles had 21 solutions. As such, each solution represented an individual connection weight of the proposed simulation system.

One can see from the right side of the Figure 7.1 that Gbest val. (mean square error) had varied non-uniformly and non-linearly with progression of the iterations (epochs) and there is a rapid decrease of the mean square error near epochs 24, 42, and 46, which supports the presented optimal results.

Another result window using the trainpso training function has been presented in this work, as shown in Figure 7.2.

As seen on the left side of this figure, the relation between the Gbest val. (the mean square error) vs. the no. iterations has been presented for another training test, which has been mentioned in Figure 7.1.

At the right side of Figure 7.2, the searching zone (space) has been presented between the dimension 1 (the x- axis) and the 27 dimensions (the y-axis). The intersection point of the red dashed lines represented the best location of solution (best solution of weights). One can see from this figure that the particles of the proposed system had moved toward the direction of the best solution which is the intersection of the red dashed lines, as mentioned before that each particle had a single solution for the weights of the proposed simulation system.

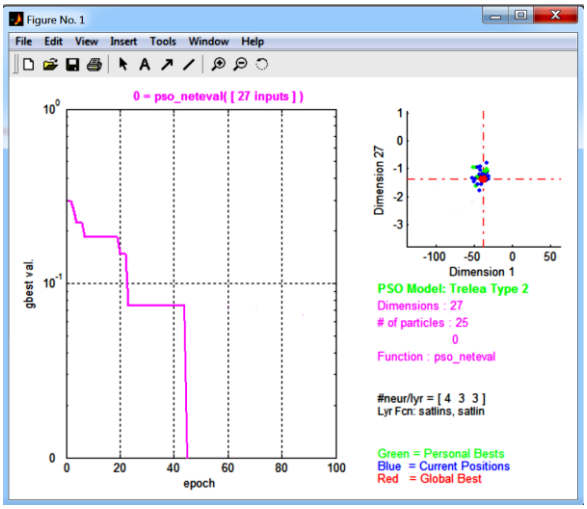


**Figure 7.2.** The second output results using trainpso training function.

### 7.3 Comparison With Results Of Related Works

There are three important results of previous works related to the proposed work. These works will be discussed below. One can see that the obtained optimal results in this work is much better than that of these related works when comparing the performance results.

In reference [16] had proposed a Back-propagation neural network for a wireless sensor network. They used the trainlm (Levenberg-Marquardt) training function for learning the network and used linear activation functions for the hidden and output layers. The performance result of this work has been presented in Figure 7.3. One can see from this figure that the mean square error of this work had reached to (1.2642×10-10) at epoch 218, which is more than that of the proposed work. Thus, one can see that the optimal performance result of the proposed work is much better than that of this related work. In [17] proposed a Back-propagation Neural Network based on Multi-layer Perceptron Neural Network to carry out the localization of a wireless sensor network. In this work, 10 neurons were used for the hidden layer, three neurons were used for the output layer, the tan-sigmoid (non-linear) activation function was used for the hidden layer, and the linear activation function was used for the output layer. The Trainlm (Levenberg-Marquardt) function was used for training.

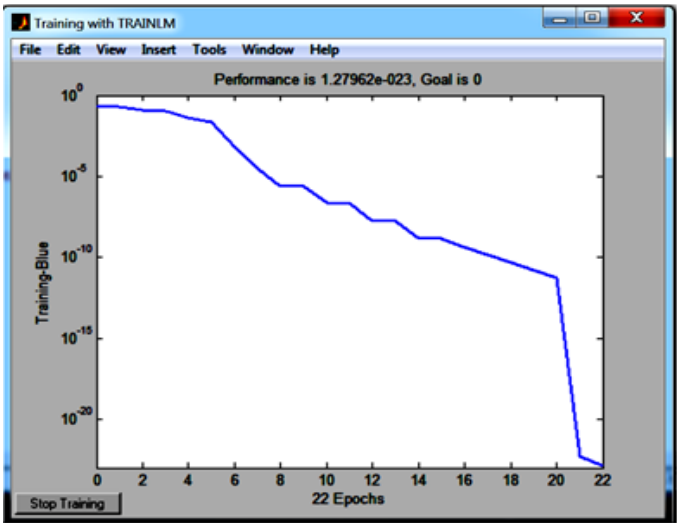


**Figure 7.3.** Performance result of the BB neural network of [16].

Figure 7.4. One can see from this figure that the MSE (Mean-Square-Error) reached the 1.278×10-23 value in 22 epochs. Thus, one can conclude that the output results of the proposed simulation system shown in Figure 7.2 are much better than that of this related work.

In reference [18] proposed a Back-propagation Neural Network for a sensor network that used non-linear activation functions for the hidden and output layers and the traingdx (Gradient Descent with Momentum and Adaptive Learning Rate) training function for learning the network. The performance result for this related work has been shown in Figure 7.5. One can see from this figure that the MSE (Mean-Square-

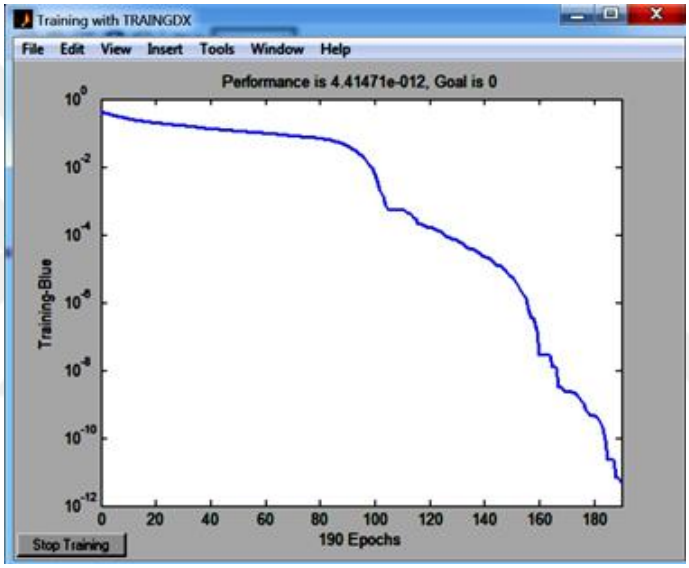


**Figure 7.4.** Performance result of the BB neural network of [17].

Error) reached (4.4×10-12) at epoch 190, which is greater than that of the proposed work that shown in Figures 7.1, and 7.2.

Table 7.1 shows the comparison between the proposed simulation results and the related work results.

**Table 7.1.** Comparison between the proposed simulation and related work.

| Work | Hidden layer activation function | Output layer activation function | Training function | No. epochs | Mean Square error |
|---|---|---|---|---|---|
| Muhammed et. al., 2012 | Linear | Linear | trainlm | 218 | $1.264\times10^{-10}$ |
| Shikha B., 2013 | Non-linear | Non-linear | trainlm | 82 | $1.28\times10^{-23}$ |
| Guo W. et. al., 2014 | Non-linear | Non-linear | traingdx | 190 | $4.414\times10^{-12}$ |
| Proposed simulation using trangda | Linear | Linear | traingda | 87 | 0 |
| Proposed simulation using Trainpso | Linear | Linear | trainpso | 46 | 0 |

Another important result was shown during the execution of the simulation software using the ISE design suite software using trainpso compared to using of traingda training function. After a primary result is presented on the computer screen, one can see from the output results that the proposed simulation software using the traingda training function was larger than of using trainpso training function. This lead to the execution time required when using the Trainpso training function being less than the execution time required when using the Traingda training function. Thus, this training system makes the system much faster.

### 7.4 VHDL Conversion Results Using Trainpso Training Function

After executing the proposed simulation software by the ISE Design Suit software package using the trainpso training function, the primary output results have been presented in Figures 7.5.

One can see from Figure 7.5 that the number of Slice Look Up Tables occupied 3% of the size of the FPGA and the number of Used as Logics items occupied 3% the

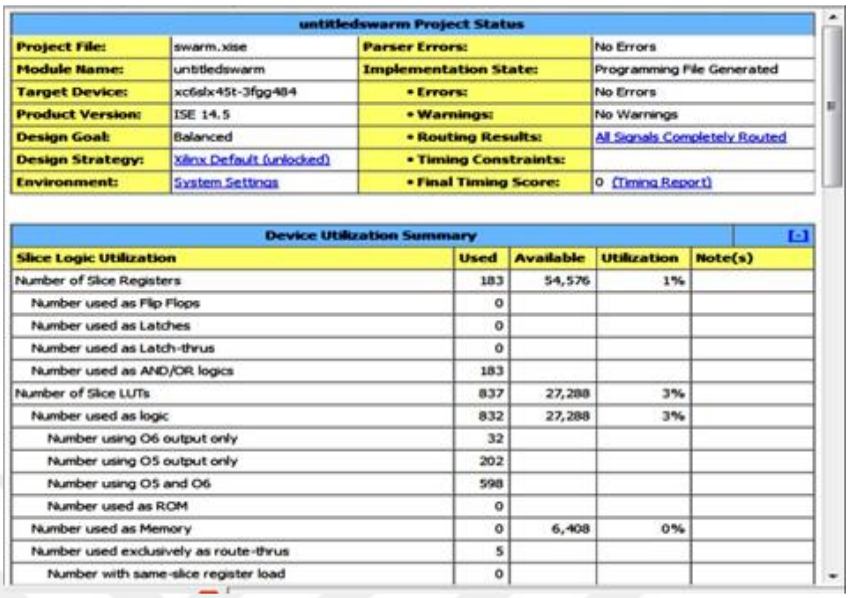

| untitledswarm Project Status | | | |
|---|---|---|---|
| Project File: | swarm.xise | Parser Errors: | No Errors |
| Module Name: | untitledswarm | Implementation State: | Programming File Generated |
| Target Device: | xc6slx45t-3fgg484 | • Errors: | No Errors |
| Product Version: | ISE 14.5 | • Warnings: | No Warnings |
| Design Goal: | Balanced | • Routing Results: | All Signals Completely Routed |
| Design Strategy: | Xilinx Default (unlocked) | • Timing Constraints: | |
| Environment: | System Settings | • Final Timing Score: | 0 (Timing Report) |

| Device Utilization Summary [-] | | | | |
|---|---|---|---|---|
| Slice Logic Utilization | Used | Available | Utilization | Note(s) |
| Number of Slice Registers | 183 | 54,576 | 1% | |
| Number used as Flip Flops | 0 | | | |
| Number used as Latches | 0 | | | |
| Number used as Latch-thrus | 0 | | | |
| Number used as AND/OR logics | 183 | | | |
| Number of Slice LUTs | 837 | 27,288 | 3% | |
| Number used as logic | 832 | 27,288 | 3% | |
| Number using O6 output only | 32 | | | |
| Number using O5 output only | 202 | | | |
| Number using O5 and O6 | 598 | | | |
| Number used as ROM | 0 | | | |
| Number used as Memory | 0 | 6,408 | 0% | |
| Number used exclusively as route-thrus | 5 | | | |
| Number with same-slice register load | 0 | | | |

**Figure 7.5.** The first primary results using ISE design suit software package with trainpso training function.

### 7.5 Conclusion and Discussion On Obtained Results Of The FSO.

For any given work of a scientific research, three types of results should be presented for realizing good and accepted performance of a specific designed system. These are: theoretical, simulation, and practical results. Theoretical results represent results of the used mathematical expressions. Simulation results represent the executing outputs of the used software package that signify the proposed system. Practical results represent outputs of the designed and implemented circuit of the proposed system. For a good and accepted proposed design, the simulation and practical outputs must realize the theoretical expressions calculations.

In this section, the theoretical and practical results of the receiver circuit and FSO communication system of the proposed system have been presented and discussed.

### 7.6 Discussion On Obtained Results Of The FSO Communication

After designing and implementing the FSO communication link, several results have been presented using theoretical calculations and practical measurements. As shown

from the results figures, the practical measurements approached the theoretical calculations, which is discussed as follows:

Figure 7.6 represents the theoretical relation between the attenuation loss in dB and the link range in meter, while the attenuation loss represents the Mie-scattering loss. As shown in this figure, the attenuation loss linearly increases when increasing the link range, which realizes Equation (3.18). The attenuation loss starts with a zero dB value at link a range of 0 meters and finishes with a value of 48.2×10-3 dB at link a range of 50 meters.

Figure 7.7 demonstrates the theoretical relation between the received power in dB and the link range in meter. As shown in this figure, the received power linearly decreases when increasing the link range, which realizes Equation (3.19). The received power starts with a value of -23.188 dB at a range 0 meters and finishes with a value of -23.238 dB at a range of 50 meters.

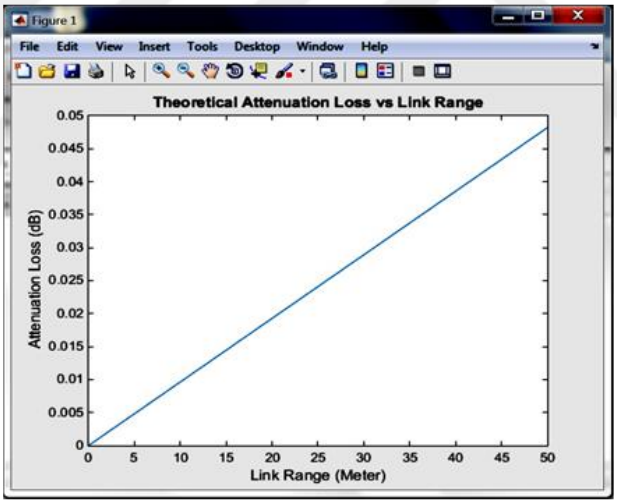


**Figure 7.6.** Theoretical relation between attenuation loss and the link range.

Figure 7.8 represents the practical relation between the attenuation loss in dB and the link range in meter. The attenuation loss represents the Mie-scattering loss. As shown in this figure, the attenuation loss approximately linearly increases when increasing the link range, and there are some fluctuations in the measurement readings, which have occurred due to the following reasons:

1. High lack of accuracy of the used instruments (testing devices).

2. Lack of accuracy of the measurement readings.

3. Continuous timely changing of the environmental conditions which effects the attenuation loss and received power readings.

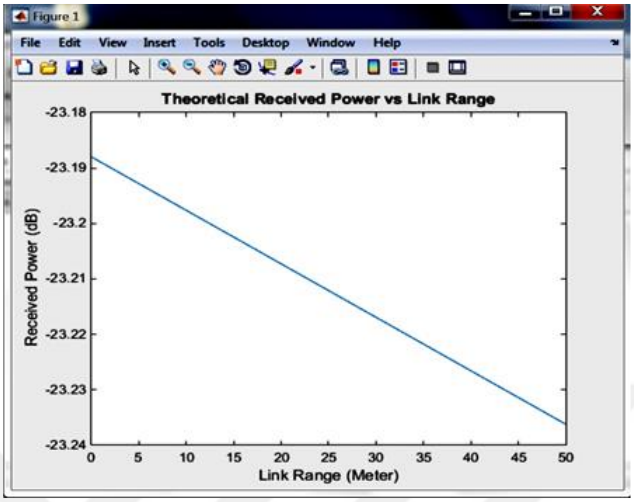


**Figure 7.7.** Theoretical relation between received power and the link range.

As shown in Figure 7.8, the attenuation loss starts with zero dB value at a link range of meters and finishes with value 48.2×10-3 dB at a link range of 50 meters.

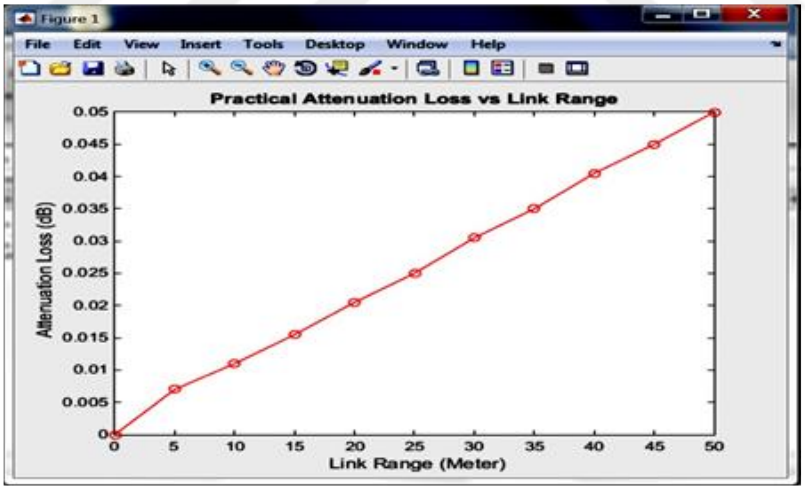


**Figure 7.8.** Practical relation between attenuation loss and the link range.

As shown in Figure 7.9, the received power starts with a -23.188 dB value at a link range of zero meters and finishes with value -23.236 dB at a link range of 50 meters.

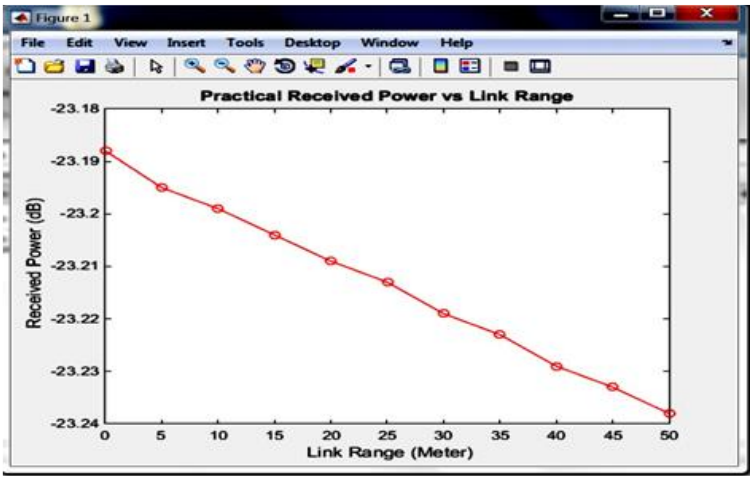


**Fig. 7.9** Practical relation between received power and link range.

Figure 7.10 shows in single graph the theoretical and practical attenuation loss in dB with the link range in meters. As shown in this figure, there is a proximity between these two relations, and one can observe that the practical attenuation loss is slightly higher than that of theoretical attenuation loss along the 50 meter link range, which has occurred due to the above mentioned reasons. The practical relation in Figure 7.10 has been drawn using 11 measurement readings through a 50 meters link range, at steps of 5 meters. One can observe that the attenuation loss for the two relations of Figure 7.10 has been linearly increased when increasing the link range along 50 meters. As shown in same figure, the theoretical relation is a pure increasing line, but the practical relation increasing line has some of slight fluctuations, again, which has been occurred due to the above-mentioned reasons.

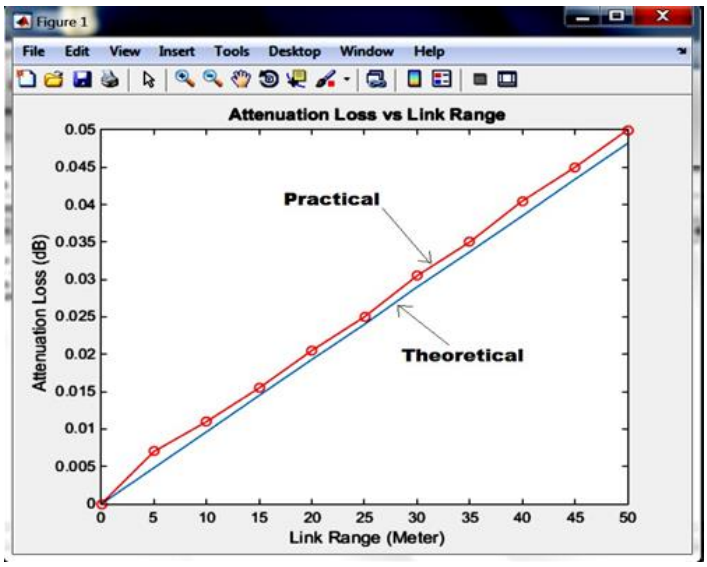


**Figure 7.10.** Comparison between practical and theoretical relation between attenuation loss and the link range.

Figure 7.11 shows in single graph the theoretical and practical received power in dB with the link range in meters. As shown in this figure, there is a proximity between these two relations, and one can observe that the practical received power is slightly lower than that of theoretical received power along the 50 meter link range, which has occurred due to the above mentioned reasons. The practical relation in Figure 7.11 has been drawn using 11 measurement readings through a 50 meter link range, at a step of 5 meters. One can observe that the received power for the two relations of Figure 7.11 has been linearly decreased when increasing the link range along 50 meters. As shown in same figure, the theoretical relation is a pure increasing line, but the practical relation increasing line has some of slight fluctuations, again, which has been occurred due to the above-mentioned reasons.

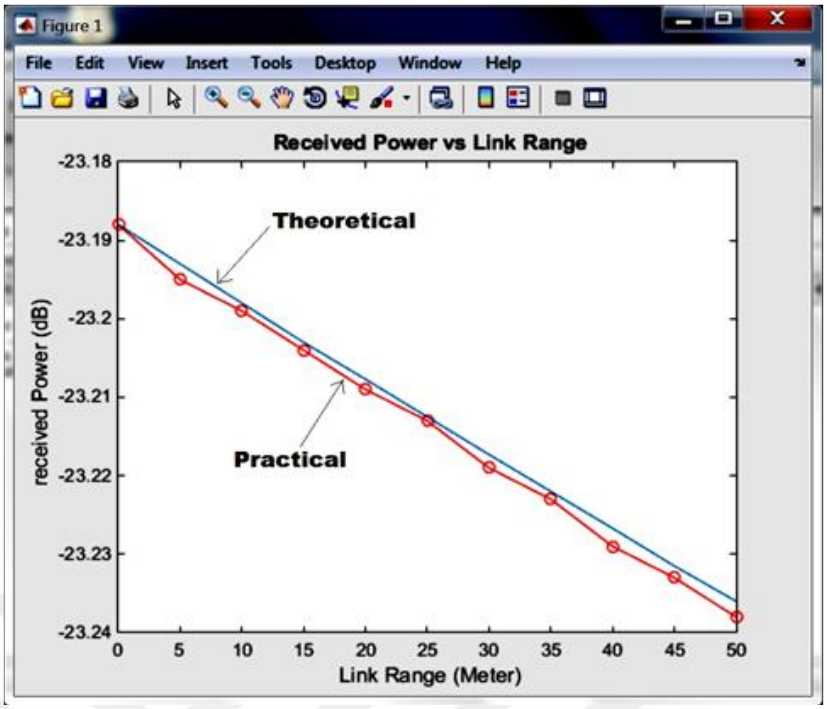


**Figure 7.11.** Comparison between practical and theoretical relation between received power and the link range.

### 7.7 Discussion On Measured Results Of The Ir Laser Receiver Circuit.

This section presents and discusses the transmitted and received data represented by the NORMAL level data that is represented by a pulse with duration of 1 msec. The measurement readings have been achieved by using real oscilloscope. The output of this oscilloscope has been presented on the screen of the laptop computer.

Figure 7.12 demonstrates the shape of the transmitted laser pulse, which has been detected by PIN photodiode circuit. As shown, this pulse represents the transmitted pulse at the side of the laser transmitter diode. The duration of this pulse is 1 msec as shown in Figure 7.12, and this pulse has an amplitude of 1.002 $V_{p.p}$ (Peak-to-Peak voltage), which realizes the design requirements. This pulse represents the NORMAL level data. As shown, this pulse is considered as a pure pulse, because the duration of this pulse is 1 msec that can easily be generated by the laser diode in this range of duration. When this duration is decreased to approximately 1×10-5, this pulse can be distorted because the response limitation of the used integrated in the laser transmitter circuit.

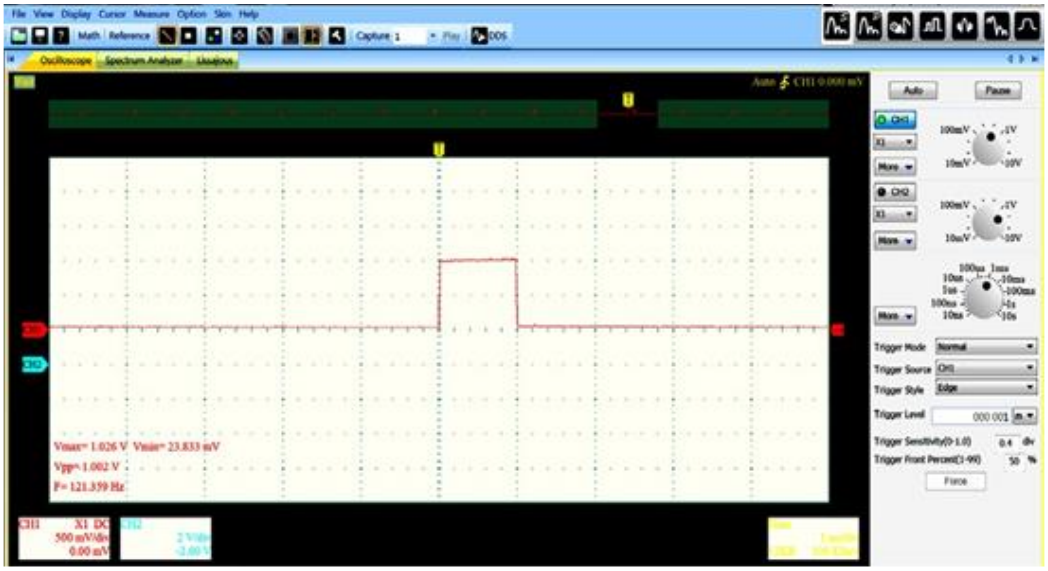

**Figure 7.12.** The transmitted pulse of the IR laser diode.

Figure 7.13 shows the received pulse beyond the stage of the PIN detector diode circuit. As shown, this pulse has an amplitude of 38.345 $mV_{p.p}$ and a duration of 1 msec. Thus, one can observe the attenuation of the transmitted pulse after 50 meters, where the transmitted laser pulse has been attenuated by Mie-Scattering effects of the FSO channel. So, one can observe that the duration had not changed along the link range, which signifies the purity of the received pulse after the 50 meter range.

**Figure 7.13.** Real oscilloscope presenting for the received laser pulse at the input of the Low Noise Amplifier.

Figure 7.14 shows the received pulsed after the stage of the Low Noise Amplifier. As shown in this figure, the duration of the pulse is 1 msec, and it has amplitude of 1.916 $V_{p.p}$. Thus, one can observe that the received pulse has been amplified by a factor of 50, which is the Gain of the Low Noise Amplifier.

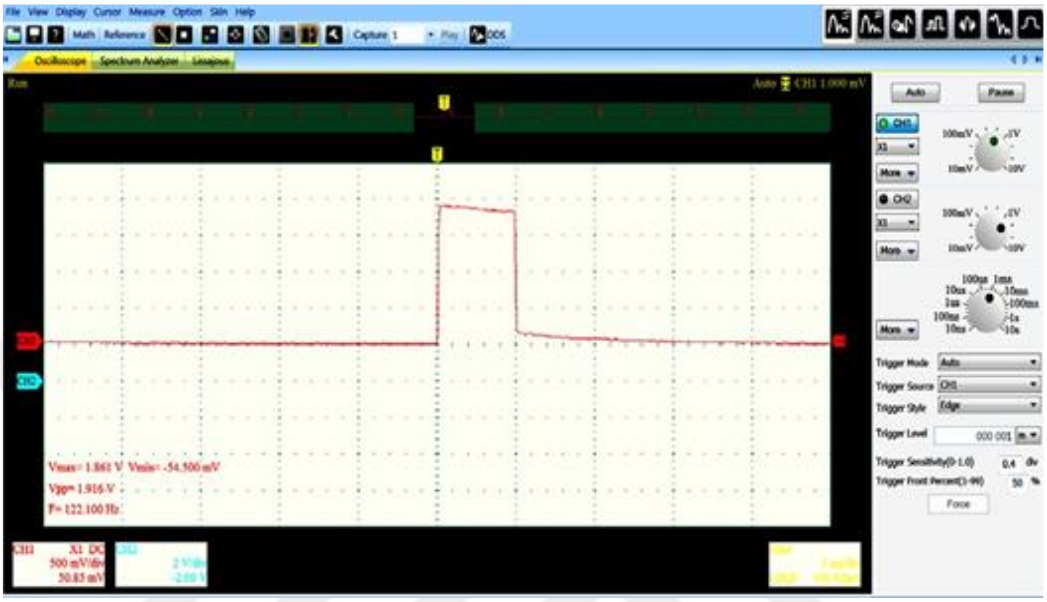

**Figure 7.14.** Real oscilloscope presenting for the received laser pulse at the output of the Low Noise Amplifier.

One can see the distortion that occurred at the base of the pulse due the response limitation of this amplifier which is 2-20000 Hz. Thus, one can say that the received pulse at the of the Low Noise Amplifier retains the same duration of the transmitted pulse, but it is amplified due the gain of this amplifier and distorted due the response limitation of the same amplifier.

Figure 7.15 demonstrates the received pulse after the stage of 50 Hz Notch Filter. The duration of the shown pulse is still 1 msec. Because the Gain of this stage (The Notch Filter) is 1.9, the amplitude of the pulse measured after this stage is 3.663 Volts. As shown in this figure, the received pulse has been distorted more than that after Low Noise Amplifier because the frequency components in range (48-52) have been deleted due the function of the 50 Hz Notch Filter. Thus, the received pulse after this stage has been distorted at the top and base of the received pulse.

Figure 7.16 demonstrates the received pulse after the stage of Low Pass Filter. Again, The duration of the shown pulse is still 1 msec. Because the Gain of this stage (The Notch Filter) is 1, the amplitude of the pulse measured after this stage is 3.611 Volts. As shown in this figure, the received pulse has been distorted more and more than after the 50 Hz Notch Filter. This is because the frequency components ≥ 1 kHz were deleted due to the function of the Low Pass Filter. Thus, the received pulse after this stage has been more distorted at the base of the received pulse.

Figure 7.17 illustrates the received pulse after the stage of Voltage Comparator. As shown in this figure, the duration of the received pulse is still 1 msec and the amplitude is 5 Volts. One can observe the received pulse is a pure pulse due the reshaping process of the Voltage Comparator.

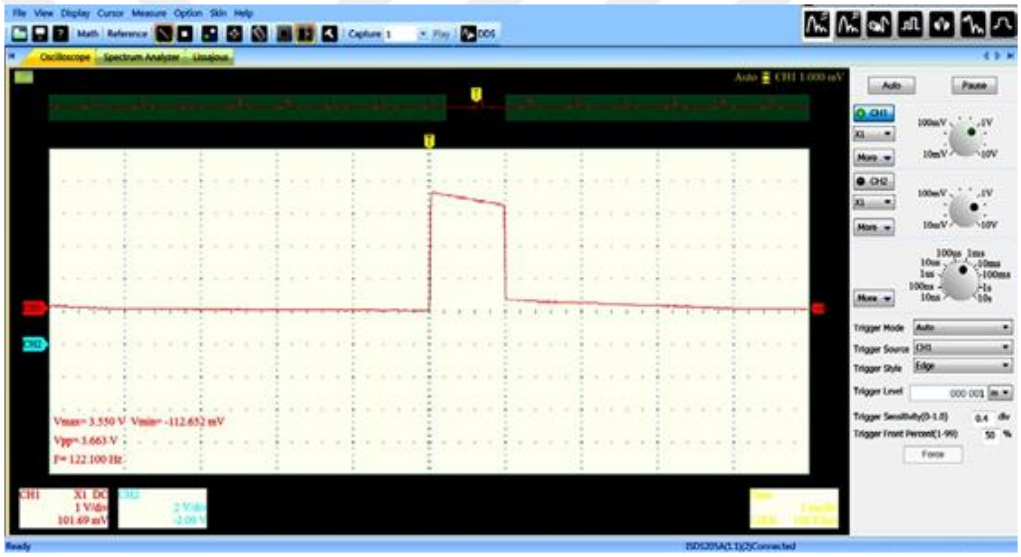

**Figure 7.15.** Real oscilloscope presenting for the received laser pulse at the output of the 50 Hz Notch Filter.

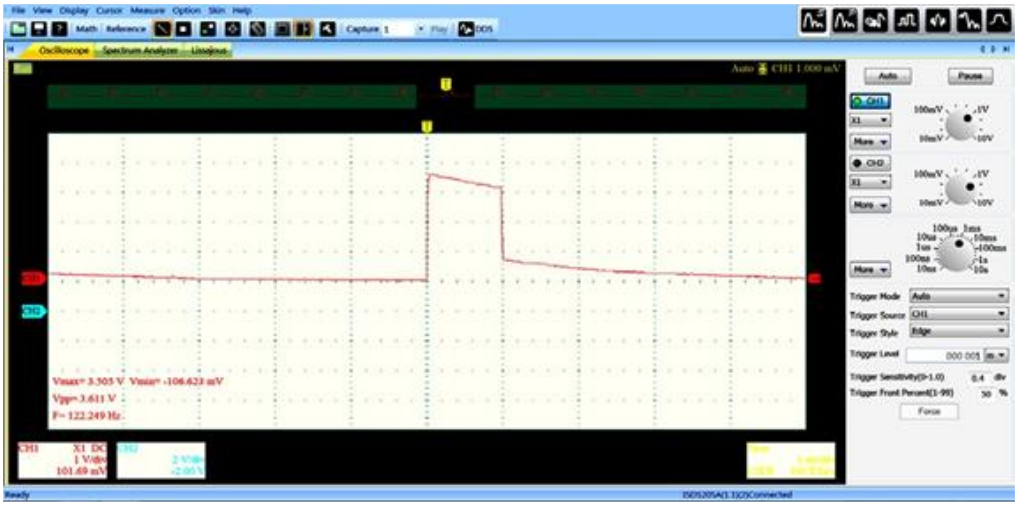

**Figure 7.16.** Real oscilloscope presenting for the received laser pulseat the output of the Low Pass Filter.

Figure 7.17 illustrates the received pulse after the stage of Voltage Comparator. As shown in this figure, the duration of the received pulse is still 1 msec and the amplitude is 5 Volts. One can observe the received pulse is a pure pulse due to the reshaping process of the Voltage Comparator circuit, whereas, the output signal of this circuit is either 1 or 0, the 1 signal will be represented by +5Volts and the 0 signal will be represented by zero Volts. As mentioned in chapter five, the threshold of the used voltage Comparator was 3 volts, so the Voltage Comparator circuit produces +5 volt when the received pulse at the output of the Low Pass Filter is ≥ 3 volt and produces 0 volt when the received pulse voltage is lower than 3 volts.

Due to above mentioned measurement readings, one can conclude that any time the received pulse may be distorted by the FSO link or inside the receiver circuit, the received pulse can be reshaped to a pure pulse that entered to the Data Receiver Unit.

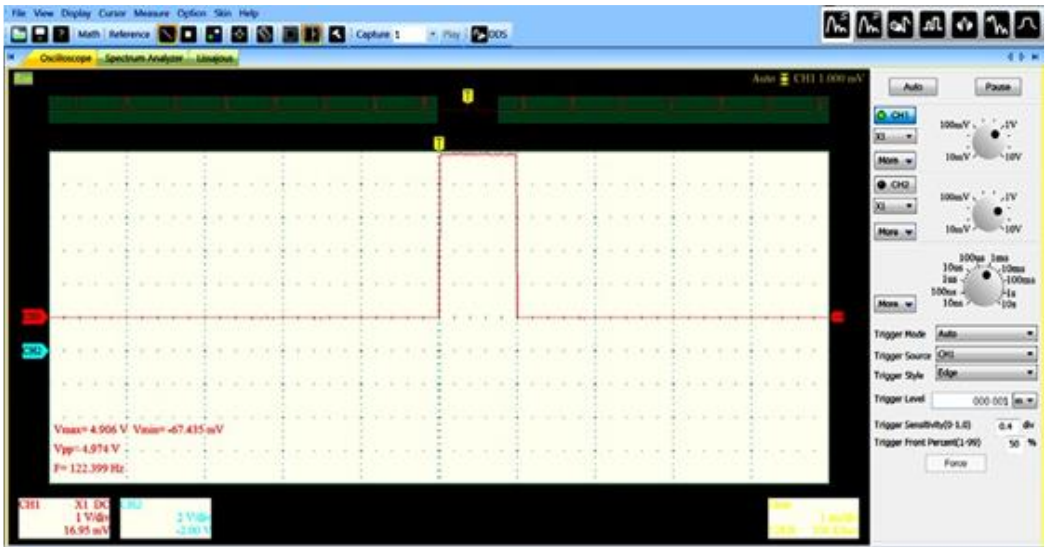

**Figure 7.17.** Real oscilloscope presenting for the received laser pulse at the output of the Voltage Comparator.

## 7.8 Discussion on Result Obtained from Proposed ADC Methods

The following comparison of ADC architecture is to find the suitable one for WSN, the selection of ADC depends on the application and specification such as sample rate and power consumption, so that the choosing of architecture of ADC method in WSN is a critical point.

A proper choosing of architecture design of analog to digital converter lead to save of energy.

Time interleaved ADCs need for multiple sets of analog hardware, which leading to high power consumption with fast sampling rates. In Flash converters method a large number of comparators used to give a high resolution, making them impractical in most applications requiring more than 8 bits of resolution. interpolation and Folding could help to reduce the number of require comparators, but the architecture is still not well suited for low-power applications. The Multi-step analog-to-digital converter also requires a large number of analog hardware, resulting in excessive power consumption for application in distributed sensor networks. Another ADC architectures, such as Successive Approximation,Delta-Sigma, Integrating and Algorithmic, have been reported to work with low-power consumption, low supply voltage and with moderate resolution and speed. A comparative of reported low power ADCs of various architectures reported is given in table (7.2) [75].

**Table 7.2.** Performances of some ADCs of version architecture.

| Architecture | Supply voltage | Power(µW) |
|---|---|---|
| Delta-Sigma[7] | 1.8 V | 108 |
| Successive Approximation[7] | 1V 0.5 V | 30 0.85 |
| Successive Approximation[8] | 1V | 25 200nW 19 |
| Pipeline[9] | 1.8V | 385mW |
| Logarithmic[10] | 1.8V | 89-271 |
| Integrating[7] | 3.3 V | -- |
| Algorithmic[7] | 2.8 V 2V | 8.18 + 9.71 1 + 1.3 |
| Pulse-period coding | 5V | 4.8mW |

## 7.9 Conclusions

In this work, an intelligent wireless sensor network for $NO_2$ gas sensing has been designed, simulated and implemented. The proposed system involves two main parts: the wireless sensor network and the intelligent system. The wireless sensor network has been utilized for: 1) reading the sensors output signals, 2) converting these signals to pulses with specific periods, 3) transmitting these pulses to the pulse period decoders at the receiver circuits, and 4) these decoder circuits translate these pulses to binary data that can be driven to an intelligent system and stored in an FPGA. The intelligent system has been used for processing the incoming binary data from the wireless sensor network and presenting a specific decision.

The proposed automation system has been designed and implemented as a prototype with the mentioned considerations in chapters five and six. Using these considerations, one can use the Back-propagation neural network as an intelligent system for the proposed intelligent wireless sensor network and the proposed ADC to

convert the analog signal to digital signal which is a powerful network for presenting severe decision.

The Pulse-period coding can be use as ADC method where can obtain a faster and low power consumption Therefore, the probability of error is occurred only on a single bit, whereas the probability of error of the related or traditional wireless sensor networks is performed on multi-bits or pulses (usually 8-bits). It then stands to reason that the probability of error of the proposed transmission technique is much less than traditional WSN systems due to the transmission of only a single bit for representing each character.

The Trainpso function (which is particle swarm optimization function) can be used as a training function for the proposed neural network, whereas, one can obtain an optimal result of performance for this neural network because the mean square error can reach zero at epoch 46 to get the best error value for this network when using only three neurons in the hidden layer.

### 7.10 Suggestions for Future Work

For a future work, one can develop or improve the function of the proposed intelligent WSN by proposing the following important points:

1- The sensor of the proposed intelligent WSN can be increased for enlarging the coverage area of the proposed system, at the same time the practical circuit of the system can be more complex and the size of the proposed simulation software can be enlarge, so one must choose an appropriate FPGA for storing this software.

2- Increasing the levels of the sensor output signal and increasing the output data of the proposed intelligent WSN can increase the accuracy of the results, but at the same time the proposed simulation software can enlarge in size, cause the proposed simulation system for this situation must involve more than four lines for the input data, and more than four lines for the output data, for this reason the resolution ( the no. the bits of data that represents the given level) can also

increases and so the durations of the transmitted laser pulse, and finally, the complexity of practical circuit of the overall proposed system can increase too.

3- The proposed system can be faster more and more by decreasing The duration of the transmitted pulses more and more, but the bandwidth of the transmitted signals can also increases too.

4- Using a microprocessor for processing the incoming data from the sensors instead of the FPGA, one can get a flexible WSN with multi- processing modes, but at the same time the proposed system will be slower, cause the FPGA is faster than the microprocessor and the microcontroller. One can use any type of sensors in the proposed intelligent WSN, such as light, sound, pressure…., etc. that produces the same good and accepted results, which make the proposed WSN more applicable system.

5- One can increase the link range of the laser communication system of the proposed intelligent WSN either by increasing the overall gain of the receiver circuit, or by increasing the transmitted power of the IR laser diode.

6- One can use high speed CMOS or any another type of high speed and low power Integrated Circuits (ICs) for increasing the speed and decreasing the consumed power of the proposed practical circuit, which supports the performance of the proposed intelligent WSN.

**REFERENCES:**


1. Brauer, M., Henderson, S. B., Kirkham, T., Lee, K. S., Rich, K. and Teschke, K., 2002. Review of the health risks associated with nitrogen dioxide and sulfur dioxide in indoor air, The University of British Columbia,

2. Dimitroulopoulou, C., Ashmore, M. R., Byrne, M. A. and Kinnersley, R. P., 2001. Modelling of indoor exposure to nitrogen dioxide in the UK, Atmospheric Environment, 35, 2, 269-279.

3. Mullen, N. A., Li, J., Russell, M. L., Spears, M., Less, B. D. and Singer, B. C., 2016. Results of the California Healthy Homes Indoor Air Quality Study of 2011–2013: impact of natural gas appliances on air pollutant concentrations. Indoor Air, 26, 2, 231-245.

4. Wang, J., Zhang, W., Cao, R., You, X. and Lai, H., 2016. Analysis of nitrogen dioxide in environment. Advances in Bioscience and Biotechnology, 7, 06, 278-290.

5. Cotton, S., 2013. Lanthanide and actinide chemistry, John Wiley & Sons, UK.

6. Chan-Yeung, M., Ashley, M. J. and Grzybowski, S., 1978. Grain dust and the lungs, Canadian Medical Association Journal, 118, 10, 1271-1274.

7. Gurney, J. W., Unger, J. M., Dorby, C., Mitby, J. K. and Von, E., 1991. Agricultural disorders of the lung, Radiographics, 11, 625-634.

8. https://nuclearweaponarchive.org/Nwfaq/Nfaq5.html, Retrieved on 20.05.2018.

9. Porterfield, W. W., 2013. Inorganic chemistry, second edition, Academic press, San Diego.

10. National Research Council, 2007. Chapter 12: Nitrogen Dioxide in Emergency and Continuous Exposure Guidance Levels for Selected Submarine Contaminants, National Academies Press, USA.

11. Hansel, N. N., Breysse, P. N., McCormack, M. C., Matsui, E. C., Curtin-Brosnan, J. and Williams, D. A. L., 2008. A longitudinal study of indoor nitrogen dioxide levels and respiratory symptoms in inner-city children with asthma, Environmental health perspectives, 116, 10, 1428-1432.

12. https://www.cdc.gov/niosh/npgd0454, Retrieved on 25.01.2019.

13. https://www.govinfo.gov/app/collection/fr, Retrieved on 29.10. 2011.

14. Pinjare, S. and Arun, K., 2012. Implementation of Neural Network Back Propagation Training Algorithm on FPGA, International Journal of Computer Applications 52, 6, 1-7.

15. Muhammed, K., Muhammed, B. and Muhammed, T., 2012. FPGA Based Neural Wireless Sensor Network, Conference: the 13th International Arab Conference on Information Technology (ACIT), organized by CCIS, Zarqa University, Jordan.

16. Shikha, B., 2013. ANN for Node Localization in Wireless Sensor Network, International Journal of Advanced Research in Electrical, Electronics and Instrumentation Engineering, 2, 5, 1724-1731.

17. Guo, W. and Juan, W., 2014. Design and Implementation of Wireless Sensor Network Nodes Based on BP Neural Network, Journal of Chemical and Pharmaceutical Research, 47, 777-780.

18. Te-Jen, S., Ming-Yuan, H. and Yuei-Jyun, S., 2011. An Adaptive Particle Swarm Optimization for the Coverage of Wireless SensorNetwork, Springer-Verlag Berlin Heidelberg, 218, 386-391.

19. Mehrjoo, S., Shanbehzadeh, J., and Sarrafzadeh, A., 2012. Swarm Intelligence Based Clustering In Wireless Sensor Networks. In Iaeng Transactions On Engineering Technologies, 7, 389-402.

20. Haiping, H., Junqing, Z., Ruchuan, W. and Yisheng, Q., 2014. Sensor Node Deployment in Wireless Sensor Networks Based on Ionic Bond-Directed Particle Swarm Optimization, An International Journal of Applied Mathematics & Information Sciences, 8, 2, 597-604.

21. Kavitha1, K. and Mohamed, M., 2014, Particle Swarm Optimization Based QoS Aware Routing for Wireless Sensor Networks, IJSRD – International Journal for Scientific Research & Development, 2, 07, 284-292.

22. Kulkarni, R. V. and Venayagamoorthy, G. K., 2010. Particle swarm optimization in wireless-sensor networks: A brief survey. IEEE Transactions on Systems, Man, and Cybernetics, Part C (Applications and Reviews), 41, 2, 262-267.

23. Xunqian, T., Jun Lin, Yanju J. and Guanyu Z., 2017. Global Optimization of Wireless Seismic Sensor Network Based on the Kriging Model and Improved Particle Swarm Optimization Algorithm, Springer U.S.

24. Benrekia, F., Attari, M. and Bouhedda, M., 2013. Gas sensors characterization and multilayer perceptron (MLP) hardware implementation for gas identification using a field programmable gate array (FPGA). 13, 3, 2967-2985.

25. Silva, M. R. L. F., de Carvalho, G. H. S., Monteiro, D. C. and Machado, L. S., 2015. Distributed target location in wireless sensors network: an approach using FPGA and artificial neural network. Wireless Sensor Network, 7, 05, 35-48.

26. Yasin, A. and Sabaneh, K., 2016. Enhancing Wireless Sensor Network Security using Artificial Neural Network based Trust Model. International Journal Of Advanced Computer Science And Applications, 7, 9, 222-228.

27. Andrey, S. and Alexander, B., February 2012. Energy-Aware Gas Sensing using wireless Sensor Network, 9th European Conference, Trento, Italy.

28. Hanan, A. R. and Aied, K., 2016. Design and implementation of interface unit communicated by a laser system within wireless sensor Network, Eng and Tech journal, 34, 13, 2507-2517.

29. Gaura, E., Girod, L., Brusey, J., Allen, M. and Challen, G., 2010. Wireless sensor networks: Deployments and design frameworks. Springer Science & Business Media, USA.

30. Suraiya, T., 2011. Wireless Sensor Networks, InTech. Corp, 9, 51000 Rijeka, Croatia.

31. Pedro, J., Thiemo, V., Peter, C. and Luca, M., 2010. Real-World Wireless Sensor Networks, Springer-Verlag Berlin Heidelberg, USA.

32. Subhas, C. M. and Henry, L., 2010. Advances in Wireless Sensors and Sensor Networks, Springer-Verlag Berlin Heidelberg, USA.

33. Waltenegus, D. and Christian, P., 2010. Fundamentals of Wireless Sensor Networks: Theory and Practice, John Wiley & Sons Ltd, The Atrium, Southern Gate, Chichester, West Sussex, PO19 8SQ, United Kingdom.

34. Geoff, V. M. and Yen, K. T., 2010. Wireless Sensor Networks: Application-Centric Design, InTech., Corp, Janeza Trdine 9, 51000 Rijeka, Croatia.

35. Gilbert, E. P. K., Kaliaperumal, B. and Rajsingh, E. B., 2012. Research issues in wireless sensor networkapplications: a survey. International Journal of information and electronics engineering, 2, 5, 702-716.

36. Grindvoll, H., Vermesan, O., Crosbie, T., Bahr, R., Dawood, N. and Revel, G. M., 2012. A wireless sensor network for intelligent building energy management based on multi communication standards-A case study, Journal of Information technology in construction, 17, 43-61.

37. Rajkumar, V. B., Jadhav, K. and Vidya, S., 2012. Wireless sensor networks issues and applications. International Journal Computer Technology & Applications, 3, 5, 1667-1673.

38. Maraiya, K., Kant, K., and Gupta, N. 2011. Wireless sensor network: a review on data aggregation. International Journal of Scientific & Engineering Research, 2, 4, 1-6.

39. Takahiro, H., Vladimir, I., Zadorozhny I. and Erik, B., 2010. Wireless Sensor Network Technologies for the Information Explosion Era, Springer-Verlag Berlin Heidelberg, USA.

40. Dishongh, T. J. and McGrath, M., 2010. Wireless sensor networks for healthcare applications. Artech House, UK.

41. Arun, K. M. and Jennifer, C. R., 2008. Free-Space Laser Communications: Principles and Advances, Springer Science & Business Media, USA.

42. Abdulsalam, G. A., November 2014. Free Space Optical Communications-Theory and Practices, InTech Corp, UK.

43. Jahan, A. F., Samiul, E. and Naveed, A., August 2014. Development of Carbon Monoxide Detecting Device Using MQ-7 Sensor Along with its Statistical Analysis, BRAC University, Dhaka.

44. Muhammad, H. R., 2011. Microelectronic Circuits: Analysis and Design, Cengage Learning, Inc, Second Edition, Canada.

45. Samuel, D. R. and Ojongbede, H. A., 2014. Microcontroller Based Security System with Intruder Position. IOSR Journal of Electrical and Electronics Engineering, 9, 1, 01-08.

46. Jawla, S., 2013. Intensity modulation formats in optical communication system. International Journal of Scientific & Engineering Research, 4, 12, 584-589.

47. Monn, C., 2001. Exposure assessment of air pollutants: a review on spatial heterogeneity and indoor/outdoor/personal exposure to suspended particulate matter, nitrogen dioxide and ozone, Atmospheric environment, 35, 1, 1-32.

48. Takahiro, N., 2010. Laser Diodes and Their Applications to Communications and Information Processing, John Wiley & Sons, Canada.

49. Abdulsalam, G. A. and Khaleel, S. A., 2014. Free Space Optical Communications-Theory and Practices, The Authors, Licensee InTech Corp, UK.

50. Alphan, S., 2007. Solid-State Lasers and Applications, Taylor & Francis Group, LLC., UK.

51. Hamid, H., 2009. Near-Earth Laser Communications, Taylor & Francis Group, LLC, USA.

52. Mingbo, N., Julian, C. and Jonathan, F. H., 2012. Terrestrial Coherent Free-Space Optical Communication Systems, InTech, UK.

53. Ming, L. and Milorad, C., 2017. Coherent Free Space Optics Communications Over the Maritime Atmosphere with Use of Adaptive Optics for Beam Wavefront Correction, Optical Society of America, 6, 1453-1462.

54. Kazi, M. S., Mehedi, H., Karmaker, B. and Liton, K. B., Scattering Effect on Terrestrial Free Space Optical Signal in Tropical Weather Condition, IOSR Journal of Electronics and Communication Engineering (IOSR-JECE), 10, 4. 12-18.

55. Arockia, B., Arputha, V. and Durairaj, S., 2015. Comparison of Different Models for Ground-Level Atmospheric Turbulence Strength (Cn2) Prediction with a New Model According to Local Weather Data for FSO Applications, Optical Society of America, 54, 4, 802-815.

56. Van, D., Moene, A. F., Graf, A., Simmer C. and Holtslag, A. M., 2014. Estimation of the Refractive Index Structure Parameter from Single-Level Daytime Routine Weather Data, Optical Society of America, 53, 26, 5944-5960.

57. Dima, B., 2015. Free-Space Optical Channel Simulator for Weak-Turbulence Conditions, Optical Society of America, 54, 31, 9055-9059.

58. Ahm, N. Z. R. and Mohamed, S., March 2014. Dramatic Atmospheric Turbulence Effects on Submarine Laser Communication Systems (SLCS) and Free Space Optics (FSO), International Journal of Advanced Research in Computer Engineering & Technology (IJARCET), 3, 3, 656-667.

59. Bernhard, E., 2010. Simplified Channel Model for Simulation of Free- Space Optical Communications, Journal of Optical Communications and Networking, 2, 5, 293-304.

60. Yang, F., Cheng, J. and Tsiftsis, T. A., 2014. Free-space optical communication with nonzero boresight pointing errors. IEEE Transactions on Communications, 62, 2, 713-725.

61. Bouhadda, M., Abbou, F. M., Serhani, M., Chaatit, F. and Boutoulout, A., 2016. Analysis of dispersion effect on a NRZ-OOK terrestrial free-space optical transmission system. Journal of the European Optical Society-Rapid Publications, 12, 1, 1-6.

62. Barranco, G. F., Sheard, B. S., Dahl, C., Mathis, W. and Heinzel, G., 2018. A low-power, low-noise 37-MHz photoreceiver for intersatellite laser interferometers using discrete heterojunction bipolar transistors, IEEE Sensors Journal, 18, 18, 7414-7420.

63. Nihal, K., 2008. Electronic Circuit Design: from Concept to Implementation, Taylor & Francis Group, USA.

64. John, A. F., 2011. Focus on Artificial Neural Networks, Nova Science Publishers, Inc, USA.

65. Vittorio, C., Massimo, B., Pierluigi, C. and Bruno, D., 2010. Applications of Mathematics in Models, Artificial Neural Networks and Arts, Springer Science & Business Media, USA.

66. Shashi, S., July 2014. A Gentle Introduction to Back- propagation, Numeric Insight, 7, 1, 15-27.

67. Osamah, I. and Bayan, M., 2019. An overview on wireless sensor networks and finding optimal location of nodes, Periodicals of Engineering and Natural Sciences, 7, 3, 1196-1011.

68. Verma, N. and Chandrakasan, A., Jun 2007. An ultra low energy 12-bit rateresolutionscalable SAR ADC for wireless sensor nodes, IEEE J. Solid-State Circuits, 42, 6, 1196-1205.

69. Brunsilius, J., Siragusa, E., Kosic, S., Murden, F., Yetis, E., Luu, B. and Barlow, A., 2011. A 16b 80ms/s 100mw 77.6 db snr cmos pipeline adc. In 2011 IEEE International Solid-State Circuits Conference 186-188.

70. Dian, P., Diaz, D., Santika, K. and Bens, P., 2011. An Application of Backpropagation Artificial Neural Network Method for Measuring The Severity of Osteoarthritis, International Journal of Engineering and Technology, 11, 03, 102-105.

71. Daniel, S. Y., Ian, C., Daming, S. and Wing, W. Y., 2010. Sensitivity Analysis for Neural Networks, Springer-Verlag Berlin Heidelberg, UK.

72. David, J. L., 2008, Artificial Neural Networks, Humana Press, a part of Springer Science & Business Media, LLC, USA.

73. Lee, J., Rhew, H. G., Kipke, D. and Flynn, M., 2010. A 64 channel programmable closed-loop neurostimulator with 8 channel neural amplifier and logarithmic ADC, IEEE Solid-State Circuits, 45, 9, 1935-1945.

74. Sameh, K. and Dominique, B., 2015. Particle Swarm Optimization with Adaptive Inertia Weight, International Journal of Machine Learning and Computing, 5, 5, 368-374.

75. Kavitha, V. and Kirupa, G., 2018. Efficient and Optimal Routing Using Ant Colony Optimization Mechanism for Wireless Sensor Networks, Periodicals of Engineering and Natural Sciences, 6, 1, 171-181.

**THESIS APPENDIX**

**Appendix A:** FPGA field-programmable gate array

SPARTAN-6 FPGA SP605 EVALUATION KIT

LOW-COST, CONNECTIVITY
FPGA DESIGN PLATFORM

# SPARTAN-6 FPGA SP605 EVALUATION KIT

**Accelerated Development**

- Fewer resources under tighter deadlines, new standards, and shifting requirements make for a challenging design environment
- Market expectations for higher performance and more intelligent features require new approaches to developing electronic systems
- Today's systems call for advanced memories, connectivity, digital signal, and embedded processing, all working together

**Simpler and Smarter Methodologies**

- Xilinx Targeted Design Platforms enable software and hardware designers alike to leverage open standards, common design methodologies, development tools, and run-time platforms
- Design teams can spend less time developing the infrastructure of an application and more time building differentiating features into the end application
- Targeted Design Platforms from Xilinx and its network of third parties provide system designers with simpler and smarter methodologies for creating FPGA-based system-on-chip solutions

## Accelerate your Designs – Right Out of the Box

The Spartan®-6 FPGA SP605 Evaluation Kit conveniently delivers all the basic components of the Xilinx Base Targeted Design Platform for developing broadcast, wireless communications, automotive, and other cost- and power-sensitive applications that require transceiver capabilities in one package. Along with the development board, cables, and documentation, the new kit provides an integration of hardware, software, IP, and pre-verified reference designs so development can begin right out of the box.

## Value-added Productivity

With everything you need in one package, the Spartan-6 FPGA SP605 Evaluation Kit provides value-added productivity gains that you can't get from à la carte development system assemblies. Functional infrastructure that already looks like your basic architecture makes you more productive as you ramp up a new design, enabling quicker time-to-innovation for differentiating your products versus your competition. Multiple design examples provide insight and a kick-start on how to implement system IP to optimize your unique application.

## Integrated, Easy-to-Use Solutions

The Spartan-6 FPGA SP605 Evaluation Kit provides a flexible environment for higher-level system design including applications which need to implement features such as high-speed serial transceivers, PCI Express®, DVI, and/or DDR3. The SP605 development board includes an industry-standard FMC (FPGA Mezzanine Card) connector for scaling and customization to specific applications and markets. The integration of Xilinx development tools help streamline the creation of systems that adhere to complex requirements.

For more information, support, documents and reference designs, or to purchase, please visit **www.xilinx.com/sp605**

XILINX®

**Appendix A:** FPGA field-programmable gate array

SPARTAN-6 FPGA SP605 EVALUATION KIT

## What's Inside the SP605 Evaluation Kit

- SP605 Base Board with the XC6LX45T-FGG484-3 CES FPGA
- ISE® Design Suite Logic Edition: (device-locked) for Spartan-6 LX45T FPGA
  - Includes ChipScope™ Pro and the ChipScope Pro Serial I/O Toolkit
  - Includes PlanAhead™ Design Analysis Tool
  - Timing Driven Place and Route, SmartGuide™, and SmartXplorer Technology
- Documentation
  - Hardware Setup Guide
  - Getting Started Guide
  - Hardware User Guide
  - Reference Designs User Guide
- Schematics and PCB files
- Universal 12V power supply
- Cables: 2 USB, 1 Ethernet, 1 DVI-VGA adapter
- Reference Designs and Demos
  - Board Diagnostic Demo
  - Base System Reference Design featuring DSP48, Ethernet, Memory, and Serial Transceiver integration
  - Multiboot Reference Design, featuring fail-safe configuration
  - Hardened Memory Controller Reference Design
- Reference designs, demos, documentation, and applications delivered on USB FLASH drive to get started quickly

## BOARD FEATURES

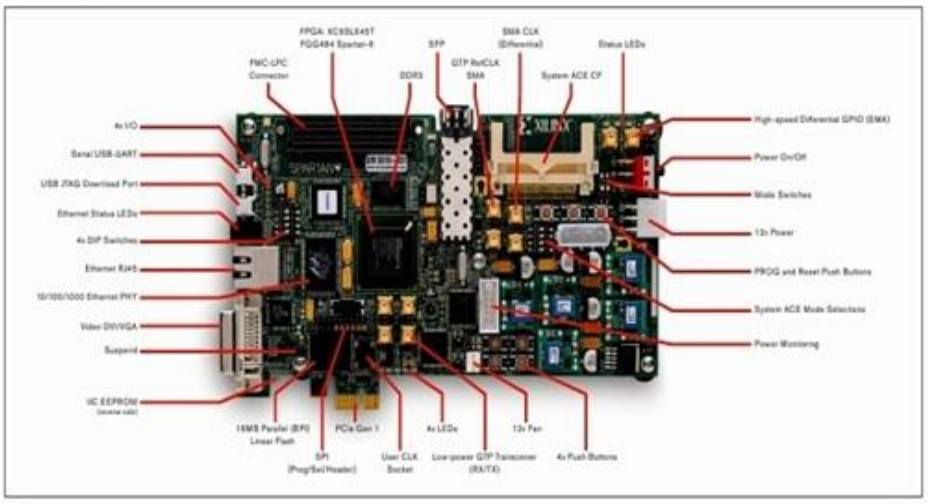

## Take the NEXT STEP

For more information, support, documents, and reference designs, or to purchase, please visit **www.xilinx.com/sp605**

**Part Number: EK-S6-SP605-G**


**Corporate Headquarters**
Xilinx, Inc.
2100 Logic Drive
San Jose, CA 95124
USA
Tel: 408-559-7778
www.xilinx.com

**Europe**
Xilinx Europe
One Logic Drive
Citywest Business Campus
Saggart, County Dublin
Ireland
Tel: +353-1-464-0311
www.xilinx.com

**Japan**
Xilinx K.K.
Art Village Osaki Central Tower 4F
1-2-2 Osaki, Shinagawa-ku
Tokyo 141-0032 Japan
Tel: +81-3-6744-7777
japan.xilinx.com

**Asia Pacific Pte. Ltd.**
Xilinx, Asia Pacific
5 Changi Business Park
Singapore 486040
Tel: +65-6407-3000
www.xilinx.com


XILINX®




Printed in the U.S.A. PN 2421

**Appendix B:** IR Infra-Red

EGiSMOS

6mm Laser Module Series

## 850nm, Infrared Laser Module

### Application

Industrial areas / Medical / Biochemical / Laser Tag

### Property

Wavelength Range = 850nm (others optional)

### Introduction

Egismos created compact laser series that have very attractive price tag. Our standard modules are emitting 780nm and 850nm wavelengths, however custom wavelength are also available. Other characteristics like TTL or custom optics is also available upon a customer's request.

| Specifications(T=25℃) | | |
|---|---|---|
| **Items** | **Symbols** | **S638501D, S638505D** |
| Mode | | CW |
| Wavelength | λ | 850nm |
| Lens | | PMMA |
| Spot | D/R | Dot |
| Spot Size | D | <15x 30mm at 10m |
| Diameter x Length | Φ x l | 6x10.5mm (without PCB) |
| Output Power | Po | <1mW, <5mW |
| Power Stability | | <10% |
| Divergence Angle | mrad | <1 |
| Operating Voltage(DC) | Vo | 3V |
| CW Operating Current | Io | 25~30mA, 40mA max |
| Operating Temperature | To | -10℃~ +50℃ |
| Storage Temperature | Ts | -40℃~ +80℃ |
| Housing Material | | Brass |
| Mean time to failure | | >5000 hrs |

EGiSMOS
www.egismos.com
tel:+1-360-3893347
sales@egismos.com

Dcc no: EG-QS-T-PM-ST-0021 Form no: EG-QR-T-QA-0003 Date:2015.04.16

**Appendix B:** IR Infra-Red



# Silicon Photodiode

# TIL100

Optoelectronic Products



**General Description**

The TIL100 is a high-speed PIN photodiode operating in a reverse-bias mode. It is spectrally matched with the TIL38 emitter. This photodiode was designed for infrared remote-control system.

**Low Capacitance**
**High Photosensitivity With Fast Response**

**Absolute Maximum Ratings**

**Maximum Temperature**

| | |
|---|---|
| Operating Temperature | −25°C to +100°C |
| Storage Temperature | −25°C to +100°C |
| Pin Temperature (Soldering, 3 s) | 260°C |

**Maximum Power Dissipation**

| | |
|---|---|
| Total Dissipation at $T_A$ = 25°C | 150 mW |
| Derate Linearly at 25°C | 2 mW/°C |

**Maximum Voltage**

| | | |
|---|---|---|
| BV | Breakdown Voltage | 30 V |

**Package Outline**

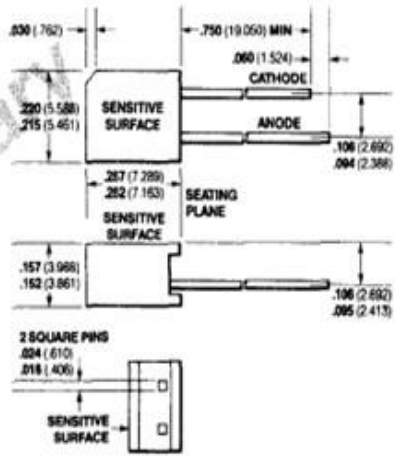


**Notes**
All dimensions in inches bold and millimeters (parentheses)
Tolerance unless specified = ±.015 (±.381)

**Electrical Characteristics** $T_A$ = 25°C

| Symbol | Characteristic | Min | Typ | Max | Units | Test Conditions |
|---|---|---|---|---|---|---|
| $C_T$ | Total Capacitance | | 35 | 50 | pF | $V_R$ = 3 V, H = 0, f = 1 MHz |
| $t_r$ | Rise Time | | | 100 | ns | $V_R$ = 10 V, $R_L$ = 1 kΩ |
| $t_f$ | Fall Time | | | 100 | ns | $V_R$ = 10 V, $R_L$ = 1 kΩ |
| $I_L$ | Light Current | | 10 | | μA | $V_R$ = 10 V, H = 250 W/cm² at 940 nm |
| $I_D$ | Dark Current | | | 50 | nA | $V_R$ = 10 V, H = 0 |

## **Appendix C:** NO2 Sensors

e2v

**MiCS-2710**
**$NO_2$ Sensor**

This datasheet describes the use of the MiCS-2710. The package and the mode of operation illustrated in this document target the detection of nitrogen dioxide ($NO_2$).

### FEATURES

- Low heater current
- Wide detection range
- High sensitivity
- Fast thermal response
- Miniature dimensions
- High resistance to shocks and vibrations

### IMPORTANT PRECAUTIONS

**Read the following instructions carefully before using the MiCS-2710 sensor described in this document to avoid erroneous readings and to prevent the device from permanent damage.**

- The sensor must not be wave soldered without protection, or exposed to high concentrations of organic solvents, ammonia, or silicone vapours, to avoid poisoning the sensitive layer.
- Heating powers above the maximum rating of 120 mW can destroy the sensor due to overheating.
- This sensor is to be placed in a filtered package that protects it against any water or dust projection.
- For any additional questions, email enquiries@e2v.com or telephone +44 (0)1245 493493.

### OPERATING MODE

The recommended mode of operation is a constant power mode. A heater power of $P_H$ = 43 mW is applied. This causes the temperature of the sensing resistor ($R_S$) to reach about 220 °C.

Detection of the pollution gases is achieved by measuring the sensing resistor $R_S$ during operation.

### SENSOR RESPONSE

The sensor response to $NO_2$ in air is represented in Fig. 1.

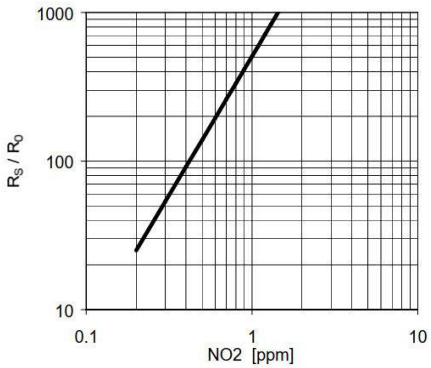


The sensor resistance $R_S$ is normalised to the resistance under air ($R_0$).

**Fig. 1: $R_S/R_0$ as a function of gas concentration at <5% RH and 25 °C.**



e2v technologies (uk) limited, Waterhouse Lane, Chelmsford, Essex CM1 2QU United Kingdom Telephone: +44 (0)1245 493493 Facsimile: +44 (0)1245 492492
e-mail: enquiries@e2v.com Internet: www.e2v.com Holding Company: e2v technologies plc
e2v technologies inc. 4 Westchester Plaza, PO Box 1482, Elmsford, NY10523-1482 USA Telephone: (914) 592-6050 Facsimile: (914) 592-5148 e-mail: enquiries@e2vtechnologies.us



A1A-MiCS-2710 Version 2, July 2008
104168

# **Appendix C:** NO2 Sensors

## MEASUREMENT CIRCUIT

Fig. 2 shows the pin connections of the MiCS-2710 gas sensor. A simple circuit to measure the pollution level is proposed in Fig. 3. The heating voltage $V_H$ is applied to pins 3 and 1. A load resistor $R_L$ is connected in series with $R_S$ to convert the resistance $R_S$ to a voltage $V_S$ between pins 2 and 4. $R_S$ can then be calculated by the following expression:

$$R_S = R_L / (V_{CC} - V_S) \times V_S$$

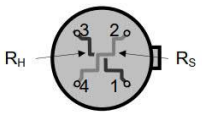


| Pin | Connection |
|---|---|
| 1 | Heater ground |
| 2 | Sensor pin |
| 3 | Heater power |
| 4 | Sensor pin |

**Fig. 2: Equivalent circuit of MiCS-2710 (top view)**

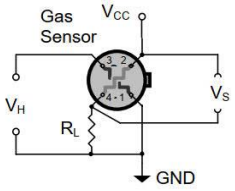


**Fig. 3: Measurement circuit for pollution gas detection**

## ELECTRICAL SPECIFICATIONS

### Maximum Ratings

| Rating | Symbol | Value/ Range | Unit |
|---|---|---|---|
| Maximum sensor supply voltage | $V_{CC}$ | 2.5 | V |
| Maximum heater power dissipation | $P_H$ | 50 | mW |
| Maximum sensor power dissipation | $P_S$ | 1 | mW |
| Relative humidity range | $R_H$ | 5 – 95 | %RH |
| Ambient operating temperature | $T_{amb}$ | -30 – 85 | °C |
| Storage temperature range | $T_{sto}$ | -40 – 120 | °C |
| Storage humidity range | $RH_{sto}$ | 5 – 95 | %RH |

### Operating Conditions

| Parameter | Symbol | Typ | Min | Max | Unit |
|---|---|---|---|---|---|
| Heating power | $P_H$ | 43 | 30 | 50 | mW |
| Heating voltage | $V_H$ | 1.7 | - | - | V |
| Heating current | $I_H$ | 26 | - | - | mA |
| Heating resistance | $R_H$ | 66 | 59 | 73 | Ω |

### Sensitivity Characteristics

| Characteristic | Symbol | Typ | Min | Max | Unit |
|---|---|---|---|---|---|
| $NO_2$ detection range | FS | | 0.05 | 5 | ppm |
| Sensing resistance in air (see note 1) | $R_0$ | 2.2 | 0.8 | 8 | kΩ |
| Sensitivity factor (see note 2) | $S_R$ | 55 | 6 | 100 | - |

**Notes:**

1. Sensing resistance in air ($R_0$) is measured under controlled ambient conditions, i.e. synthetic air at 23 ± 5 °C and <5 ± 5% RH.
2. Sensitivity factor ($S_R$) is defined as $R_S$ at 0.25 ppm of $NO_2$ divided by $R_S$ in air. Test conditions are 23 ± 5 °C and <5 ± 5% RH.

## **Appendix C**: NO2 Sensors

### PACKAGE AND FILTER OUTLINE

**(All dimensions nominal and in millimetres)**

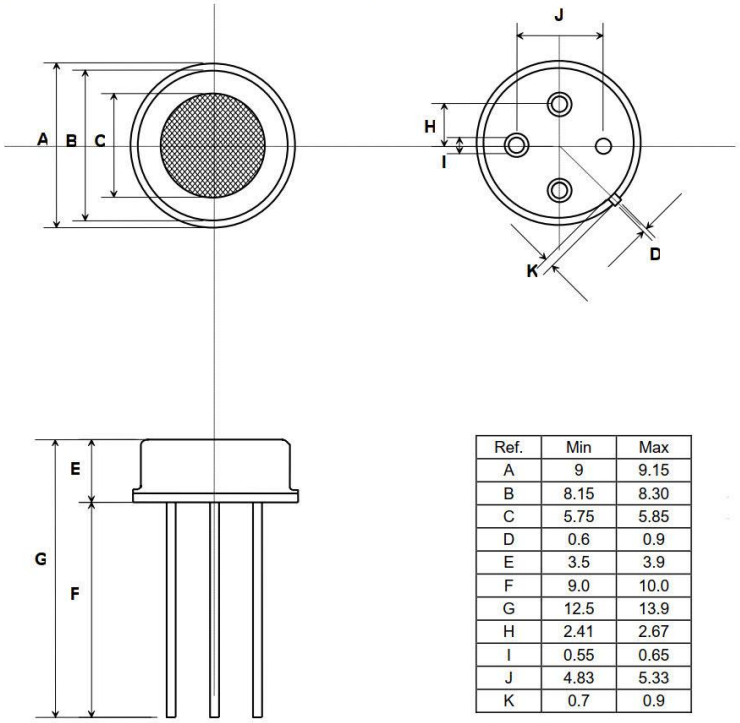


| Ref. | Min | Max |
|---|---|---|
| A | 9 | 9.15 |
| B | 8.15 | 8.30 |
| C | 5.75 | 5.85 |
| D | 0.6 | 0.9 |
| E | 3.5 | 3.9 |
| F | 9.0 | 10.0 |
| G | 12.5 | 13.9 |
| H | 2.41 | 2.67 |
| I | 0.55 | 0.65 |
| J | 4.83 | 5.33 |
| K | 0.7 | 0.9 |

**Outline Notes:**

1. A perfect pin alignment is not guaranteed.
2. The metallic mesh is optional.

e2v semiconductor gas sensors are well suited for leak detection and applications requiring limited accuracy. Their use for absolute gas concentration detection is more complicated because they typically require temperature compensation, calibration, and sometimes as well, humidity compensation. Their base resistance in clean air and their sensitivity can vary overtime depending on the environment they are in. This effect must be taken into account for any application development (117-5.0).

## CURRICULUM VITAE

**Name** : Mohammed Hussein Ali.

**EDUCATION INFORMATION** (Institute and year):

**Bachelor's Degree**: Al-Mustansiryia University (collage of computer and software Engineering) 2002-2006.

**Master's Degree** : SRM University (collage of Information Technology Engineering) 2010-2012.

**PhD Degree** : Aksaray University (collage of Electrical, Electronic and Computer Engineering) 2017- 2021.

**PROFESSIONAL EXPERIENCE AND AWARDS:**

1. (2006) work as IT engineer with (GTSI company) for one year.
2. (2006-2007) work as software engineer at general directory of Budget and Programs (Iraqi MOD).
3. (2006-2010) work as network and system engineer in IDN (Iraqi Defence Network).
4. (2012-2015) work as formal lecturer at Cihan university.
5. Selected to teach Database course and system building course in Greenwich university/UK.
6. (2017-2018) work as coordinator and Lecturer at Al Rasheed Collage University.
7. currently work as IT manager and trainer of cyber security at IN2 company.

## PUBLICATIONS, PRESENTATIONS AND PATENTS

Articles Published in International Peer-Reviewed Journals

1. Yusuf Erkan Yenice and Mohammed Hussein Ali, 2020**.** A novel Analog to Digital Converter for push mode Wireless Sensor Networks, International Journal of Psychosocial Rehabilitation, Vol. 24, Issue 10, 2020 ISSN: 1475-7192.

https://www.psychosocial.com/article/PR300094/22489

2. Mohammed Hussein Ali and Yusuf Erkan Yenice, 2020. Using a Backpropagation Neural Network in WSN for NOx Detection, Solid State Technology Volume: 63 Issue: 6 Publication Year: 2020.

http://www.solidstatetechnology.us/index.php/JSST/article/view/4398